An MCNP Feasibility Study for a Switchable Radioactive Gamma Source for SPECT Gamma Camera Calibration or Blood Irradiation

by

Ruxandra Ioana Dranga

A thesis submitted to the Faculty of Graduate and Postdoctoral Affairs in partial fulfillment of the requirements for the degree of

Master of Applied Science

in

Biomedical Engineering

Carleton University
Ottawa, Ontario

Abstract

Gamma radiation sources are used for a multitude of applications, including nuclear medicine applications. The current study investigated the feasibility of a switchable radioactive gamma source for two applications: as a calibration source for SPECT gamma cameras; and as a blood irradiator. The source was based on a sequence of (α, n) reactions followed by (n, γ) reactions. MCNP5 parametric studies were performed to investigate the effects of different moderators (*e.g.,* heavy water, deuterated polyethylene or high density polyethylene), neutron absorbers (*e.g.,* $Sm_{natural}$ or $Gd_{natural}$) and geometries, on the calculated gamma flux and dose rate for the proposed source design. The results show that, although technically feasible, the applicability of the proposed source for the two intended applications is not feasible because of cost constraints for larger source designs, and low gamma fluxes and dose rates obtained for smaller source designs.

Acknowledgements

I would like to acknowledge the contribution and support of the following people, who helped make this research possible, have enhanced my learning experience and allowed me to explore the world of computer modelling for healthcare applications: my supervisor, Prof. Glenn McRae for providing me with the amazing opportunity to explore this new concept, for his advice, and his direction; my friend Ragnar Dworschak, and my colleagues at Canadian Nuclear Laboratories - Jeremy Whitlock, Geoff Edwards, Bruce Wilkin, Fred Adams for their technical help and being there to bounce ideas off when I needed.

I would also like to thank Canadian Nuclear Laboratories for giving me time off to attend the courses and being flexible with my schedule when I needed to work on my research. Finally, I would like to thank Best Medical Canada Inc., for funding the preliminary part of the study.

Table of Contents

List of Tables

List of Figures

List of Appendices

List of Symbols

A	atomic mass (number of protons plus number of neutrons)
α	Alpha particle (^4_2He)
β	Beta particle
barn	unit for cross-section (1 barn = 10^{-24} cm)
Bq	Becquerel, SI unit of activity (1 disintegration per second)
Ci	Curie, traditional unit of activity (1 Ci = 3.7×10^{10} Bq)
E	energy of a particle
E_{dep}	energy deposited in a cell calculated with MCNP5 using the F6 tally
eV	Electron-volt, unit of energy (1 eV = 1.602×10^{-19} J)
ε(E)	stopping cross-section
f	fission
f^{α}_{kl}	fraction of all decays of nuclide k that led to an alpha particle with an energy E_{kl}
F4	tally used in MCNP5 to output particle flux in particles/cm^2/source particle
F6	tally used in MCNP5 to output energy deposited in a volume in MeV/g
γ	Gamma radiation
Gy	Gray, unit of absorbed radiation dose (J/kg)
λ	decay constant
M_a	average atomic weight of air
MeV	mega electron-volt (10^6 eV)
n	neutron
N	number of atoms in a sample
N_A	Avogado's number (6.022×10^{23} atoms / mole)
p	proton
R	particle range in the material of interest
R_a	particle range in air
ρ	density of material

ρ_a	density of air
σ_e	elastic scattering cross-section
σ_f	fission cross-section
σ_γ	radiative capture cross-section
σ_i	inelastic scattering cross-section
Σ_a	macroscopic absorption cross-section
Σ_s	macroscopic scattering cross-section
Sv	Sievert, unit of equivalent radiation dose ($Sv = Gy \times w_r$)
$T_{1/2}$	half-life of an isotope
w_r	radiation weighting factor
Z	number of protons
ξ	logarithmic energy decrement per collision
Φ^g	rate at which alpha particles pass through an interface

List of Abbreviations

ALARA	As Low As Reasonably Achievable
CD_2	Deuterated Polyethylene
D_2O	Heavy Water
DNA	Deoxyribonucleic Acid
HDPE	High Density PolyEthylene
ICRP	International Commission on Radiological Protection
MCNP	Monte Carlo N-Particle - probabilistic computer code used to model particle interaction
PET	Positron Emission Tomography
QC	Quality Control
SOURCES-4C	Computer code used to calculate neutron source strength from (α, n) reactions
SPECT	Single Photon Emission Computed Tomography
SRGS	Switchable Radioactive Gamma Source
SRNS	Switchable Radioactive Neutron Source
TA-GVHD	Transfusion Associated Graft-Versus-Host Disease

1 Chapter: Introduction

This chapter presents the motivation for investigating the feasibility of a new gamma source concept, which allows the user to manually and mechanically activate and deactivate the production of gamma radiation, as needed. Subsequently, the objectives of the research are presented, followed by an outline of this thesis and a general overview of the computational models implemented for the feasibility study.

1.1 Motivation

Gamma radiation sources are being used for various everyday applications, from portal monitors for homeland security [1] to food and blood sterilization [2], and as calibration sources in nuclear medicine [3][4]. Since the September 2001 attack on the United States, the use of radiation sources has been subjected to enhanced scrutiny and regulations. Hence, countries around the world started looking into the possibility of replacing current radiation sources with alternative designs that seek to improve health, safety and security, while maintaining an equivalent or improved performance level of the device [5].

Two main applications of gamma radiation sources provided the motivation behind the feasibility study:

1) ^{57}Co flood sources used to calibrate gamma cameras for nuclear imaging devices [3][4]; and
2) The gamma sources used in self-contained blood irradiators for irradiation and sterilization procedures [5].

In general, the current sources work well, however, a number of disadvantages and/or limitations were identified, including:

1) The sources need to be replaced every 1-2 years (*e.g.,* for ^{57}Co flood sources) [6], or 5 years (*e.g.,* ^{60}Co sources) [5], depending on the type of radionuclide used to generate the gamma radiation.
2) ^{137}Cs sources, although they have a long shelf-life, needing replacement every 30 years because of the long half-life of ^{137}Cs, primarily use cesium chloride as the radioactive material, which poses potential hazards to workers, and public safety and security [5].
3) These sources are continuously active, that is, the radioactive material continuously emits gamma radiation as it decays. Permanent shielding needs to be in place in order to minimize the dose to personnel and follow the ALARA (As Low As Reasonably Achievable) radiation protection principle [7].

In order to address some of these disadvantages and limitations, the feasibility of a new switchable radioactive gamma source was investigated. The source was designed to eliminate the need for frequent replacement of the radioactive sources, eliminate the use of cesium chloride as the gamma emitter, aid in the simplification of storage, transportation and handling procedures, and further reduce the time of radiation exposure and the dose received by medical personnel.

1.2 Objective of the Research

The objective of this research was to explore the feasibility of a new concept for a gamma source that would provide significant advantages over current gamma sources. The proposed design would allow the user to start and stop the source remotely and only when needed, thus reducing the radiation exposure of personnel involved in handling and operating the radioactive gamma source. Also, the shelf-life of the gamma source would be increased by using radionuclides that have a longer half-life than ^{57}Co, or ^{60}Co, thus eliminating the need for frequent source replacements.

The basic principle behind the new flood source design is the production of gamma rays via a sequence of two nuclear reactions: an (α, n) reaction, followed by an (n, γ) reaction. The (α, n) reaction can be mechanically switched "ON" and "OFF", hence, allowing the user to have full control over the subsequent production of gamma radiation. The neutrons produced via the (α, n) reaction are slowed down to thermal energies (*i.e.,* energies lower than 0.1 eV) to maximize their absorption by isotopes that will produce gamma rays via an (n, γ) reaction.

To achieve the objective of this research, a number of sub-tasks were carried out:

- Monte Carlo simulations were performed using MCNP5 computer code [8] to investigate the interaction of neutrons produced by the neutron source with the surrounding materials. Various geometries, source materials (*i.e.,* for both (α, n) and the (n, γ) reactions), and materials used to slow down neutrons were investigated.

- Average gamma flux and dose rates were calculated for the modelled gamma source design.
- Calculated average gamma flux and dose rate were compared with the requirements for the two applications of interest: a SPECT gamma camera calibration flood source, and a self-contained blood irradiator, respectively.

1.3 Outline of the Thesis

Following this introduction, the next Chapters lay the foundation for this research, the analysis, and the discussions to follow. Chapter 2 introduces the basic physics concepts that apply in this research and gives an overview of two applications for the proposed design (*i.e.,* a calibration flood source for gamma cameras used in nuclear medical imaging and a self-contained blood irradiator). In addition, the chapter includes a general overview of the two computer codes used in the analysis: MCNP5 and SOURCES-4C. Chapter 3 discusses the methodology developed and implemented for the parametric studies performed to investigate the feasibility of the source design for the two applications introduced in Chapter 2.

In Chapter 4, the study results are summarized and discussed. The feasibility of the switchable radioactive gamma source design is discussed with reference to current gamma sources and their requirements for the two medical applications. Chapters 5 and 6 discuss the limitations associated with the current research and the recommendations for future research, respectively. Lastly, Chapter 7 provides a conclusion for the current thesis.

A number of appendices are also included which contain supporting information to aid with the results and discussion sections in Chapter 4.

1.4 General Overview of the SRGS Design

Mechanically activated "ON" or "OFF" neutron sources based on (α, n) reactions have been reported [9]. This earlier work provides the foundation for the current research, which investigated the feasibility of a mechanically activated radioactive gamma source (referred to as the switchable radioactive gamma source, SRGS) based on (α, n) reactions coupled to (n, γ) reactions.

The SRGS design was based on two main processes:

1) production of neutrons via an (α, n) reaction, and
2) production of gamma rays via an (n, γ) reaction.

The first process can be mechanically controlled so that the neutron source can be turned "ON" and "OFF" on demand. In the "OFF" position, no neutrons are produced, thus turning off the gamma production as well. The gamma source was modelled using a planar geometry (see Figure 1), so that it could be used for the intended applications:

1) a flood source for calibration of gamma cameras, and
2) a self-contained blood irradiator.

These applications are described in detail in Section 2.2.1, and Section 2.2.2. A planar source geometry is appropriate for these planar applications. Figure 2 illustrates the configuration of the proposed SRGS and the gamma camera, while Figure 3 shows a self-contained blood irradiator. Details on the neutron and gamma sources will be presented in Section 3.1.2.1 and Section 3.1.2.2.

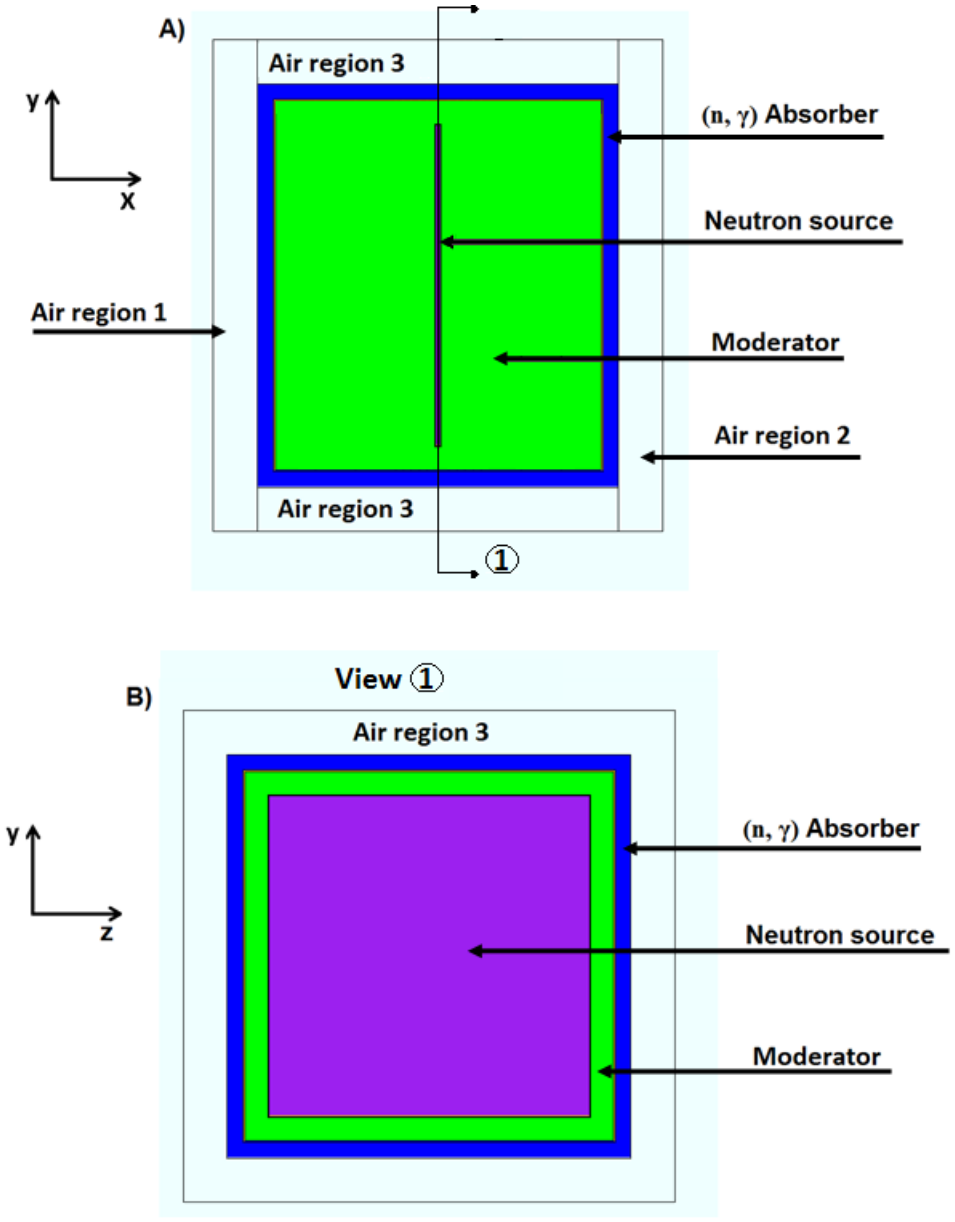

Figure 1 Example of a modelled design for the SRGS. (A) XY view; (B) ZY view. The source is symmetrical about the y-axis, thus, the gamma flux or dose rate calculated in air region 1 or region 2 (Figure 1A), which would be facing the gamma camera during calibration activities or the blood bags for irradiation, is the same (confirmed with MCNP calculation). These two regions were modelled separately in MCNP to be able to tally the flux and dose rates (see Section 2.3.1) independently and compare them with the gamma flux and gamma dose rate required by the intended applications. Figure 1B is a cross-sectional view through the centre of the neutron source (view 1).

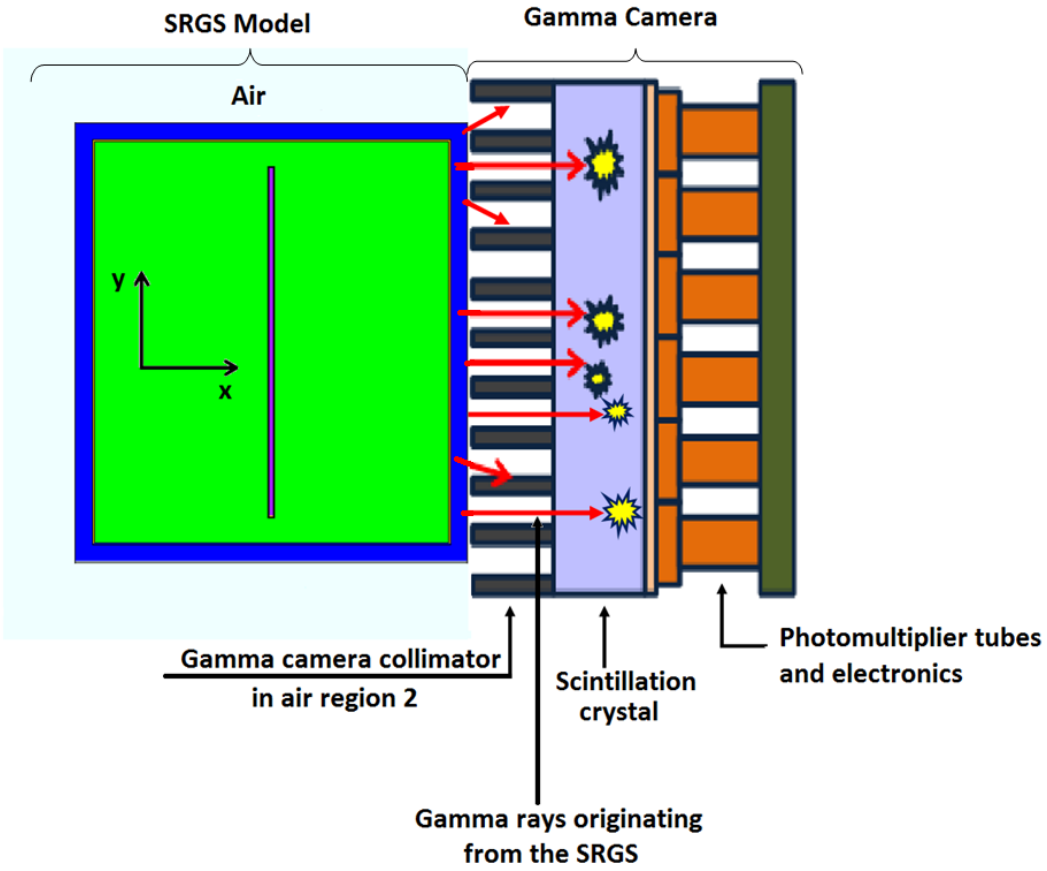

Figure 2 Illustration of the SRGS used as a calibration flood source for a SPECT gamma camera. The collimator was not modelled in MCNP5 in the air region facing the camera, because its presence would lower the calculated average gamma flux. If the gamma flux results calculated without a collimator are not comparable to the requirements for a SPECT gamma camera calibration, then the added complexity of modelling the collimator is not required. Also, calibration tests for gamma cameras used in SPECT imaging are performed both with (extrinsic tests) and without (intrinsic tests) the collimator present (see Section 2.2.1), thus, ignoring the presence of the collimator in the MCNP models is an appropriate representation for intrinsic calibrations tests.

Figure 3 Picture of a self-contained blood irradiator.
The SRGS would be located inside the equipment and the user would not have access to the radioactive source. Picture of the blood irradiator obtained online from Best Theratronics Limited, www.theratronics.ca/product_gamma.html, Accessed March 15, 2015.

The neutron source used for the switchable gamma source was an ^{241}Am-^{9}Be source and was located in the center of the SRGS so that the design was symmetric with respect to the center of the source. ^{241}Am is an alpha (α)-emitting radioisotope used in 'off-the-shelf' devices such as smoke detectors and, although it requires special handling procedures, it has better public acceptance than other α-emitting radioisotopes (*e.g.,* ^{210}Po[1]). Natural beryllium is composed of ^{9}Be, which can produce neutrons when bombarded with α particles (Section 3.1.2.1). Of all neutrons produced by ^{241}Am-^{9}Be (α, n) reactions, 88% are fast neutrons, *i.e.,* they have energies above 1 MeV (Figure 8, Section 3.1.2.1). These energies are too high for efficient gamma production, thus, in order to increase their probability of being absorbed by the neutron absorber and produce gamma (γ) radiation (see Section 2.1.2 and Figure 5), the neutrons are slowed down (or moderated) from fast energies (*i.e.,* >1 MeV) to thermal energies (*i.e.,* <0.1 eV). This

[1] A pure α-emitter, ^{210}Po is lethal in very small amounts (10-20 μg). It drew particular media attention after 2006, because it was used to poison Alexander Litvinenko, a Russian spy living in United Kingdom [10].

was achieved by surrounding the source with a moderating material such as deuterated polyethylene (CD_2[2]), heavy water (D_2O) or high density polyethylene (HDPE[3]) at thicknesses between 0 cm and 20 cm (Section 3.1.2.2 and Section 3.1.3). The moderating material was then encased in a neutron-absorbing, gamma-emitting material (referred to as the (n, γ)-absorber) such as $Sm_{natural}$ or $Gd_{natural}$. These two (n, γ)-absorbers were chosen because of their strong thermal neutron absorbing properties; they have two of the highest thermal neutron absorption cross-sections (Section 2.1.2).

[2] The chemical formula for deuterated polyethylene is CD_3-$(C_2D_4)_n$-CD_3, where n is the number of repeating units in the polymer. The notation used to denote deuterated polyethylene in this thesis is CD_2.
[3] The chemical formula for HDPE is CH_3-$(C_2H_4)_n$-CH_3. This polymer has densities between 0.93 g/cm^3 and 0.97 g/cm^3 [11].

2 Chapter: Background Information

This Chapter summarizes the background information that provides the foundation for the computational analysis performed for the feasibility study. General information on radiation, radioactive decay and interaction of radiation with matter is first presented, followed by the two applications of interest for the proposed gamma source, and a description of the computer codes used for this research.

2.1 Basic Physics Background Information

2.1.1 Radiation and Radioactive Decay

The majority of nuclides found in nature are unstable and are referred to as radionuclides. These unstable radionuclides undergo a process known as radioactive decay, through which they emit energy in the form of alpha (α) or beta (β) radiation, and transform into a new radionuclide. This process continues until they transform into one of the 259 stable nuclides [12][13]. The radioactive decay process that is important for this project is α decay, because it provides the foundation for the neutron source. Radiative capture of neutrons produced by the neutron source is also of interest because it will be used to produce the gamma radiation needed to calibrate SPECT gamma cameras (Section 2.2.1) or irradiate blood bags (Section 2.2.2). A description of radiative capture and its application to this study is discussed in Section 2.1.1.2.

The rate of decay of a sample of radioactive atoms is known as the "activity" of the sample. It is traditionally measured in Curies (Ci), where 1 Ci equals to 3.7×10^{10} Becquerel (Bq), and 1 Bq represents one disintegration per second (dps) [13].

The Becquerel is the SI unit. Activity (A) is defined as [13]:

$$A = \lambda \times N \qquad (1)$$

where λ is the decay constant, and N is the number of atoms in the sample. The decay constant is related to the half-life ($T_{1/2}$) of the sample:

$$\lambda = \frac{\ln 2}{T_{1/2}} \qquad (2)$$

The half-life represents the time in which half the sample will decay.

2.1.1.1 Alpha decay

Some radionuclides decay by emission of alpha (α) particles, which are highly energetic helium ($^{4}_{2}He_{2}$) nuclei [12]. Alpha decay can be represented by:

$$^{A}_{Z}X_{N} \rightarrow \quad ^{A-4}_{Z-2}Y_{N-2} \quad + \quad ^{4}_{2}He_{2} \quad + \quad 2e^{-} \qquad (3)$$

where *X* is the radioisotope undergoing α decay (also referred to as the "parent radioisotope"), *Y* is the radioisotope it transforms into (also referred to as the "daughter product"), *Z* is the number of protons, *N* is the number of neutrons, and *A* is the atomic mass (*i.e.,* the number of protons plus the number of neutrons).

The neutron source used in this research is an (α, n) source, where the ^{241}Am is the α-emitting radioisotope and the ^{9}Be is the α-absorbing, neutron-emitting (or (α, n)-absorbing) radioisotope (Section 1.4). Following general equation (3), the decay of ^{241}Am [13] can be represented as:

$$^{241}_{95}Am_{146} \rightarrow \quad ^{237}_{93}Np_{144} \quad + \quad ^{4}_{2}He_{2} \quad + \quad 2e^{-} \qquad (4)$$

The average energy of the α particle released by the decay of ^{241}Am is 5.48 MeV[4] [14] (see also Section 3.1.2.1).

2.1.1.2 Gamma radiation

There are various schemes that result in a nucleus being in an excited state: emission of beta (β) particles (*e.g.,* β^- decay of ^{133}Xe to one of the excited states of ^{133}Cs, which in turn decays by gamma emission to the ^{133}Cs ground state [15]), or absorption of a neutron [16]. Gamma radiation emitted by an excited nucleus as a result of absorption of a neutron is a process known as radiative capture, denoted (n, γ) [16]. The (n, γ) reaction that describes radiative capture is:

$$ {}^{A}_{Z}\Gamma_{N} + n \rightarrow {}^{A+1}_{Z}\Gamma_{N+1} + \gamma \qquad (5) $$

where Γ is the radioisotope absorbing a neutron, n is the interacting free neutron and γ is the emitted gamma ray.

Radiative capture is the process used in the design of the SRGS to produce the gamma radiation, by absorption of the neutrons created via the (α, n) reaction. Three (n, γ) reactions used in this feasibility study are those of ^{149}Sm and ^{155}Gd and ^{157}Gd:

$$ {}^{149}_{62}\mathrm{Sm}_{87} + n \rightarrow {}^{150}_{62}\mathrm{Sm}_{88} + \gamma \qquad (6) $$

$$ {}^{155}_{64}\mathrm{Gd}_{91} + n \rightarrow {}^{156}_{64}\mathrm{Gd}_{92} + \gamma \qquad (7) $$

$$ {}^{157}_{64}\mathrm{Gd}_{91} + n \rightarrow {}^{158}_{64}\mathrm{Gd}_{92} + \gamma \qquad (8) $$

[4] The electron-volt is a unit of energy (1 eV = 1.602×10^{-19} J).

Radiative capture of ^{149}Sm, ^{155}Gd and ^{157}Gd was studied because they have the highest thermal neutron absorption cross-section (*i.e.,* they readily absorb neutrons with energies lower than 0.1 eV and produce gamma rays). The concept of cross-section is discussed in more detail in Section 2.1.2 below.

2.1.2 Interaction of Particles with Matter

As neutrons, gamma rays or α particles travel through a medium, they interact with atoms, resulting in radioactive decay, and/or reactions such as (n, γ), (n, 2n), (n, fission), (α, n), *etc*. The strength of these interactions are described using cross-sections for neutrons and gamma rays, and specific ionization and stopping power for charged particles such as α particles [17].

Let p be the probability of an interaction and N the number of trials. The probability of an interaction does not change from one trial to another. The mean (average) number of interactions, μ, in N trials would be:

$$\mu = Np \qquad (9)$$

The probability of no interactions would be 1 - p, and the probability of no interactions in N trials would be:

$$P(0) = (1-p)^N \qquad (10)$$

which can be written as:

$$P(0) = e^{\ln(1-p)^N} = e^{N\times\ln(1-p)} \qquad (11)$$

A Taylor expansion can be used to re-write $\ln(1-p)$:

$$\ln(1-p) = 0 - p - \frac{1}{2}p^2 - \frac{1}{3}p^3 - \frac{1}{4}p^4 - \frac{1}{5}p^5 \ldots \qquad (12)$$

Because p is very small, then equation (12) can be approximated as:

$$\ln(1-p) \approx -p \qquad (13)$$

and equation (11) becomes

$$\begin{aligned} P(0) &= e^{-Np} \\ &= e^{-\mu} \end{aligned} \qquad (14)$$

where the last form of equation (14) used equation (9). The probability that there will be no interactions depends on the mean number of interactions, μ. Equation (14) may be applied to describe various types of interactions, for each type, μ will define a mean number of interactions with respect to some variable that is case-specific. For example, for radioactive decay, the mean number of interactions will be defined with respect to time. This mean value is called the decay constant, λ, which has units of 1/time, such that, the mean number of interactions for some time t is given by $\lambda \times t$. Hence, for radioactive decay,

$$P(0) = e^{-\mu} = e^{-\lambda t} \qquad (15)$$

If we start with N_0 nuclei in a sample, then the number of nuclei that do not decay will be $N_0 \times P(0)$, resulting in the standard exponential decay equation:

$$N(t) = N_0 \times e^{-\lambda t} \qquad (16)$$

Another example describes the interaction between neutrons and a medium. If neutrons are travelling in some direction x, along which they can interact with nuclei in a target, then the mean number of interactions, μ, can be defined with respect to the length travelled (Σ, also known as the macroscopic cross-section), which has units of 1/length (*i.e.,* 1/cm). Thus, the mean number of interactions for some length x is $\mu = \Sigma \times x$. Hence, for neutrons travelling a distance, x, the probability of not interacting will be:

$$P(0) = e^{-\mu} = e^{-\Sigma x} \qquad (17)$$

If the neutrons are packaged in the form of a flux (neutrons/cm^2-s), I_0, then that portion of the flux, I, that is not lost because of interactions in distance x, will be $I_0 \times P(0)$.

$$\therefore I(x) = I_0 \times e^{-\Sigma x} \qquad (18)$$

The macroscopic cross-section is also defined as $\Sigma = \sigma \times N$, where σ is the microscopic cross-section and N is the total number of atoms in 1 cm^3 volume. The microscopic cross-section represents a measure of the propensity of a neutron (or gamma ray) to interact with an atom. The cross-section is often imagined to be an effective interaction area that the nucleus of an atom in a target medium presents to an incoming neutron (Figure 4) [18].

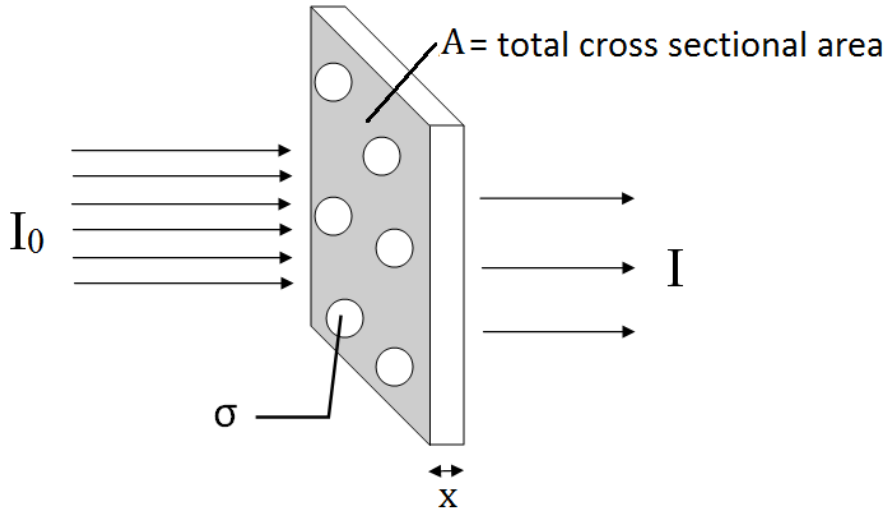

Figure 4 Interaction of a flux of neutrons (neutrons / cm^2-s), I_0, with a material of thickness x (cm). σ represents the "effective area" presented by the medium to the incoming neutrons.

The microscopic cross-section is measured in barns, where 1 barn = 10^{-24} cm^2 [17]. It depends on the type of nuclei present in the target medium, on the energy of the neutron or gamma ray, as well as the type of interaction (*e.g.,* scattering, capture, fission). A neutron can interact with matter in a number of different ways, and each type of interaction is characterized by a specific cross-section: elastic scattering (σ_e), inelastic scattering (σ_i), radiative capture (σ_γ), fission (σ_f). Cross-section values have been evaluated experimentally and published by the National Nuclear Data Center in various databases (or libraries). The library used to perform computational analysis for this research was ENDF/B-VII.0. Figure 5 below illustrates the cross-section values[5] (in barns) evaluated for various incident neutron energies (in eV) for the (n, γ) reactions on ^{149}Sm, ^{155}Gd and ^{157}Gd (Section 2.1.1.2). These isotopes were chosen for this research because their thermal neutron (*i.e.,* energies <0.1 eV) absorption cross-sections are

[5] The cross-section data were plotted using the online tool from the National Nuclear Data Centre, http://www.nndc.bnl.gov/sigma/, Accessed 2015 November 22.

10,000 to 100,000 times larger than those of most other isotopes [19]. In general, the neutron absorption cross-section values for fast neutrons (energies >1 MeV), are significantly lower than those for thermal neutrons. For example, for ^{149}Sm, ^{155}Gd and ^{157}Gd, the cross-section values for fast neutrons are 1,000,000 to 10,000,000 times lower than the values at thermal neutrons (energies <0.1 eV) (see Figure 5). In order to take advantage of the high thermal neutron absorption cross-sections of these isotopes, and increase the probability of neutrons being absorbed and producing gamma radiation, the source neutrons were moderated to thermal energies (see Section 2.1.2.3 for more information on neutron moderation).

The neutron absorption cross-section of isotopes other than ^{149}Sm, ^{155}Gd and ^{157}Gd will be smaller, hence, resulting in a lower gamma flux and gamma dose rate for the investigated SRGS models. Targeting the neutrons resonance region (*i.e.,* energies between 1 eV and 1 MeV) would increase the probability of absorption of neutrons and consequently the production of gammas when compared with that of fast neutrons, however, the neutron resonance cross-sections will be at least 100 times lower than the thermal absorption cross-sections (see Figure 5 for an example).

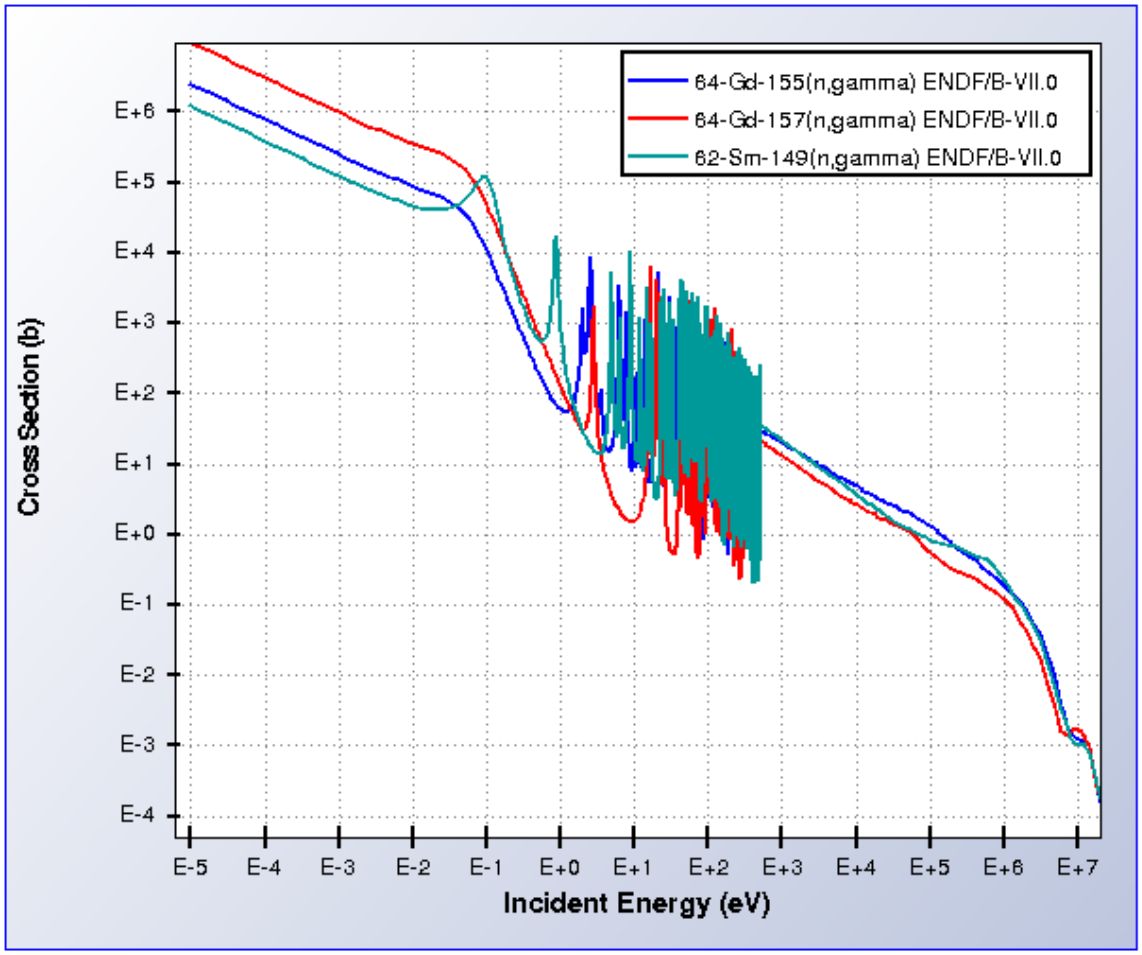

Figure 5 Cross-section data for (n, γ) reaction on ^{149}Sm, ^{155}Gd and ^{157}Gd

2.1.2.1 Alpha Particles

Alpha particles were used in this research to produce the neutrons via (α, n) reactions. The range of the α particle limits the design of the neutron source, because it leads to constraints on the separation between the α-emitting plate and the α-absorbing, neutron-emitting plate (see Section 3.1). Alpha particles are the least penetrating type of radiation. They are double positively charged ions, with high mass and high initial energies (typically between 3 MeV - 7 MeV [20]), hence, they have high momentum.

Because of their high relative momentum, they do not undergo significant deflection when they interact with atomic electrons [17]. Their penetration range (*i.e.,* their ability to move through matter) is very small, and even a thin layer of paper or the dead layer of human skin is sufficient to stop α radiation [12]. The range of an alpha particle is defined as the point at which it stops and captures electrons to form a helium atom with no net charge [17]. The range depends on the initial kinetic energy of the particle and on the type of material it travels through. Ranges for α particles travelling in any medium can be estimated based on their range in air, using the Bragg-Kleeman equation [17]:

$$R = R_a\left(\frac{\rho_a}{\rho}\right)\sqrt{\frac{M}{M_a}} = 3.2\times10^{-4}\,\frac{\sqrt{M}}{\rho}\,R_a \qquad (19)$$

where R is the range in the material of interest, ρ is the density of the material, M is the atomic weight of the material, ρ_a is the density of air (1.23×10^{-3} g/cm^3, at 15 °C and 1 atm), M_a is the average atomic weight of air (14.9 u, at 15 °C and 1 atm), R_a is the range in air. The range for α particles in air at 15 °C and 1 atm can be approximated as follows [12]:

$$R_a = \begin{cases} 0.56\times E & \text{for} \quad E < 4\ \text{MeV} \\ \\ 1.24\times E - 2.62 & \text{for} \quad 4 < E < 8\ \text{MeV} \end{cases} \qquad (20)$$

where E is the energy of the α particle in MeV. For an α particle with an energy of 5.48 MeV such as that originating from the decay of ^{241}Am, which was used for the (α, n) source in this feasibility study, the range in air is 4.2 cm [17].

The range of alpha particles in the ^{241}Am-^{9}Be neutron source was estimated to be 2.17×10^{-3} cm, using equation (19), with M = 9.01218 u, ρ = 1.85 g/cm^3 and R_a = 4.2 cm

(calculated using equation (20)). This range is small, which limits the required separation between the alpha emitter and the (α, n)-absorber (Section 3.1).

2.1.2.2 Gamma Rays

Gamma rays originating from a source interact with atomic electrons in the different media surrounding the source, being either absorbed or attenuated [17]. The three main methods through which gamma rays interact with matter are [17]:

- *photoelectric effect*

  In the photoelectric effect, the gamma ray interacts with an electron of an atom, disappearing because the gamma ray transfers its energy to the electron, as the electron is knocked out of its orbit. The vacant electron location is then filled by an outer shell electron, resulting in secondary emissions of x-rays, as the outer electron transitions to fill this vacancy. The photoelectric effect is one of the gamma interactions by which a gamma camera used for SPECT imaging detects gamma radiation originating from the SRGS or a radiopharmaceutical injected in a patient (Section 2.2.1).

- *pair production*

  In pair production, the gamma ray with a minimum energy of 1.02 MeV (see Appendix B.1 for calculation) disappears in the strong electric field of a nucleus, resulting in a positron-electron pair being produced [17].

- *Compton scattering*

  Compton scattering (or Compton effect) is the process through which a gamma ray interacts with an electron of an atom, by scattering. In this type of interaction,

the γ-ray does not disappear, and it continues to travel through and interact with the surrounding material. Eventually, as it loses energy through scattering, the γ-ray will disappear via one of the other two methods (*i.e.*, photoelectric effect or pair-production). Compton scattering is important for this research because γ radiation produced by the SRGS will have a range of energies, and will interact with the surrounding media, potentially scattering away from the air regions where the gamma camera would be located (see Section 1.4, Figure 2).

2.1.2.3 Neutron Moderation

Neutrons produced via (α, n) reactions have a wide energy spectrum, from a few eV up to as high as 11 MeV, thus, to take advantage of the high absorption cross-section of materials such as Sm or Gd at low energies, the neutrons need to be thermalized (see Section 2.1.2). Neutrons are uncharged particles that interact with matter through different processes: elastic scattering, inelastic scattering, or absorption by surrounding atoms, leading to various types of nuclear reactions such as (n, γ), (n, α), (n, xn[6]), (n, p[7]), (n, f[8]) [21]. Fast neutrons, *i.e.,* neutrons that have energies of several MeV, interact with surrounding atoms primarily via elastic scattering, resulting in a neutron energy decrease with every interaction. This process is known as "neutron moderation" [21]. As the neutron energy decreases, the likelihood of the neutron being absorbed by surrounding

[6] (n, xn) reaction where one neutron interacts with the parent radioisotope resulting in a daughter product and 2 or 3 neutrons being emitted. It could also refer to an (n, n) interaction, which represents elastic scattering.
[7] (n, p) reaction where one neutron interacts with the parent radioisotope resulting in a daughter product and one proton (p).
[8] (n, f) reaction where one neutron interacts with the parent radioisotope resulting in a fission (f) reaction.

atoms increases [21], *i.e.,* the absorption cross-section is higher for thermal (or slow) neutrons (<0.1 eV) (see Section 2.1.2, Figure 5).

Two factors were considered to determine the moderating material used in this research:

1) the logarithm of the fractional energy loss per collision, and
2) neutron absorption.

The logarithm of the fractional energy loss when a neutron collides with a nuclide of atomic mass A is known as the "logarithmic energy decrement", and is defined as [22]:

$$\xi = 1 + \frac{\alpha}{1-\alpha}\ln\alpha \qquad (21)$$

where ξ is the logarithmic energy decrement per collision, and α is defined as

$$\alpha = \frac{(A-1)^2}{(A+1)^2} \qquad (22)$$

These equations show that the energy decrement (*i.e.,* the fraction of energy lost by the neutron with every collision) is independent of the energy of the neutron, but it is dependent on the atomic mass of the interacting medium [22]. For example, using equation (22), the value of α for hydrogen is equal to 0.000, for deuterium it is equal to 0.113, and for beryllium it is equal to 0.640. Consequently, the ξ values for hydrogen, deuterium and beryllium are 1.000, 0.722, and 0.206, respectively (see Table 1). Thus, as the atomic mass increases, the value of α increases, and the logarithmic energy decrement decreases. This shows that lighter atoms are better at causing the neutron to lose energy during a collision, hence making them better moderators.

The total number of collisions (n) required to bring a neutron from initial energy E_0 to final energy E [22] can be estimated using:

$$n = \frac{1}{\xi}\ln\left(\frac{E_0}{E}\right) \qquad (23)$$

Table 1 summarizes the logarithmic energy decrement and the number of collisions calculated for different nuclides. The initial neutron energy is assumed to be 4 MeV (approximately the average neutron energy for the neutrons produced by the neutron source used in this study - see Section 3.1.2.1, Figure 8) and the final energy is assumed to be 0.1 eV (*i.e.,* the upper boundary for the thermal neutron energy range). Table 1 shows that the heavier the nuclide, the higher the number of collisions required to thermalize neutrons and, thus, the less effective the nuclide is at slowing down neutrons.

Table 1 Calculated logarithmic energy decrement and total number of collisions required to slow down a neutron from 4 MeV to 0.1 eV for various nuclides

Nuclide	A (g/mol)	α	ξ	n (# collisions)
H	1.00794 [14]	0.000	1.000	18
D	2.01410 [14]	0.113	0.722	24
Be	9.01218 [14]	0.640	0.206	85
C	12.01070 [14]	0.716	0.158	111
O	15.99940 [14]	0.779	0.120	146

Neutron absorption was the second factor that influenced the choice of moderator. The logarithmic energy decrement and the number of collisions provide information on the effectiveness of atoms to slow down neutrons (*i.e.,* moderate), however, the neutrons must survive the collision (*i.e.,* the absorption probability should be low) for the moderator to be effective [20][23]. When a neutron interacts with an atom, it can scatter or be absorbed, depending on the microscopic cross-section for the particular reactions

(Section 2.1.2). An effective moderator would decrease the energy of neutrons without absorbing them; this is described using the "moderating ratio":

$$\text{moderating ratio} = \xi \frac{\Sigma_s}{\Sigma_a} \qquad (24)$$

where Σ_s is the total macroscopic scattering cross-section, and Σ_a is the total macroscopic absorption cross-section. The macroscopic cross-sections for mixtures are defined using:

$$\Sigma = \sum_{i=1}^{m} N_i \sigma_i \qquad (25)$$

where Σ is the macroscopic cross-section, N_i is the number density of isotope i, and σ_i is the microscopic cross-section for isotope i.

Three moderating materials have been investigated for the proposed SRGS to determine its feasibility as a SPECT gamma camera calibration flood source or as a blood irradiator: deuterated polyethylene (CD_2), heavy water (D_2O), and high density polyethylene (CH_2, referred to as HDPE) (see Section 1.4). Table 2 summarizes the thermal energy spectrum-averaged microscopic cross-sections for the atoms in these moderators, obtained from reference [23]. Deuterium, carbon and oxygen have lower thermal neutron absorption cross-sections than hydrogen, resulting in higher moderating ratios for CD_2 and D_2O than for H_2O and CH_2. The calculated moderating ratios for CD_2, D_2O, H_2O and CH_2 are summarized in Table 3. These values show that fewer neutrons are lost by absorption when the moderator is D_2O or CD_2 than H_2O or CH_2, hence, making these two deuterium-based moderators better in terms of neutron economy. For this reason, D_2O and CD_2 were chosen for this feasibility study. For comparison, HDPE, a hydrogen-based moderating material, was also investigated.

Table 2 Energy spectrum-averaged microscopic absorption cross-sections and scattering cross-sections for thermal neutrons

Nuclide	σ_a (barns)	σ_s (barns)
H	0.29	20.5
D	0.0005	3.4
C	0.003	4.7
O	0.0002	3.8

Table 3 D_2O, H_2O, CH_2 and CD_2 moderating ratios and calculated macroscopic absorption cross-section and scattering cross-sections

Material	ξ	Moderating Ratio	Σ_s	Σ_a
H_2O	0.925	71	1.4961	0.0194
CH_2 (or HDPE)	0.913	72	1.9052	0.0243
D_2O	0.508	4487	0.3522	0.00004
CD_2	0.491	906	0.2325	0.00013

2.2 Background Information on Applications of Interest for the Gamma Source

2.2.1 Medical Imaging and the History of SPECT

Nuclear imaging is used to investigate the biological function of tissues and organs by detecting ionizing radiation originating from the area being investigated. The two methods used to investigate physiological processes such as blood flow through the heart, brain function, or lung capacity [24][25][26], are Positron Emission Tomography (PET) and Single Photon Emission Computed Tomography (SPECT). Both methods are based on measuring gamma radiation.

In the case of SPECT, current medical imaging procedures use a gamma emitting radioisotope bound to a pharmaceutical drug to form a compound that is also known as a radiopharmaceutical, which is injected into the bloodstream. Depending on the pharmaceutical drug used, the radiopharmaceutical will target a specific organ or tissue. When injected into the body, the drug is selectively taken-up by the targeted tissue or

organ. As the radioisotope decays, it emits gammas of known energy (*e.g.,* ^{99m}Tc, decays with a gamma of 140.5 keV energy). Recently published work also investigated the possibility of a neutron-activated SPECT (nSPECT) imaging technique [27]. In nSPECT, patients would be injected with a stable, neutron-absorbing isotope that would then be activated using a high-output electric neutron source attached to the SPECT imaging system. The proposed system would produce information similar to the current SPECT procedure, but allow the medical staff to control the radiation dose given to patients [27].

In the case of PET, a positron emitting radioisotope is injected in the bloodstream. As this radioisotope decays, it emits a positron that travels only a very short distance (<5 millimeters [28]) in the tissue before it annihilates with an electron producing two equal energy gammas (511 keV) travelling 180° away from each other. This annihilation process is the opposite of pair production (Section 2.1.2.2).

Single Photon Emission Computed Tomography (SPECT) dates back to the 1960s and the seminal emission tomography experiments carried out by Dr. David Kuhl and Roy Edwards, and the groundbreaking invention of the Anger scintillation camera [29]. Nowadays, SPECT imaging is widely applied because of its high image accuracy and fast response for image rendering.

Gamma cameras are, and continue to be, the most widely used nuclear imaging devices [3][4]. They have been extensively utilized to investigate neurological diseases such as Alzheimer's, brain function and blood flow, diagnose heart ailments and cancers, and examine lung capacity [24][25][26][30]. To ensure that these devices are performing according to specifications, are providing reliable results, and their performance is not

significantly changing over time, a set of quality control (QC) tests is required. These tests include system uniformity and spatial resolution tests; some of these tests being performed on a daily basis, before any patient procedures are carried out [3][31][32].

System uniformity tests are intended to check the ability of the gamma camera to reproduce a consistent image when it is exposed to a uniform flux of gamma radiation. Spatial resolution tests are intended to check the ability of the gamma camera to distinguish between two very closely spaced objects [32]. Calibration tests can be either intrinsic (*i.e.,* the collimator is not present) or extrinsic (*i.e.,* with a collimator), and they are performed by "flooding" the gamma camera with a uniform gamma flux (γ/cm^2-s) from a solid disk of ^{57}Co [32]. Current ^{57}Co sources are designed as flat, rectangular or circular sheets of ^{57}Co, with activities of 5, 10, 15 or 20 mCi (185 - 740 MBq) [33][34]. They come in multiple sizes (*e.g.,* 40 cm × 40 cm, 60 cm × 40 cm) and they are designed to cover the entire surface area of the gamma camera. The ^{57}Co source gives off gamma radiation with main energies of 122 keV (85.6%) and 136 keV (10.7%), which are very close to the gamma energy emitted by the main radionuclide used for clinical applications, *i.e.,* ^{99m}Tc (140.5 keV) [14]. Uniformity tests should be performed with a gamma energy similar to that used during patient procedures, in order to ensure that the pulse height setting is correctly calibrated for the intended application [32]. When calibration tests are performed with gamma energies other than those of the radioisotope used during the medical procedures, the user must ensure that the correction factors applied to calibrate the gamma camera are acceptable for the clinical procedures [32]. Using a similar gamma energy spectrum during the calibration procedure would ensure that the camera and photomultiplier tubes are seeing the appropriate energy peak for the

intended application (*e.g.,* 140.5 keV for ^{99m}Tc) and are producing a uniform image. Gamma cameras are sensitive to the small amounts of ^{56}Co and ^{58}Co that can be found as impurities in the ^{57}Co flood sources, resulting in non-uniformity patterns being observed in the acquired images because of the high count rate in the detector [35]. This high count rate is caused by the broad tail of high energy photons (>500 keV) emitted by ^{56}Co and ^{58}Co and is increased in the central part of the field-of-view compared with the useful field-of-view [35]. The half-lives of ^{56}Co (78.8 days) and ^{58}Co (70.8 days) are shorter than the half-life of ^{57}Co (271 days), hence, as the flood source ages, and the impurities decay, experimental data show improvements in the flood-field uniformity image obtained [35]. Thus, the gamma energy spectrum of the proposed SRGS needs to be considered in this research.

2.2.2 Blood Irradiators

Blood irradiators are self-contained units that contain x-rays sources [36], or radioactive sources such as ^{137}Cs and ^{60}Co [5][37]. The decay of ^{137}Cs produces gamma rays with an energy of 662 keV (with a probability of 94.4% per decay) [5], and that of ^{60}Co produces two gamma rays with energies of 1.173 MeV (99.88%) and 1.333 MeV (100%) (with approximately equal probability per decay) [5][14]. Blood irradiators are primarily used to prevent a rare but deadly complication that can result from blood transfusions, known as "transfusion associated graft-versus-host-disease" (TA-GVHD) [37][38]. This disease, although arising in less than 1% of patients undergoing blood transfusions, is deadly for those who develop it and can be prevented entirely by the irradiation of blood with gamma radiation [38]. A radiation dose between 20 - 40 Gy

[5][39] must be administered to the blood bags in order for such a process to be effective. The currently "recommended dose for blood irradiation in the United States is 25 Gy delivered to the midplane of the blood container" and a minimum of 15 Gy anywhere else in the container [5].

T-cells are primarily responsible for TA-GVHD because they have the ability to divide and multiply, resulting in a potential immune response in the host body [5]. Treating the T-cells in the donated blood with high doses of gamma radiation destroys their genetic DNA, preventing them from replicating and triggering the immune response. Loss of cell function or damage of the blood cell is not expected to occur as long as the total doses are lower than 50 Gy [37][40], although the doses deposited by the gamma blood irradiator are high (5 - 10 times higher than the LD_{50}[9] [21]). The effect of the gamma radiation on other cells such as red blood cells or platelets is minimal because these cells do not have the genetic material needed for cell replication. Damage to the mitochondrial DNA in the platelets does not prevent them from performing their intended function (*i.e.,* prevent bleeding by supporting blood clotting) [5].

2.3 An Introduction to Monte Carlo Method and the MCNP Computer Code

The Monte Carlo method is a type of algorithm developed to solve mathematical problems using probabilities and probability theory. This algorithm predicts the mean behaviour of a system by performing a large number of random trials that simulate the events responsible for that behaviour [41]. In the eighteenth and nineteenth centuries, this method was used to perform simulations to provide confirmation of mathematical

[9] A 4 Gy acute gamma dose to the whole-body, without treatment, is fatal in 50% of the exposed individuals. This value is called the lethal dose in 50% of the population exposed, or LD_{50}.

functions and corroborate theoretical results [41][42]. For example, the method was used in the "Buffon's needle" experiment to estimate the value of π by randomly throwing identical needles onto a lined background [42].

The modern Monte Carlo algorithm has been developed from the nuclear weapons work of Fermi, von Neumann and Ulam at Los Alamos National Laboratory during World War II [8][41][42]. This algorithm has been used to solve complex problems that are analytically difficult, and require numerous assumptions and simplifications for a deterministic solution. It involves sampling probability density functions that define the modelled system, and performing simulations for a large number of trials, leading to estimates of the expected mean values for variables that characterize the system.

Radiation transport and its interaction with matter is one application of the Monte Carlo method. For example, consider an isotropic source of neutrons, and assume that the neutrons are emitted in a random direction, one at a time [42]. As they travel through the medium surrounding the source, the neutrons interact with atoms, undergoing either scattering or absorption [42]. The length that each neutron travels in a random direction before it collides with an atom is called the track length, and it is proportional to the effective mean free path of the particle or $1/\Sigma_{total}$, where Σ_{total} is the total macroscopic cross-section in units of 1/cm.

The Monte Carlo method uses a sequence of random numbers uniformly distributed between 0 and 1 to mirror the experimentally observed distribution of neutron track lengths [8][41], which follow the probability density function: $P(0) = e^{-\Sigma_{total} x}$ (equation (17), Section 2.1.2). After the distance to the next collision is calculated (*i.e.,*

the track length), a decision is made on the type of interaction the neutron will experience. This decision is based on the cross-section value associated with each event (*i.e.,* σ_s or σ_a[10], see Section 2.1.2) and generated random numbers. If this event is scattering, then the probabilistic decision depends on the scattering cross-section as a function of the scattering angle; if the event is neutron absorption, the neutron is absorbed (or "killed") [42]. This random neutron "walk" algorithm is performed until the neutron is either absorbed or it reaches the outer boundary of the system [8][42]. Tracking a large number of neutrons using this algorithm results in an appropriate representation of the simulated system.

2.3.1 The MCNP Computer Code

Monte Carlo N-Particle (MCNP) is a probabilistic computer code, developed based on the Monte Carlo method presented above. It is currently applied to a wide range of applications, from reactor physics and shielding calculations, to dose calculations for biomedical and radiological applications, space shielding analysis, and aerospace applications [8]. The code has been validated for various applications based on published benchmark data, to ensure it produces accurate results [43]. In MCNP, the user can model any general three-dimensional geometry and track the interaction of neutrons, photons and electrons (or coupled neutron-photon-electron) with matter. These interactions include elastic and inelastic scattering, absorption or fission, and are parameterized with cross-sections (see Section 2.1.2).

[10] σ_s = scattering cross-section; σ_a = absorption cross-section.

MCNP is recommended for complex three-dimensional problems, when solving the neutron transport equation directly cannot be accomplished without making simplifying assumptions and approximations. MCNP simulates the behaviour of particles in the modelled environment by sampling transport probability density functions and the reaction cross-sections over a large number of particle "histories", to reach an acceptable accuracy (*i.e.,* relative uncertainties in the calculated results lower than 10% [8]). In MCNP, a particle such as a neutron is tracked from the point of birth (*i.e.,* the source) to the point of death (*i.e.,* when the particle is absorbed, or escapes) [8], which defines the particle history. An example of a random history of a source neutron, representative of the cases modelled in this feasibility study is illustrated in Figure 6 below. For a history, MCNP first produces a pseudo-random number sequence which will be used to define all the processes the neutron will undergo from birth to death [8]. The energy of the neutron, and the "direction of flight" [8] are determined based on a random number from the generated sequence, and the user-definition provided using the source routine SDEF. The track length of the neutron with the chosen energy and direction is calculated using another random number, as described in Section 2.3. Two situations may present once the track length is calculated:

- If this track length is equal to or greater than the distance to the surface that the neutron is heading towards, the neutron is transported to that surface, surface tallies (if specified) are calculated, and then it is processed to cross into the next cell (*i.e.*, a new track length is calculated based on the new medium properties) [8].

- If the track length is less than the distance to the surface, then the neutron will undergo an interaction with a nucleus in the medium. Based on a random number and the macroscopic cross-section for each nuclide in the medium, the collision nuclide is identified. In processing the collision between the neutron and the chosen nuclide, MCNP also takes into consideration the thermal motion of the atom [8]. The type of collision is randomly determined based on cross-section values for different reactions (*e.g.,* (n, xn), (n, p), (n, γ) - see Section 2.1.2.3). Subsequently, the new neutron energy and direction are determined, and the process is repeated until the particle is killed.

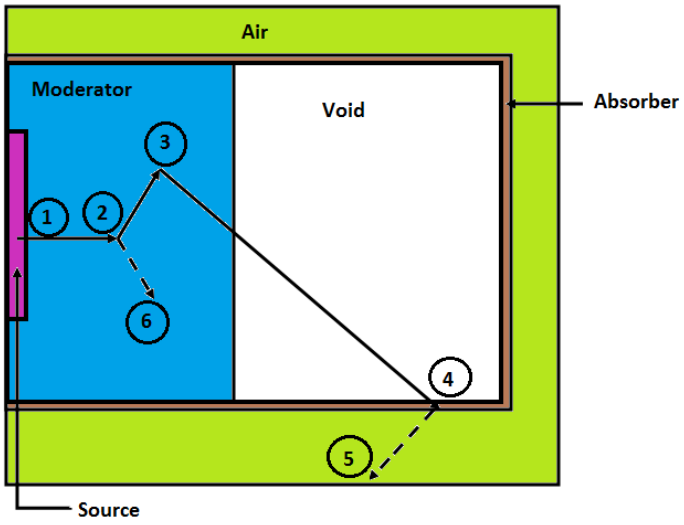

Figure 6 Neutron history illustration (1/2 of the modelled gamma source). 1) Neutron originating from the ^{241}Am-^{9}Be source; 2) Neutron scattering off the moderator and gamma production; 3) Neutron scattering; 4) Neutron absorption and gamma production; 5) gamma leakage; 6) gamma capture

In MCNP, the user models the geometry by defining various "cells", which are bound by simple surfaces such as planes, cylinders, or spheres. A cell is defined by the intersection or union of surfaces that represent the outer boundary of the region where a

specific material is found. For example, in Figure 6, the absorber region is one cell, surrounded by the air region as another cell. The materials can be specified based on their isotopic compositions either by mass% (also referred to as wt% in this thesis), or as atom density of each isotope in the material. In the MCNP simulations performed for this research, material compositions were defined based on wt%. The user defines which continuous-energy cross-section data library the code will use to calculate the reaction cross-sections. This leads to modelled particle behaviour that is closer to that of the physical system since it eliminates the need for interpolation between discrete cross-section values, as is the case with a multi-group data library. The neutron cross-section data library used throughout the current research was the ENDF/B-VII.0 library and the gamma cross-section data library used was mcplib04 [8]. The models were run on a cluster which uses the Red Hat Enterprise Linux server 5.5 on 20 nodes, each node with dual Intel Xeon L5640 CPUs and 96 GB RAM. Each model was run using 8 CPUs in parallel and 100 million histories, which translated into a computational time of 6-8 hours. Examples of MCNP input files are provided in Appendix D.1 and Appendix D.2.

An MCNP simulation only provides the results (*e.g.,* current, flux, energy deposition) that the user requests by specifying the desired type of output tally. The code provides seven standard tally types, which can be modified by the user in different ways to provide the desired output information from a modelled system [8]. The two tallies that were used to calculate average neutron and gamma fluxes, dose rates and energy deposition were the "F4 tally" and the "F6 tally".

The flux tally (F4) produced average flux results in a user-specified cell, in units of particles per unit area per source particle, in this case a source neutron. The average flux was calculated using MCNP, by solving the following equation [8]:

$$\overline{\phi_V} = \frac{1}{V}\int dE \int dt \int dV \int d\Omega \Psi(\vec{r}, \hat{\Omega}, E, t) \qquad (26)$$

where $\overline{\phi_V}$ is the average flux in a cell of volume V, which is the volume in cm^3 calculated by the code for the tallied cell, Ψ is the angular flux in units of particles/cm^2/sh/MeV per steradian (1 sh = 10^{-8} s).

The F4 tally was also modified in the MCNP models, by specifying flux-to-dose conversion factors for both neutrons and gammas, to calculate the dose rates in rem/h or Sv/h (100 rem/h = 1 Sv/h). These flux-to-dose conversion factors, taken from the MCNP manual [8], and published in ICRP-21, are summarized in Table 4. These factors account for the conversion between flux to absorbed dose rate in Gy/h and from absorbed dose rate to equivalent dose rate in rem/h.

The dose deposition tally (F6) was the second type of standard tally that was used. This tally output the energy deposited in the tallied volume, in MeV/g. The energy deposited, $H(t)$, is calculated using MCNP by solving the following equation [8]:

$$H(t) = \frac{\rho_a}{m}\int dE \int dt \int dV \int d\Omega \sigma_t(E) H(E) \Psi(\vec{r}, \hat{\Omega}, E, t) \qquad (27)$$

where ρ_a is the atom density in atoms/barn-cm, m is the cell mass in grams, $\sigma_t(E)$ is the microscopic total cross-section in barns, *H(E)* is the heating number in MeV/collision, and Ψ is the angular flux in units of particles/cm^2/sh/MeV per steradian (1 sh = 10^{-8} s).

This calculated energy deposited value was then be converted to Gy/h as follows:

$$\text{Dose rate}\left(\frac{\text{Gy}}{\text{h}}\right) = E_{dep}\left(\frac{\frac{\text{MeV}}{\text{g}}}{\text{source neutron}}\right) \times \text{source strength}\left(\frac{\text{n}}{\text{s}}\right) \times 10^{6}\left(\frac{\text{eV}}{\text{MeV}}\right) \times 10^{3}\left(\frac{\text{g}}{\text{kg}}\right)$$
$$\times 1.602 \times 10^{-19}\left(\frac{\text{J}}{\text{eV}}\right) \times 3600\left(\frac{\text{s}}{\text{h}}\right) \qquad (28)$$

where E_{dep} is the energy deposited calculated using the F6 tally in MeV/g/source neutron, 1 eV = 1.602×10^{-19}J, and 1 Gy = 1 J/kg.

Table 4 Flux-to-Dose Conversion Factors Applied in MCNP to Calculate Neutron and Gamma Dose Rates (Values Summarized from MCNP Manual [8])

Energy (MeV)	Flux-to-dose factor for neutrons [(rem/h)/unit flux][11]	Energy (MeV)	Flux-to-dose factors for gammas [(rem/h)/unit flux]
2.5E-8	3.85E-6	0.01	2.78E-6
1.0E-7	4.17E-6	0.015	1.11E-6
1.0E-6	4.55E-6	0.02	5.88E-7
1.0E-5	4.35E-6	0.03	2.56E-7
1.0E-4	4.17E-6	0.04	1.56E-7
1.0E-3	3.70E-6	0.05	1.20E-7
1.0E-2	3.57E-6	0.06	1.11E-7
1.0E-1	2.08E-5	0.08	1.20E-7
5.0E-1	7.14E-5	0.1	1.47E-7
1.0	1.18E-4	0.15	2.38E-7
2.0	1.43E-4	0.2	3.45E-7
5.0	1.47E-4	0.3	5.56E-7
10.0	1.47E-4	0.4	7.69E-7
20.0	1.54E-4	0.5	9.09E-7
		0.6	1.14E-6
		0.8	1.47E-6
		1.0	1.79E-6
		1.5	2.44E-6
		2.0	3.03E-6
		3.0	4.00E-6
		4.0	4.76E-6
		5.0	5.56E-6
		6.0	6.25E-6
		8.0	7.69E-6
		10.0	9.09E-6

[11] Note: MCNP flux-to-dose conversion factors are defined in rem/h/unit flux, instead of using the SI unit, Sv (100 rem/h = 1 Sv/h).

2.4 SOURCES-4C Computer Code and Its Application to This Research

SOURCES-4C was used to model the ^{241}Am-^{9}Be (α, n) reaction and calculate the source strength for the neutron source investigated in this research [44][45]. The modelled system was represented by a slab of radioisotopes emitting α particles (*i.e.,* ^{241}Am, α particle energy 5.48 MeV) in close contact with a low-Z target material (*i.e.,* ^{9}Be) [45] (see Section 3.1.1 and Section 3.1.2.1). The α particles started in the α-emitting region, crossed the boundary between the two regions and were slowed down (or attenuated) and absorbed by the low-Z material, resulting in production of neutrons via the (α, n) reaction. The estimated range for α particles originating from ^{241}Am was calculated to be 2.14×10^{-3} cm (Section 2.1.2.1), while the plate of ^{9}Be modelled in this study was 0.5 cm, which is 233 times larger than the range of the α particles. Thus, the thickness of the plate is much larger than the range of the alpha particles emitted by the source, which is consistent with the methodology implemented in SOURCES-4C [45].

The input file for SOURCES-4C is described in Appendix D.3 and it contained:

- Material information (*e.g.,* nuclide types and their weight percentages) for both α-emitting (^{241}Am) and α-absorbing, neutron-emitting (^{9}Be) regions.
- The type of stopping cross-sections that the code would use (*i.e.,* cross-sections for material in a solid form).

- The α particle energy groups[12] used at the interface between the α-emitting and the α-absorbing, neutron-emitting materials (*e.g.,* 52-groups linearly interpolated between 0.00001 MeV to 6.5 MeV).
- The neutron source energy group structure used to produce the neutron source output information. For the current application, 210-energy groups were used, linearly interpolated between 0 MeV and 11 MeV.

The SOURCES-4C computer code package included data libraries containing information on evaluated nuclides α decay spectra, evaluated (α, n) cross-sections and branching fractions (*i.e.,* the fraction of α decays of the radioisotope with respect to all the different decay modes of that particular radioisotope), and α stopping cross-sections [45].

The methodology implemented in the code made use of the data libraries provided with the installation package to calculate the rate at which α particles pass through the interface between the α-emitter and the α-absorber, neutron-emitter [45]. This rate of α particles passing through the interface was calculated by SOURCES-4C by solving:

$$\Phi^{g} = \frac{\lambda_k f_{kl}^{\alpha}}{4} \frac{N_k}{N} \int_{E_g}^{E_{g+1}} \frac{dE}{\varepsilon(E)} \qquad (29)$$

where Φ^{g} is the rate of α particles with energies between E_g and E_{g+1} passing through unit area of low-Z material, λ_k is the decay constant for nuclide k in the source, N_k is the atom

[12] A group is defined by a lower energy bound and an upper energy bound, between which the parameters describing the modelled problem (*e.g.,* cross-section or average energy) are constant. The specific methodology implemented in SOURCES-4C assumed a beam of α particles between the upper and lower energy bounds (*i.e.,* $E_{beam} = (E_g + E_{g+1})/2$, where E_g was the lower bound and E_{g+1} is the upper energy bound).

density of nuclide k in the source, N is the total atom density of the material, f^{α}_{kl} is the fraction of all decays of nuclide k that led to an alpha particle with an energy of E_{kl}, $\varepsilon(E)$ is the stopping cross-section [45].

As the α particles move through the absorber, they are absorbed by the low-Z material, producing neutrons. The α rate, Φ^{g}, thereby was decreased in accord with stopping cross-sections and reaction rates provided in the data libraries. Subsequently, the neutron population was calculated in each of the 210-energy groups specified by the user, as well as the total neutron flux, in neutrons/cm^2-s. The data libraries used by the code have been verified and benchmarked against experimental data [46]. The neutron flux calculated for the modelled ^{241}Am-^{9}Be source was 1.30×10^4 n/cm^2-s. The application of this source strength to the SRGS is discussed in Section 3.1.2.1.

3 Chapter: Methodology

3.1 General Information on the Neutron Source

The neutron source was the "heart" of the proposed design. The principle behind the neutron source was an (α, n) reaction that could be mechanically turned "ON" and "OFF" by the user, on demand. The feasibility of switchable radioactive neutron sources (or SRNS) has been shown at both Argonne National Laboratory [47][48] and at Sandia National Laboratories [49]. The work discussed in the current research built on the work published on switchable neutron sources and investigated the feasibility of a "switchable radioactive gamma source" (SRGS). The basic idea was to produce neutrons via an (α, n) reaction that could be mechanically turned ON and OFF by the user, and then moderate the fast neutrons (*i.e.,* energies > 1 MeV) to thermal energies (*i.e.,* < 0.1 eV) to increase their probability of being absorbed by radioisotopes that would make gamma radiation via (n, γ) reactions (Section 1.4 and Section 2.1.2, Figure 5).

Two different neutron source dimensions were investigated for this study: a 40 cm × 40 cm (referred to as the "large source") and a 6 cm × 6 cm (referred to as the "small source"). (Note: source dimensions are specified in the y- and z-directions, Figure 1, Section 1.4.). The 40 cm × 40 cm neutron source was chosen because its dimensions were similar to those of ^{57}Co flood sources that cover the entire surface area of a standard SPECT gamma camera [6] (see also Section 2.2.1). The smaller 6 cm × 6 cm neutron source feeds a 10.4 cm × 10.4 cm[13] gamma source to effectively

[13] This dimension was calculated as follows: 6 cm × 6 cm neutron source, 0.1 cm thick Zircaloy-2 container (Section 3.1.2.2) and 1.9 cm thick moderator on the y- and z-directions (Figure 8 and Section 4.2.2) and 0.2 cm thick Zircaloy-2 container around the moderator.

cover a quarter of the gamma camera, resulting in a design that would save on the cost of the (α, n)- and (n, γ)-absorbing materials, the α-emitter and the moderator required for the SRGS (see also Section 4.1.1). The SRGS was modelled as a planar, rectangular source, similar in design to the ^{57}Co flood sources (see Section 1.4).

The neutron source may be activated by mechanically bringing together two plates, one containing the α-emitter and one containing the (α, n)-absorber. The mechanism used to actuate the plates and bring them into contact was not considered nor is it discussed in this thesis. The designs for the plates are presented in Section 3.1.1. The neutron source was modelled in MCNP as an isotropic source with the neutron energy distribution corresponding to the neutron spectrum obtained from the ^{241}Am(α, n)^{9}Be reaction (see Section 3.1.2.1 for discussion on the choice of isotopes and the neutron spectrum).

3.1.1 Potential Design of the Plate Configuration for the Neutron Source

For the (α, n) reaction to be turned "ON" and "OFF" as needed, the user must be able to separate the α-emitter from the (α, n)-absorber. In a homogeneous mixture, the (α, n)-absorbing isotope surrounds the α-emitter so that each α particle produced by decay of an α-emitting radioisotope has equal probability of being captured by an (α, n)-absorbing material, thus resulting in the highest neutron flux. This is not true for lower symmetry (*e.g.,* plated) sources, for which the overall neutron production would be lower. However, such a homogeneous system that can be separated and reassembled mechanically, at the switch of a button, has not been demonstrated.

For the current research, the α-emitter and the α-absorber were non-homogeneously distributed and occupied two distinct opposing planar regions (see Figure 7). This design took advantage of the mechanical SRNS built by Argonne National Laboratory [47][48] and Sandia National Laboratories [49]. The α-emitting isotope would be plated, painted or sprayed on a plate of low neutron-absorbing material (*e.g.,* Zircaloy-2) and the (α, n)-absorber would be positioned on another plate that can be brought into contact with the α-emitter mechanically, at the switch of a button.

For the pattern illustrated in Figure 7A, the user can turn ON and OFF the neutron source by moving the plates in a direction normal to the planes. With the checkerboard pattern (Figure 7B) the plates would be moved parallel to the interface. Figure 7C illustrates how the neutron source strength may be increased by stacking plates in parallel, because α particles travelling away from one α-absorbing plate will be captured by other α-absorbing plate.

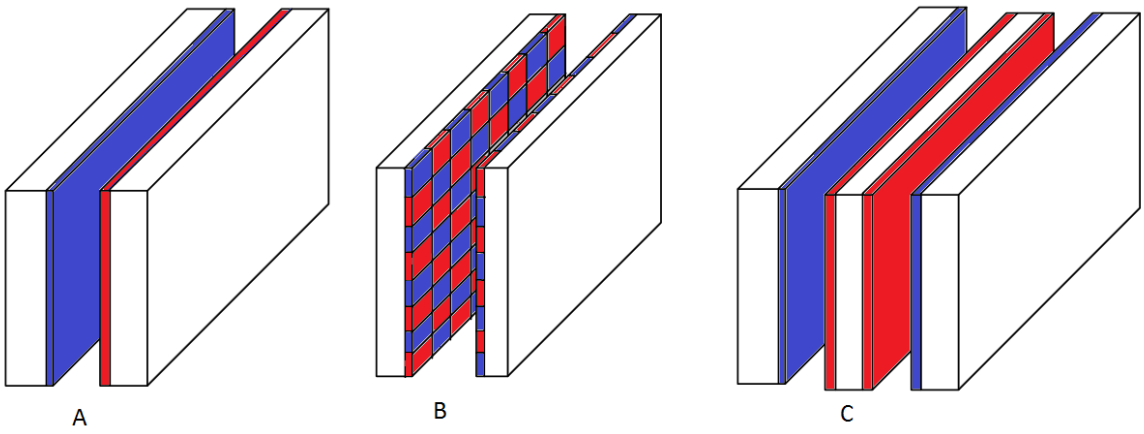

Figure 7 Plated designs for the neutron source.
A) one plate of α absorber (blue) and one plate of α emitter (red). B) Checkerboard pattern (α absorber - blue; α emitter - red); C) two plates of α emitter (red) sandwiched between plates of α absorbers (blue)

3.1.2 Source Choice and Modelling Assumptions

3.1.2.1 Neutron Source

Choosing the α-emitting and (α, n)-absorbing isotopes was the first step in investigating the feasibility of the SRGS. The criteria used to select the α-emitting radioisotope was similar to that of a switchable neutron source [49], and included the following:

1) the α-emitting radioisotope had to have a half-life long enough to eliminate the need for frequent replacements of the source (*i.e.,* a minimum of 10 years);
2) the α-emitting radioisotope had to be safe to store and transport in the "OFF" state; and
3) the α-emitting radioisotope had to have a reduced collateral radiation (*e.g.,* spontaneous fissions, or decay gamma and X-ray radiation) as it decayed.

Alpha-emitting radioisotopes such as ^{148}Gd, ^{145}Pm, ^{208}Po, ^{209}Po, ^{210}Pb, ^{227}Ac, ^{228}Ra, ^{228}Th, ^{232}U, ^{235}Np, ^{236}Pu, ^{238}Pu, ^{241}Pu, ^{241}Am, ^{243}Cm, ^{244}Cm, ^{249}Cf, ^{251}Cf, ^{252}Cf have been considered for SRNS designs [49]. The radioisotope of choice must comply with the three requirements mentioned above and emit α particles with a sufficiently high energy so that they can reach the α-absorbing isotope and be absorbed (*i.e.,* the particles have to have a sufficiently high range so that the self-shielding[14] effects caused by the material itself and the plated design of the source are minimized) [49]. Furthermore, to

[14] Self-shielding refers to the protection of nuclei inside the α-absorber by those in the outer region. If the (α, n)-absorber is thick or the energy of the α particles is not sufficiently high, the α particles will not reach the inside nuclei, be absorbed and produce neutrons. The self-shielding effects will result in a decrease in the neutron source strength.

enhance the neutron production, the α-emitting radioisotope should have a high branching ratio[15] for the production of α particles.

The choice of radioisotope for the current feasibility study was ^{241}Am. This radioisotope has a half-life of 432.2 years [14][49], a low spontaneous fission rate (5.38×10^{-7} spontaneous fissions/μs/g [49]), low energy collateral gamma radiation (60 keV [9]), and it decays primarily by α decay (a branching ratio of ~1 [14]). The low spontaneous fissions rate and collateral gamma radiation, made ^{241}Am safer than other α-emitting radioisotopes such as ^{238}Pu (44 - 766 keV gammas) or ^{227}Ac (50 - 870 keV gammas) [9]. Furthermore, the emitted α particles have an energy of 5.48 MeV (84.8% intensity[16]) [14][50] which is sufficiently high to minimize any self-shielding effects. ^{241}Am is also commonly used in 'off-the-shelf' devices such as smoke detectors and, although it requires special handling procedures common to all α-emitters [51], it has better public acceptance than other α-emitting radioisotopes (*e.g.,* ^{210}Po, see footnote 1, Section 1.4).

Suitable (α, n)-absorbing materials for neutron sources are low-Z materials because of a lower Coulomb repulsion force between the charged α particle and the nuclei of α-absorbing material. Examples of low-Z materials that are used in manufacturing of (α, n) neutron sources include Be, Li and B [9]. The chosen isotope for the neutron source in this research was ^{9}Be. Natural beryllium is composed of 100% ^{9}Be atoms. This isotope is stable and it produces the highest neutron yield when compared

[15] The branching ratio is the fraction of α decays of the radioisotope with respect to all the different decay modes of that particular radioisotope.

[16] The intensity is the percentage of alpha particles that have a particular energy out of all alpha particles produced by the decay of the radioisotope. In this case, ^{241}Am decays with an energy of 5.48 MeV 84.8% of the time.

with either B or Li (*i.e.,* 1.1×10^4 n/cm^2-s for ^{241}Am-Be *vs.* 0.4×10^4 n/cm^2-s for ^{241}Am-B and 0.012×10^4 n/cm^2-s for ^{241}Am-Li [9]).

The ^{241}Am-^{9}Be source was modelled in MCNP5, version 1.40 using the equivalent neutron energy distribution measured experimentally [52]. The modelled spectrum, presented in Figure 8, was uniformly distributed throughout a 0.5 cm thick ^{9}Be target. As illustrated in this figure, 88% of the neutrons produced via this (α, n) reaction have energies above 1 MeV. These neutrons were moderated (*i.e.,* slowed down) to the thermal range (<0.1 eV), to take advantage of the high absorption cross-section of the (n, γ)-absorbing material used in the SRGS (*i.e.,* $Sm_{natural}$ or $Gd_{natural}$, Section 2.1.2.3).

The neutron source strength was calculated using the SOURCES-4C computer code [45] introduced in Section 2.4. The source was modelled as an interface, with one region of ^{241}Am adjacent to a region of ^{9}Be. The code includes data libraries that provide information on α particle stopping cross-sections, decay spectra and branching ratios. The calculated neutron source strength for the models implemented in the current feasibility study was 1.30×10^4 neutrons/cm^2-s (Section 2.4). This value was used to normalize the MCNP results reported in Chapter 4, and to calculate the gamma flux in γ/cm^2-s and the gamma dose rate in mSv/h.

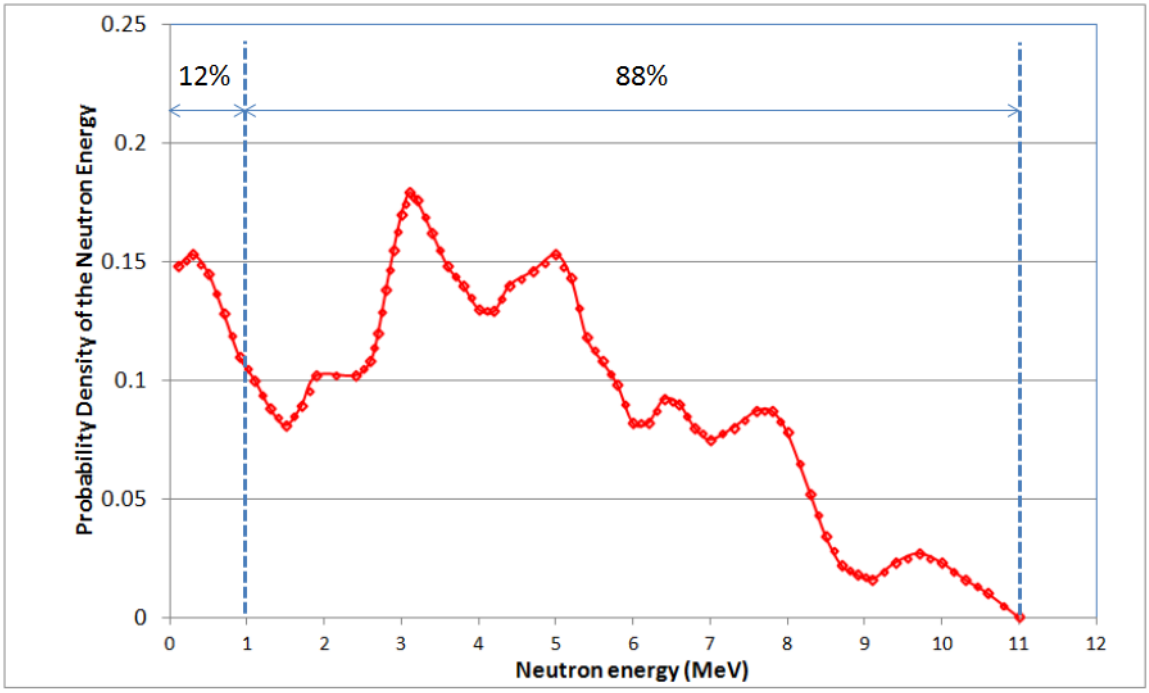

Figure 8 Neutron spectrum for the ^{241}Am - ^{9}Be source, as modelled in MCNP5. The spectrum is based on data reported in [52].

3.1.2.2 Gamma Source

The neutron source described in Section 3.1.2.1 was enclosed in a 0.1 cm thick Zircaloy-2 container. Zircaloy-2 was modelled as 1.45 wt% Sn, 0.135 wt% Fe, 0.105 wt% Cr, 0.055 wt% Ni, 0.006 wt% N, and 98.249 wt% Zr [53]. This alloy was chosen for the container material because of its low neutron absorption when compared with other structural materials used for nuclear applications [54]. Neutron economy is important for the SRGS in order to increase the number of (n, γ) reactions and decrease neutron absorption and other non-gamma producing reactions (*e.g.,* (n, p) reactions, see Section 2.1.2.3, footnote 7). This material has been extensively used to manufacture various nuclear reactor components such as fuel cladding, pressure tubes, calandria tubes,

and calandria vessels, thus, it has been well studied. Other properties that are not applicable to this study but make this alloy appropriate for nuclear applications include high corrosion resistance, good mechanical properties, and resistance to long term radiation exposure [54].

The high energy neutrons from the (α, n) source need to be moderated to take advantage of the (n, γ)-absorber high neutron absorption cross-sections at low energies (see Section 2.1.2 and Section 3.1.2.1). Three different moderators were investigated: deuterated polyethylene (CD_2, density of 1.06 g/cm^3), heavy water (D_2O, density of 1.106 g/cm^3, modelled with a purity of 99.98 wt%) and high density polyethylene (HDPE, density of 0.97 g/cm^3) (see also Section 2.1.2.3). Each moderator was encapsulated in a 0.2 cm thick shell of Zircaloy-2 that was then surrounded by the (n, γ)-absorber, followed by air. Figure 9 illustrates an example of an MCNP5 model for the 40 cm × 40 cm planar source (dimensions in the y- and z-directions), and indicates the elements described above (*i.e.,* neutron source, Zircaloy-2 containers, moderator, absorber, and air regions). The 40 cm × 40 cm neutron source was chosen because its dimensions were similar to those of ^{57}Co flood sources that cover the entire surface area of a standard SPECT gamma camera [6] (see also Section 3.1). Three air regions were identified in Figure 9: air region 1 and region 2 on either face of the planar source (x-direction), and air region 3 surrounding the source in the y- and z-directions. Air region 1 and air region 2 were tallied to calculate the gamma and neutron fluxes and the dose rates, because these two regions would be facing the gamma cameras (see Section 1.4, Figure 2). These two air regions are identical due to the symmetry of the source

(Section 1.4, Figure 1), however, they were tallied separately to calculate the flux and dose rate on each side of the source to demonstrate convergence.

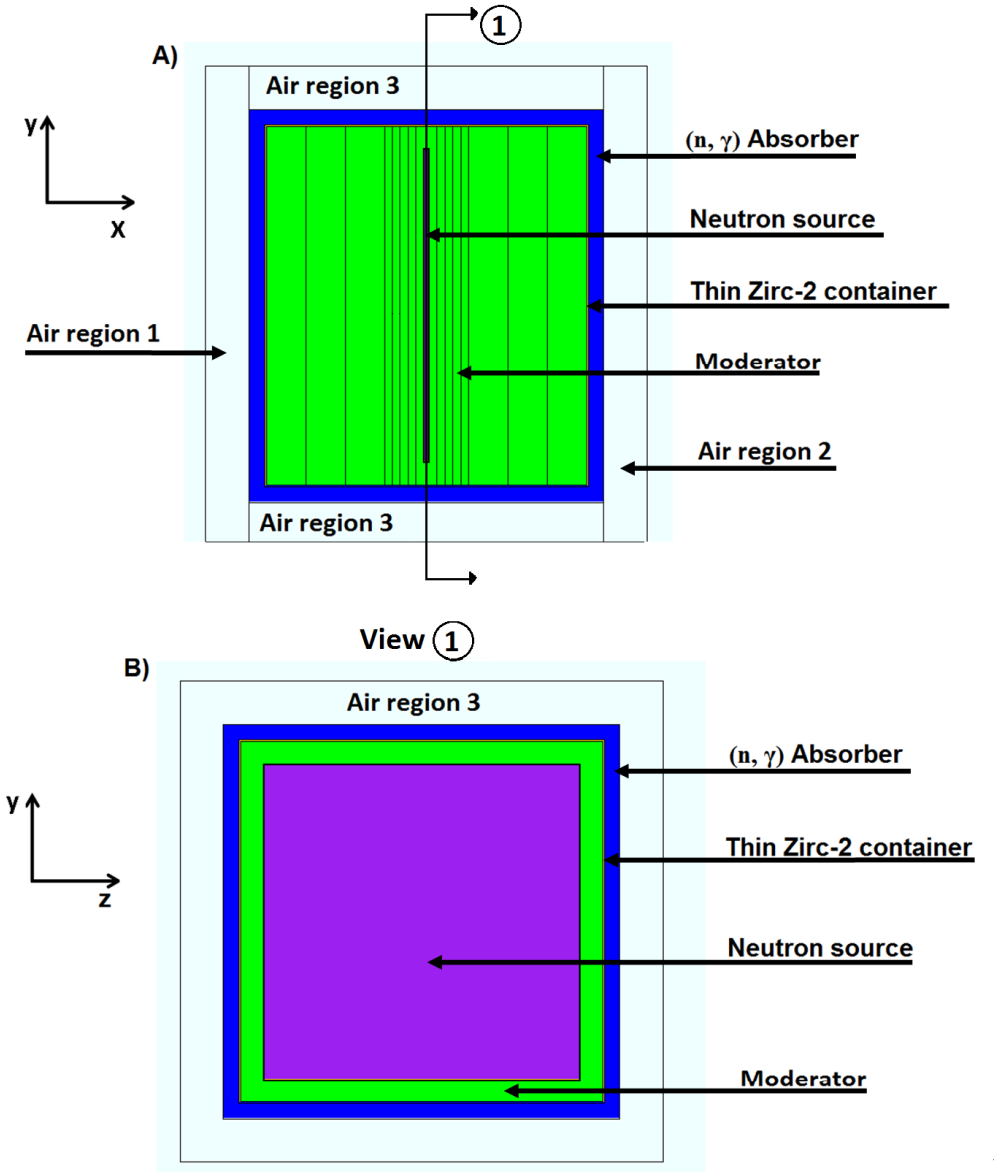

Figure 9 Example of a modelled design for the (n, γ) source. (A) XY view of a 40 cm × 40 cm source; (B) ZY view of the same gamma source, through the center of the neutron source (view 1). Air region 1 and region 2 are the regions of interest for the parametric studies and are located facing the ZY faces of the source (see also Section 1.4, Figure 2). Air region 3 represents the air region surrounding the source on all other sides that do not face the gamma cameras. Neutron loss through these sides is not desirable, as it does not contribute to the gamma production in the regions of interest (*i.e.*, region 1 and region 2). In Figure 9A), the vertical lines in the moderator, parallel to the neutron source show increasing thicknesses of moderator between 0 cm and 20 cm where intermediate results will be tabulated and used for design considerations, see Chapter 4. Figure not to scale.

The amount of moderator surrounding the neutron source results in the extent of moderation of the neutrons. For example, a thin neutron moderator (*e.g.,* <1 cm) would not be sufficient to moderate the neutrons from energies greater than 1 MeV to thermal energies lower than 0.1 eV because there would not be enough atoms present in the material to result in sufficient neutron collisions. The range of moderator thickness for the SRGS simulations was estimated from moderator thicknesses used to moderate fast neutrons in light and heavy water reactors. Pressurized heavy water reactors, which use D_2O as the moderator, have a lattice pitch (*i.e.,* the center-to-center distance between adjacent fuel regions) of 28.58 cm, such that the moderator thickness between adjacent fuel bundles is 14.1 cm to 15.4 cm (based on design of the Pickering reactors) [55]. Reactors that use light water as the moderator, have an assembly pitch of 15.24 cm [56]. The thickness of the moderator region used in the SRGS was varied between 0 cm and 20 cm maximum on either side of the planar source in the x-direction, and kept constant in the y- and z-directions (see Figure 9A). Figure 10 illustrates two types of models that were investigated:

- Model A illustrates a planar source surrounded by 3 cm of moderator on either side of the source (x-direction), encapsulated in a Zircaloy-2 container and surrounded by an absorber region and air. The empty space inside the Zircaloy-2 container that contains the moderator and the source was modelled as "void" (*i.e.,* vacuum).
- Model B illustrates a planar source surrounded by a fixed thickness of lead shield and/or reflector (1.9 cm thick), encapsulated in a thin Zircaloy-2 container, followed by an absorber region and air. The lead shield / reflector was modelled

to investigate the impact of this added region inside the source and determine whether or not it would result in an increased gamma flux and dose in the air regions facing the SPECT gamma camera or the blood bags (*i.e.,* air region 1 and region 2 in Figure 9A). Model B in Figure 10 does not contain any moderator, and the empty region inside the outer Zircaloy-2 container was modelled as void.

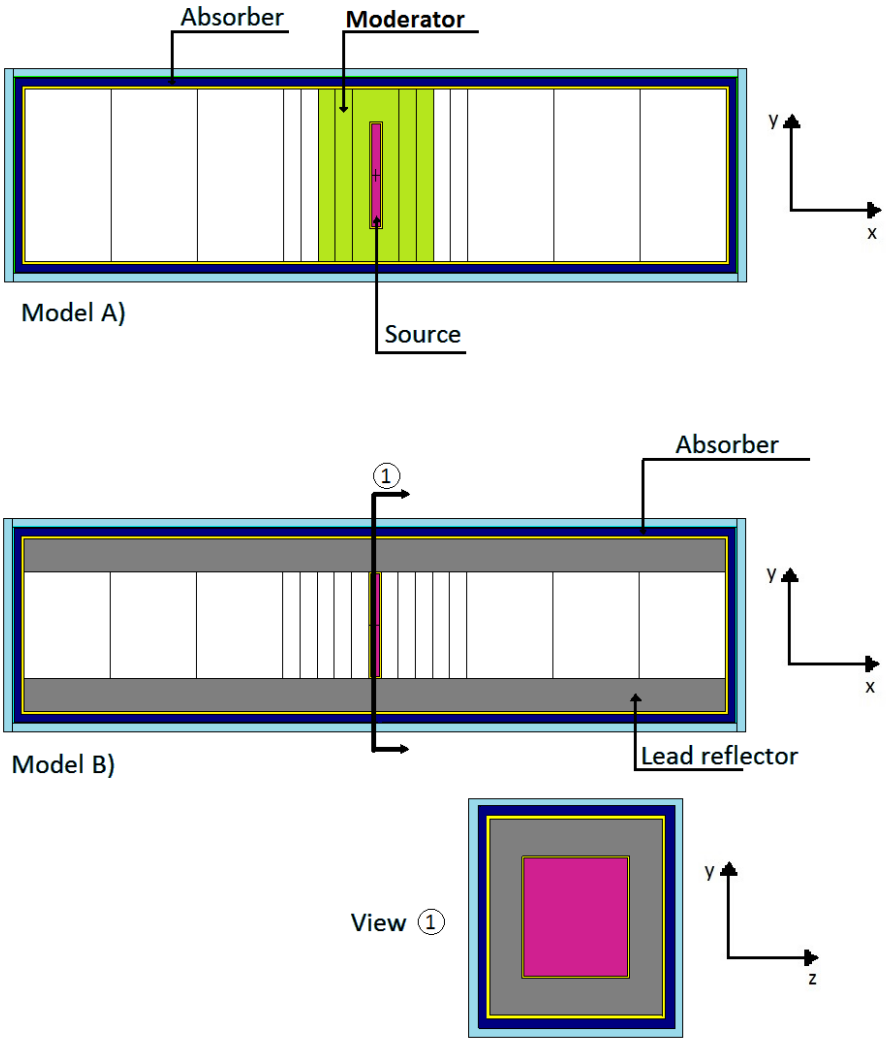

Figure 10 Example of MCNP5 models for the (n, γ) source. Model (A) X-Y view of the a SRGS with moderator surrounding the neutron source, followed by void, and the neutron absorber; Model (B) X-Y view of the similar source with no moderator but a lead reflector / shield.
In both Model (A) and Model (B), the vertical lines in the moderator, parallel to the neutron source show increasing thicknesses of moderator between 0 cm and 20 cm where intermediate results will be tabulated and used for design considerations, see Chapter 4.

3.1.3 Parametric Studies Description

The objective of this research was to test the feasibility of the SRGS for two medical applications: a SPECT gamma camera calibration source and a self-contained blood irradiator (Section 1.2). To achieve this objective, a number of parametric studies were performed to calculate the gamma flux and dose rate produced by the SRGS. The parametric studies were carried out to determine the optimal moderator thickness and absorber thickness that would result in the highest gamma flux and gamma dose rate, for two different (α, n) source sizes: 40 cm × 40 cm, and 6 cm × 6 cm. These two source dimensions were chosen based on the SPECT gamma camera calibration application (Section 3.1).

The following assumptions were made for this research. These assumptions are based on information previously presented in Chapters 2 and 3:

1) The source geometry was fixed as a planar, rectangular source, as illustrated in Figure 7 and Figure 10. This geometry was chosen because it resembles the geometry of the gamma cameras used in SPECT imaging.
2) Only the ^{241}Am - ^{9}Be source described in Section 3.1.2.1 was considered for the switchable neutron source. The source was assumed to include only two plates (one with the α-emitter and another with the (α, n)-absorber, facing each other as in Figure 7A or Figure 7B).
3) The moderating materials investigated were CD_2, D_2O, and high density polyethylene (HDPE) (Section 2.1.2.3). These materials were chosen based on information summarized in Table 1, where it was seen that lighter elements are better moderators than heavier ones. Furthermore, these materials have a long

history of being used for neutron moderation either in nuclear reactors or in research applications ([21] [55] and Section 3.1.2.2).

4) The (n, γ)- absorbing materials investigated were $Sm_{natural}$ and $Gd_{natural}$, because of their high thermal neutron absorption cross-sections *i.e.,* 49700 barn for $Gd_{natural}$ and 5922 barn for $Sm_{natural}$ [19] (Section 2.1.2).

Based on these assumptions, parametric studies were performed to calculate the average gamma flux and average gamma dose rate in air region 1 and region 2 (see Figure 9, Section 3.1.2.2) for the following investigations:

1) Investigated the effect of neutron source dimensions by modelling two different neutron sources with dimensions:
   - 40 cm × 40 cm (referred to as the "large source"), Section 4.1, and
   - 6 cm × 6 cm (referred to as the "small source"), Section 4.2.

   Neutron source dimensions are specified in the y- and z-directions. The 40 cm × 40 cm neutron source was investigated because it would cover the entire area of a standard SPECT gamma camera [6], while the 6 cm × 6 cm neutron source and the corresponding 10.4 cm × 10.4 cm gamma source would effectively cover a quarter of the gamma camera (see footnote 13, Section 3.1).

2) Investigated the effect of overall SRGS source dimensions on the calculated average gamma dose rate and gamma flux (Section 4.2.2). This parametric study was performed for the small 6 cm × 6 cm neutron source that corresponded to a 10.4 cm × 10.4 cm gamma source (see footnote 13, Section 3.1). The x-dimensions of the source were varied between 0 cm - 10 cm, 0 cm - 15 cm and 0 cm - 20 cm on either side of the planar neutron source.

3) Investigated the effect of different moderators and different moderator thicknesses. For each moderator type, the thickness was varied between 0 cm and the maximum SRGS source size, along the x-direction (*i.e.,* 10 cm, 15 cm or 20 cm), on each side of the neutron source. Along the y- and z-directions, the thickness of moderator, when present, was kept constant to result in overall gamma source dimensions of:

   - 46 cm × 46 cm for the large source design (Section 4.1), and
   - 8.4 cm × 8.4 cm (Section 4.2.1) or 10.4 cm × 10.4 cm (Section 4.2.2) for the small source design. These two gamma source dimensions were used to understand the impact of the moderator thickness in the y- and z-directions on the calculated gamma fluxes and dose rates. Furthermore, the 10.4 cm × 10.4 cm gamma source ensured effective coverage of one quarter of the gamma camera.

4) Investigated the effect of lead and carbon steel as a reflector / shield inside the source (see Figure 10B and Section 4.2.3). This investigation was performed only for the small neutron source design, using a fixed absorber type ($Sm_{natural}$) of fixed thickness (0.5 cm). The thickness of the reflector / shield was kept constant at 1.9 cm (resulting in an overall gamma source size of 10.4 cm × 10.4 cm). The investigation was conducted to determine whether the presence of a reflector such as lead or carbon steel would result in an increase in the calculated average gamma flux and dose rate in air region 1 and region 2 (*i.e.,* the air regions of interest, Figure 2 and Figure 9).

5) Investigated the effect of different (n, γ)-absorbing materials (*i.e.,* $Sm_{natural}$ or $Gd_{natural}$) and their thickness (Section 4.1 and Section 4.2). For each absorber, thicknesses of 0.1 cm, 0.2 cm, 0.5 cm and 1 cm were investigated.

4 Chapter: Results and Discussion

This chapter summarizes the results of the parametric studies introduced in Section 3.1.3. The results are discussed in terms of the impact of parameters such as source dimensions, moderator types and thicknesses, and (n, γ)-absorber types and thicknesses on the calculated average gamma fluxes and dose rates. The effect of these parameters is quantified in this chapter and the feasibility of the proposed SRGS designs for the two intended applications (*i.e.,* a flood source for SPECT gamma camera calibration, and a blood irradiator) is assessed.

4.1 Results for the Large Source

Preliminary calculations were performed for the large 40 cm × 40 cm source[17], which had a similar size as current ^{57}Co flood sources that would cover the entire surface area of a SPECT gamma camera. The neutron source was surrounded by a variable thicknesses of CD_2 moderator, as illustrated in Figure 9A), Section 3.1.2.2. The overall source dimensions were kept constant at 46 cm × 46 cm in the y- and z-directions (see Section 1.4, Figure 1). The results for the average gamma and neutron fluxes calculated in a thin air region located by the YZ faces of the source (*i.e.,* air region 1 or region 2 illustrated in Figure 9, Section 3.1.2.2) are summarized in Figure 11. For these models, the moderator thickness was varied between 0 cm and 20 cm (Section 3.1.2.2). The average gamma fluxes in γ/cm^2-s for three different $Sm_{natural}$ absorber thicknesses (*i.e.,* 0.2 cm, 0.5 cm and 1 cm) calculated in air region 1 or region 2 (*i.e.,* the region of interest,

[17] The SRGS is also referred to as the "system" in this thesis.

see also Figure 9) are shown in Figure 11A). Figure 11B) illustrates the average neutron fluxes in n/cm^2-s for the same configurations, calculated in air region 1 or air region 2. The maximum average gamma flux of 1.13×10^4 γ/cm^2-s (see Figure 11A, data point labeled 1) was obtained for the 0.2 cm $Sm_{natural}$ absorber and a 20 cm CD_2 moderator. The corresponding average neutron flux for the same region was 9.39×10^2 n/cm^2-s (see Figure 11B data point labeled 2). The computational relative uncertainty[18] for these results were <0.1%.

The results illustrated in Figure 11 show an increase in average gamma flux as the moderator thickness was increased between 0 cm and 20 cm. This behaviour was expected because a significant fraction of neutrons produced by the ^{241}Am-^{9}Be source (88%) had energies greater than 1 MeV (see Figure 8, Section 3.1.2.1), and they had to be moderated to thermal energies (<0.1eV) in order to take advantage of the high thermal absorption cross-section for ^{149}Sm (42080 barns [19]). Table 5 summarizes the percentage of gammas produced by the different $Sm_{natural}$ isotopes for 0 cm moderator, 3 cm moderator and 20 cm moderator, for an absorber thickness of 0.2 cm $Sm_{natural}$. These data show that, the higher the moderator thickness, the more thermalized the neutrons are, and the more they are absorbed by ^{149}Sm because of its high absorption cross-section for thermal neutrons (see Figure 12[19] for the energy-dependent absorption cross-section data for ^{149}Sm and ^{152}Sm). Furthermore, 33 times more gammas were produced via the (n, γ) reaction in $Sm_{natural}$ for a 20 cm thick moderator

[18] This relative uncertainty is calculated by MCNP. In MCNP this value represents the statistical precision ($S_{\bar{x}}$) as a fractional result with respect to the estimated mean value for the calculated parameter, $\bar{x}$ (*i.e.* $S_{\bar{x}}/\bar{x}$) [8].

[19] The cross-section data was plotted using the online tool from the National Nuclear Data Centre, http://www.nndc.bnl.gov/sigma/, Accessed 2015 October 10.

(1.13×10^4 γ/cm^2-s, Figure 11A, data point labeled 1), than for the 0 cm moderator case (3.44×10^2 γ/cm^2-s, Figure 11A, data point labeled 4). This result led to an average neutron flux in the tallied volume that was 3 times lower for the 20 cm moderator (9.39×10^2 n/cm^2-s, Figure 11B data point labeled 2) than for the 0 cm moderator case (2.76×10^3 n/cm^2-s, Figure 11B data point labeled 3). The implication of these results is that, as the neutrons are moderated, their probability of being absorbed by the (n, γ)-absorber increases, which results in a higher gamma flux in the air regions facing the gamma cameras (see Section 1.4, Figure 2).

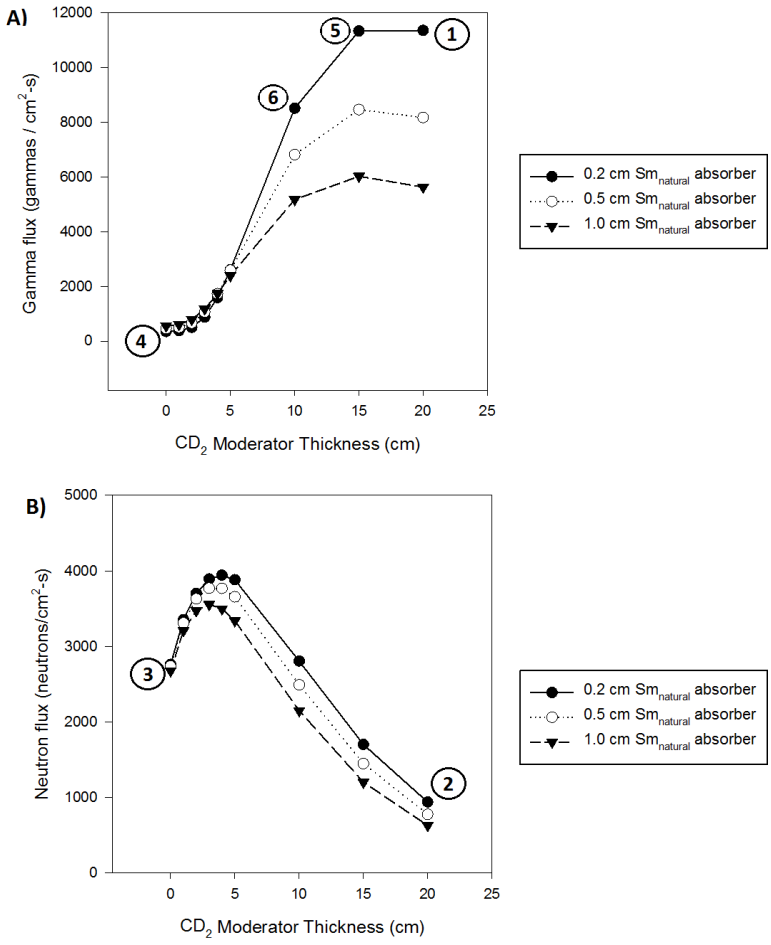

Figure 11 Calculated average flux values *vs.* CD_2 moderator thickness (cm) calculated in air region 1 or region 2 for a 40 cm × 40 cm neutron source, for different $Sm_{natural}$ absorber thicknesses. A) Average gamma flux (γ/cm^2-s) results. B) Average neutron flux (n/cm^2-s) results.

Table 5 Relative percentage of γ produced by neutron absorption in each $Sm_{natural}$ isotope from all γ produced in the (n,γ)-absorber (absorber thickness = 0.2 cm)

Isotope	σ_a (thermal neutrons) [19] (barns)	wt%[20] of Isotope in $Sm_{natural}$	Moderator thickness		
			0 cm	3 cm	20 cm
^{144}Sm	0.7	3.07	2.2%	0.6%	0.0%
^{147}Sm	57.3	14.99	15.3%	18.3%	1.8%
^{148}Sm	2.4	11.24	10.1%	3.6%	0.1%
^{149}Sm	42080.4	13.82	16.9%	44.2%	93.7%
^{150}Sm	104.4	7.38	7.4%	4.0%	0.4%
^{152}Sm	206.6	26.75	26.9%	21.9%	3.8%
^{154}Sm	8.4	22.75	21.1%	7.4%	0.2%

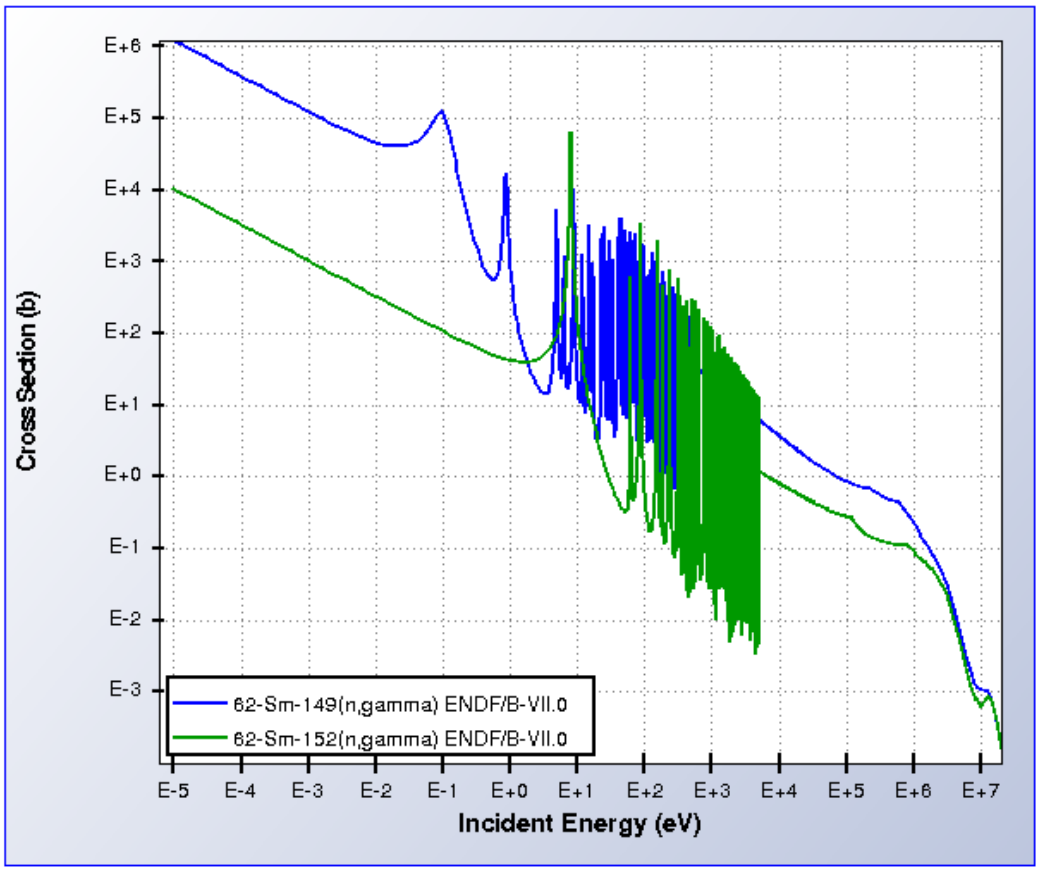

Figure 12 Cross-section data for ^{149}Sm and ^{152}Sm for the (n, γ) reaction

[20] Material compositions in MCNP were specified using mass% (also referred to as wt%), as mentioned in Section 2.3.1.

An interesting behaviour was observed for the neutron flux calculated in the air region by the YZ faces of the SRGS (see Section 1.4, Figure 1 and Figure 2), as the moderator thickness was increased. The measured average neutron flux increased between 0 cm of moderator and 3 cm of moderator, followed by a consistent decrease as the moderator thickness increased up to 20 cm (see Figure 11B). One possible explanation for this behaviour is that, as small thicknesses of moderator were added, some of the neutrons produced by the isotropically modelled neutron source were scattered towards air region 1 or region 2, instead of escaping into air region 3 (*i.e.,* the air region surrounding the gamma source on the XY and XZ faces, Section 1.4, Figure 1). However, these neutrons were not sufficiently moderated to be absorbed by $Sm_{natural}$, hence, they escaped the system. As the moderator thickness increased, the neutrons had more opportunities to collide with atoms in the moderator and lose enough energy to increase their probability of being absorbed in $Sm_{natural}$, resulting in more (n, γ) reactions.

The maximum average gamma flux calculated for this study (*i.e.,* 1.13×10^4 γ/cm^2-s, Figure 11A, data point labeled 1) was one to two orders of magnitude lower than a typical gamma flux produced by the ^{57}Co source that is currently used to calibrate the SPECT gamma cameras (*i.e.,* 4×10^5 γ/cm^2-s). Using the proposed switchable radioactive gamma source for calibration purposes would require a concomitant increase in time from a few minutes to hours. Furthermore, this source would be more expensive than a ^{57}Co source, as discussed in the next section.

4.1.1 Large SRGS Cost Discussion

The cost for the ^{241}Am and ^{9}Be used for the 40 cm × 40 cm neutron source, the CD_2 moderator and the $Sm_{natural}$ (n, γ)-absorber was estimated based on the following assumptions:

- ^{241}Am price was ~$4,000[21] (estimated mass of ^{241}Am = 2.5 g, see Appendix B.2 for calculations),
- ^{9}Be cost based on pure beryllium was ~$750 / 100 g[22] ($^{9}Be$ thickness was chosen to be twice the range of an α particle, which ensures adequate α absorption without undue neutron self-shielding (see footnote 14, Section 3.1.2.1) resulting in a mass of $^{9}Be \approx 7$ g),
- $Sm_{natural}$ price[23] was estimated for a 0.2 cm thick $Sm_{matural}$ absorber surrounding the Zircaloy-2 container encapsulating the moderator and the neutron source (mass of $Sm_{natural}$ = 18.2 kg),
- Deuterated polyethylene price[24] was estimated for 3 moderator thicknesses:
    - 20 cm (Figure 11A, data point labeled 1, mass of CD_2 = 90.1 kg),
    - 15 cm (Figure 11A, data point labeled 5, mass CD_2 = 67.7 kg), and
    - 10 cm (Figure 11A, data point labeled 6, mass CD_2 = 45.2 kg)

---

[21] Estimated price of ^{241}Am was taken from http://www.world-nuclear.org/info/Non-Power-Nuclear-Applications/Radioisotopes/Smoke-Detectors-and-Americium/ (2014 March 15).

[22] Estimated price of pure ^{9}Be was taken from http://www.chemicool.com/elements/beryllium.html (2014 March 15).

[23] Estimated price for $Sm_{natural}$ was taken from http://www.chemicool.com/elements/samarium.html (2014 March 15).

[24] Estimated price for CD_2 was based on the assumption that this material was manufactured in-house rather than bought from external suppliers, hence making it cheaper. A search for prices of pure CD_2 led to an estimated cost per 2 g of material of $3000 (http://www.polymersource.com/product.php?ID=49, 2014 March 15). The amount used in this estimate assumes that in-house manufacturing of CD_2 would cost approximately as much as 99.9 wt% pure D_2O, *i.e.,* $1,130 / kg (price obtained from http://www.sigmaaldrich.com/catalog/product/aldrich/151882?lang=en&region=CA, 2014 March 15).

- The cost of manufacturing and other component parts is not included in this estimate, but it is expected to be much smaller than the capital cost of the main component parts.

Given these assumptions, the total cost for the main components involved in the nuclear reactions for three large SRGS designs is summarized in Table 6. Based on these estimates, the designed SRGS is expensive, costing 12 - 17 times more than a ^{57}Co flood source ($10,000 [57]). The SRGS costs summarized in Table 6 used price estimates for each nuclear material based on purchasing of small quantities, not bulk amounts. Bulk buying of these materials could potentially reduce the cost of a single unit by a factor of 2 or 3. However, the high end cost of the SRGS would still be ~$50,000 to $74,000 (assuming a 15 cm moderator thickness (row 2, Table 6), because the calculated average gamma flux is the same as that of an SRGS using a 20 cm moderator thickness).

The cost of the SRGS is determined mainly by the cost of the $Sm_{natural}$ (n, γ)-absorber, and the cost of the CD_2 moderator. One option to decrease the long-term price of the flood source is to replace the neutron source (as its source strength decreases) but reuse the $Sm_{natural}$ absorber and the CD_2 moderator; this results in higher upfront costs for the SRGS (~$50,000 - $74,000), but comparable to a ^{57}Co flood source over a 10-year period (~$70,000 = $10,000/source × 7 sources in 10 years, see Section 1.1 for ^{57}Co source replacement frequency).

Another option is to investigate a smaller SRGS design, which would involve smaller amounts of moderator and (n, γ)-absorber, hence, reducing the cost of the gamma source. The calculated gamma fluxes and dose rates from smaller source designs are summarized in Section 4.2 below.

Table 6 Estimated costs for SRGS designed using a 40 cm × 40 cm neutron source. These estimates only include the cost of the main components (*i.e.,* neutron source materials, moderator and (n, γ)-absorber)

Total SRGS Cost ($)	^{241}Am cost ($)	^{9}Be cost ($)	$Sm_{natural}$ cost ($) (0.2 cm thick)	CD_2 cost ($)	CD_2 thickness (cm)	γ flux (γ/cm^2-s)
172,100	4000	100	66,000	102,000	20	1.13×10^4 (point labeled 1, Figure 11)
147,100				77,000	15	1.13×10^4 (point labeled 5, Figure 11)
121,000				51,000	10	8.51×10^3 (point labeled 6, Figure 11)

4.2 Results for the Small Source Design

The feasibility of the smaller SRGS was investigated because of the high cost of the large source (Section 4.1.1). The y- and z-dimensions of the neutron source for the small SRGS design were 6 cm × 6 cm (see Section 3.1.3). The current section summarizes results for parametric studies performed using the small neutron source to calculate the average gamma flux and dose rate. It also discusses these results with respect to the two intended applications (*i.e.*, calibration flood source for SPECT gamma camera or blood irradiator).

The parametric studies performed include:

a) Comparison between D_2O and CD_2 moderators when the (n, γ)-absorber was either $Sm_{natural}$ or $Gd_{natural}$ (Section 4.2.1).

- General characteristics of these studies include:
    - The overall gamma source size was modelled as 8.4 cm × 8.4 cm[25].
    - Four (n, γ)-absorber thicknesses were investigated: 0.1 cm, 0.2 cm, 0.5 cm and 1.0 cm.
    - Moderator thicknesses were varied between 0 cm and 20 cm (Section 3.1.2.2).
- The results of these parametric studies supported the choice for the deuterium-based moderator used in subsequent parametric studies.

b) Comparison of different gamma source sizes in the x-direction (*i.e.*, the direction facing the gamma camera), based on the maximum amount of moderator used (*i.e.*, 10 cm, 15 cm or 20 cm maximum) (Section 4.2.2).

- General characteristics of the studies reported in this section included:
    - The overall gamma source size was modelled as 10.4 cm × 10.4 cm (see footnote 13, Section 3.1.1).
    - Two moderating materials were investigated: CD_2 and HDPE. Moderator thickness was varied for each case between 0 cm and the maximum source size (10 cm, 15 cm or 20 cm on either side of the neutron source).
    - Two absorbers were investigated, $Sm_{natural}$ and $Gd_{natural}$, with thicknesses of 0.2 cm, 0.5 cm or 1 cm.

[25] This dimension was calculated as follows: 6 cm × 6 cm neutron source, 0.1 cm thick Zircaloy-2 container (Section 3.1.2.2) and 0.9 cm thick moderator on the y- and z-directions (see Figure 9 and Section 4.2.2) and 0.2 cm thick Zircaloy-2 container around the moderator.

- Gamma dose rates were calculated using two different methods:
    - The F4 tally (Section 4.2.2.1.1)
    - The F6 tally (Section 4.2.2.1.2). The F6 tally studies were performed only for a $Sm_{natural}$ (n, γ)-absorber, based on the results summarized in Section 4.2.2.1.1.
- Gamma fluxes are reported in Section 4.2.2.1.3.
- Neutron dose rates and fluxes are reported in Section 4.2.2.2. These studies were performed only for the $Sm_{natural}$ (n, γ)-absorber, based on the results summarized in Section 4.2.2.1.1.

c) Comparison of results for SRGS designs illustrated in Figure 10B, using lead and carbon steel reflector / shield (Section 4.2.3).

- General characteristics of these studies include:
    - The (n, γ)-absorber was $Sm_{natural}$ with a thickness of 0.5 cm.
    - The moderator chosen was CD_2. The thickness of the moderator was varied between 0 cm and 10 cm, 15 cm or 20 cm maximum, depending on the overall source size.

4.2.1 Comparison between D_2O and CD_2 moderators for two different absorbers: $Sm_{natural}$ and $Gd_{natural}$

A parametric study was first performed on the smaller source to investigate the effect of changing the moderating material on the calculated average gamma flux. Two moderators were investigated in this study: CD_2 and D_2O. The moderator thickness was varied for each parametric study, from a thickness of 0 cm to a maximum thickness of

20 cm along the x-direction (Section 3.1.2.2), in order to determine the optimal thickness that resulted in the maximum average gamma flux. The dimensions of the gamma source in the y- and z-directions were kept constant at 8.4 cm × 8.4 cm[footnote 25, Section 4.2]. Two absorbers were investigated: $Sm_{natural}$ and $Gd_{natural}$, with four different thicknesses: 0.1 cm, 0.2 cm, 0.5 cm and 1.0 cm. The results of the calculated average gamma fluxes in γ/cm^2-s in air region 1 or region 2 (*i.e.,* the YZ faces of the source, see Figure 9A, Section 3.1.2.2) are summarized in Figure 13 for the $Sm_{natural}$ absorber and in Figure 14 for the $Gd_{natural}$ absorber.

Figure 13 and Figure 14 show no significant differences in the calculated average gamma fluxes between the two moderators. Furthermore, the higher the neutron absorber thickness the higher the gamma fluxes obtained via the (n, γ) reaction, because more of the neutrons produced by the ^{241}Am-^{9}Be source were absorbed in the (n, γ)-absorbing material. The maximum gamma flux calculated for either $Sm_{natural}$ or $Gd_{natural}$ was obtained for a 1 cm (n, γ)-absorber thickness. These gamma fluxes are summarized in Table 7.

Table 7 Calculated average gamma fluxes for 1 cm $Sm_{natural}$ or $Gd_{natural}$ (n, γ)-absorber with CD_2 or D_2O moderators

Absorber	Moderator	Moderator thickness (cm)	Gamma flux (γ/cm^2-s)
$Sm_{natural}$	D_2O	1.0	23.8 (data point labeled A in Figure 13)
	CD_2	2.0	24.7 (data point labeled B in Figure 13)
$Gd_{natural}$	D_2O	1.0	22.7 (data point labeled C in Figure 14)
	CD_2	2.0	23.3 (data point labeled D in Figure 14)

No significant changes were observed for the calculated average gamma flux between the two moderators, when the same (n, γ)-absorber was used. The two moderators (*i.e.,* D-O-D and D-C-D) have similar densities (1.106 g/cm^3 for D_2O and 1.06 g/cm^3 for CD_2), and moderation is primarily done by the deuterium. Moreover, O and C have similar moderating properties (see Section 2.1.2.3, Table 1). Thus, D_2O and CD_2 moderate the source neutrons similarly. The maximum gamma flux was obtained at slightly different moderator thicknesses (*e.g.,* 1 cm for D_2O *versus* 2 cm for CD_2), which was expected because D_2O is a better moderator (moderating ratio of 4487) than CD_2 (moderating ratio of 906), as reported in Table 3, Section 2.1.2.3.

The calculated gamma flux differences between $Sm_{natural}$ and $Gd_{natural}$ were not significant (see Table 7). One explanation for this similarity is that both $Sm_{natural}$ and $Gd_{natural}$ are very good neutron absorbers for thermal neutrons (absorption cross-sections of 49700 barn for $Gd_{natural}$ and 5922 barn for $Sm_{natural}$ [19]), acting like "black holes" for neutrons with energies <0.1 eV (see Section 2.1.2). Although the absorption cross-section for thermal neutrons (*i.e.,* energies <0.1 eV) for $Gd_{natural}$ is higher than that of $Sm_{natural}$, the calculated gamma fluxes for the cases using $Sm_{natural}$ as the (n, γ)-absorber are 5% higher than those calculated using $Gd_{natural}$. This result can be explained by comparing the absorption cross-section graphs for ^{147}Sm, ^{155}Gd and ^{157}Gd (see Figure 5, Section 2.1.2). The ^{149}Sm graph shows a peak that is above the cross-section values for the Gd isotopes at an incident neutron energy of 0.1 eV. Moreover, the resonance peaks for ^{149}Sm are larger than those for the Gd isotopes. For the simulations shown in Table 7, the neutrons were not fully thermalized when they reached the (n, γ)-absorbing region,

thus, they most likely were absorbed at energies > 0.1 eV, where the ^{149}Sm absorption cross-sections are higher.

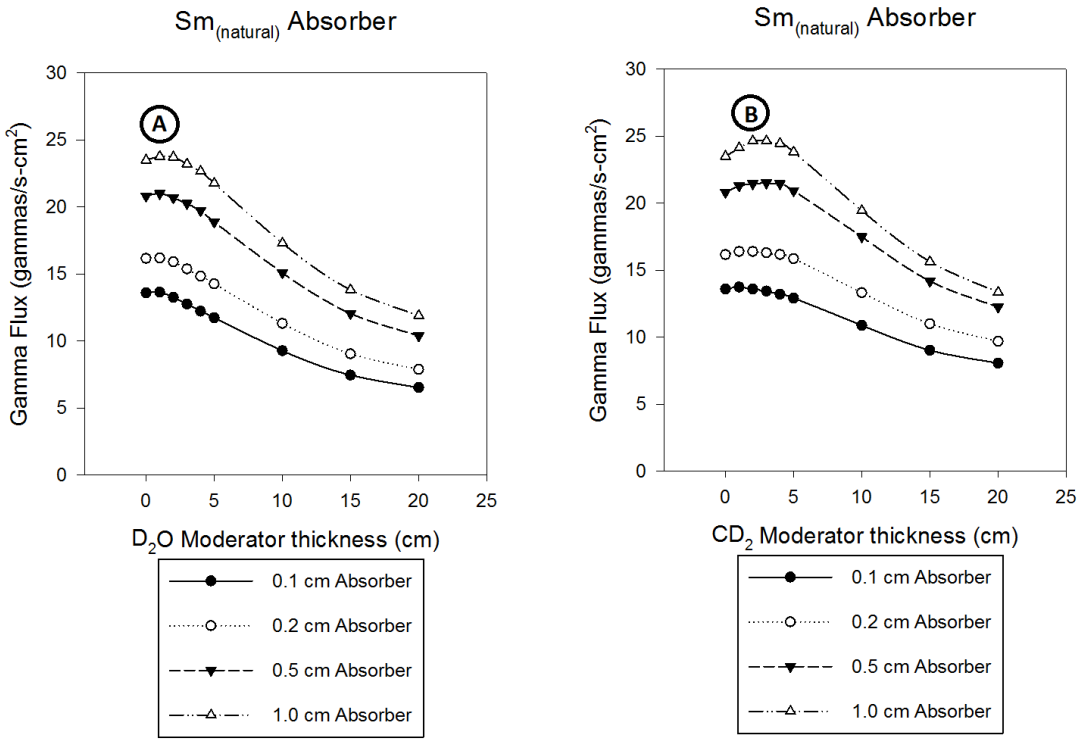

Figure 13 Average gamma flux (γ/cm^2-s) *vs.* moderator thickness (cm) for the small SRG source with CD_2 and D_2O moderators, for varying thicknesses of $Sm_{natural}$ absorber. Data points labeled A and B represent the maximum value. The computational relative uncertainties[(footnote 18, Section 4.1)] obtained were <0.1%.

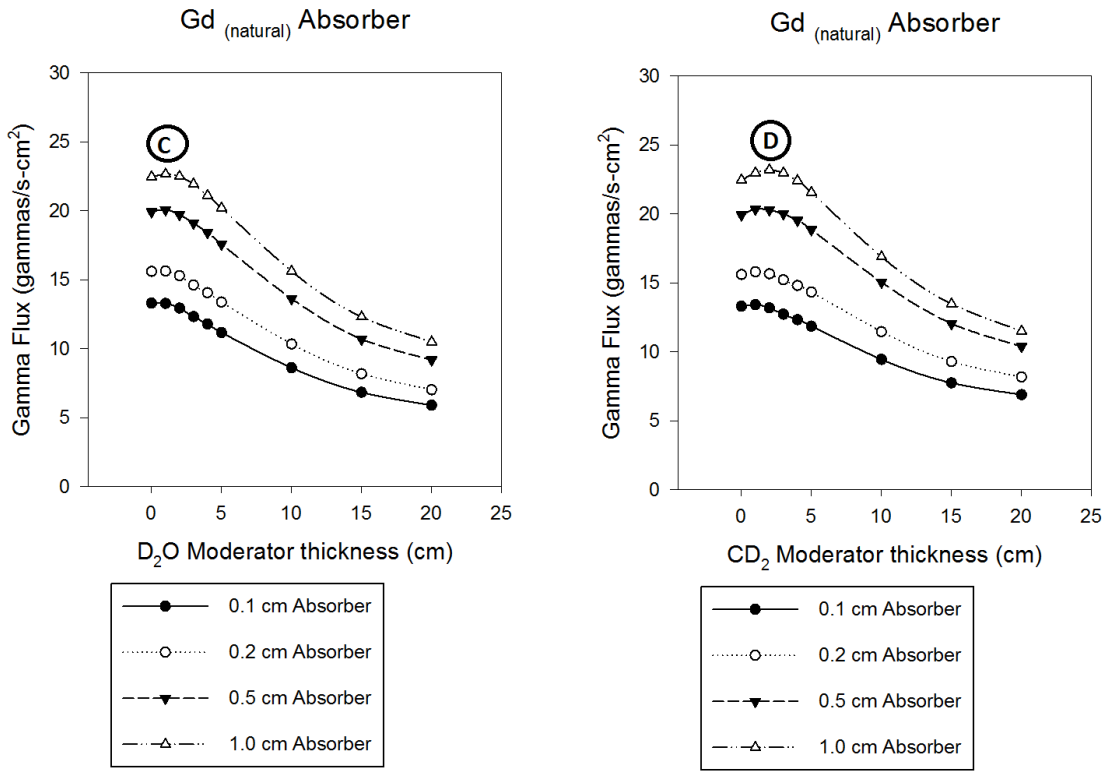

Figure 14 Average gamma flux (γ/cm^2-s) *vs.* moderator thickness (cm) for the small SRG source with CD_2 and D_2O moderators, for varying thicknesses of $Gd_{natural}$ absorber. Data points labeled C and D represent the maximum values. The computational relative uncertainties[(footnote 18, Section 4.1)] obtained were <0.1%.

The average gamma fluxes calculated for these models were significantly lower (by a few orders of magnitude) than the gamma fluxes from standard ^{57}Co flood sources (4×10^5 γ/cm^2-s) currently being used in SPECT gamma camera calibration procedures [3] (see also Section 2.2.1). The main consequence of this low flux is that calibration procedures using an SRGS would have to take a few days instead of a few minutes (*i.e.,* the current calibration time). Furthermore, the proposed mechanism to produce the gamma radiation would result in a wide range of gamma energies. Current uniformity tests recommend using gamma energies similar to those used in patient procedures, to ensure an optimal gain can be chosen for the pulse height detector used to capture the scintillation event [32]. Furthermore, the broad tail of high energy photons (>500 keV),

can confound count rates from lower energy radiopharmaceuticals [35], which leads to the detector gain being incorrectly calibrated (see Section 2.2.1). Thus, the best flood source design would have a narrow gamma spectrum that would be close to that of the isotope used during the imaging procedures [32]. The most common example is that of ^{99m}Tc, which decays by gamma rays with an energy of 140.5 keV [14].

4.2.2 Comparing Results for Different Overall Source Sizes

Further studies were performed to investigate the effect of moderator thickness and overall gamma source size on the calculated average gamma and neutron fluxes and dose rates. The new parametric studies used CD_2 and high density polyethylene (HDPE) as moderators, and $Gd_{natural}$ or $Sm_{natural}$ as (n, γ)-absorbers.

CD_2 was chosen for two reasons. First, the average gamma flux results obtained for CD_2 *vs.* D_2O (Section 4.2.1) did not show significant differences between the two moderator types. Second, during manufacturing, the deuterium in D_2O readily exchanges with the hydrogen in water vapour (*e.g.*, moisture in the air), thus impacting the D_2O purity, which makes the handling and storage process for D_2O more difficult. However, the deuterium in CD_2 is stable in the polymer, and does not exchange with the hydrogen in water vapour.

HDPE, with a density of 0.97 g/cm^3, was used to investigate the effect of a hydrogen-based moderator instead of a deuterium-based moderator on the average gamma and neutron fluxes and dose rates. The logarithmic energy decrement for hydrogen is 1.00 and the number of collisions to slow down a neutron with an initial energy of 4 MeV to an energy of 0.1 eV (*i.e.,* the upper bound for thermal energies) is 18

compared with 24 for deuterium (Section 2.1.2.3, Table 1). Therefore, fewer collisions would be required to slow down the neutrons produced by the ^{241}Am-^{9}Be source if a hydrogen-based moderator was used. This would skew the neutron spectrum towards the thermal range more-so than would a similar deuterium-based material (see Section 2.1.2.3). The ability to slow down fast neutrons with fewer collisions becomes important in a small system such as that investigated for the SRGS, because the neutrons need to be thermalized and reach the neutron absorber to produce gammas via (n, γ) reactions before they have the chance to escape the gamma source, which is more prevalent in smaller systems because of the "inverse square law"[26] [58].

For these parametric studies, the moderator region on the y- and z-directions was kept constant at 10.4 cm × 10.4 cm(footnote 13, Section 3.1) resulting in a 1.9 cm thick moderator region surrounding the neutron source (see Figure 9, Section 3.1.2.2 for a graphical illustration of the source design). The x-dimensions of the source were varied between 0 - 10 cm, 0 - 15 cm and 0 - 20 cm on either side of the planar neutron source (see Figure 10A) and for each scenario, the moderator thickness was varied between 0 cm and the maximum source size in the x-dimension. The average gamma and neutron fluxes and dose rates in air region 1 or air region 2 (*i.e.,* the areas of interest for the SPECT gamma camera application, see Figure 2, Section 1.4 and Figure 9, Section 3.1.2.2) were calculated for each overall source dimension, and were compared to investigate how they were impacted by the source size. For simplicity, throughout the rest of this analysis, the cases with a maximum 10 cm moderator on either side of the neutron source will be referred to as the "10 cm small SRGS", those with a maximum 15 cm moderator will be

[26] The neutron flux at a distance, r, from the source is proportional to $1/r^2$ [58].

referred to as the "15 cm small SRGS" and those with a maximum of 20 cm moderator will be referred to as the "20 cm small SRGS".

4.2.2.1 Calculated Average Gamma Dose Rates and Fluxes

The average gamma fluxes (γ/cm^2-s) were calculated using the F4 tally. The average gamma dose rates (mSv/h or mGy/h) were calculated using two different methods (tallies):

1) the F4 tally and applying the flux-to-dose conversion factors (Section 2.3.1, equation (26)), and
2) the F6 tally which calculates the energy deposited in the cell in MeV/g (Section 2.3.1, equation (27)).

4.2.2.1.1 Average Gamma Dose Rates Calculated using the F4 Tally

The comparison between average gamma dose rate results for the $Gd_{natural}$ absorber parametric studies using CD_2 moderator *vs.* HDPE moderator are summarized in Figure 15 for the 10 cm small SRGS, Figure 16 for the 15 cm small SRGS and Figure 17 for the 20 cm small SRGS. The comparison between average gamma dose results for the $Sm_{natural}$ absorber parametric studies using CD_2 moderator *vs.* HDPE moderator are summarized in Figure 18 for the 10 cm small SRGS, Figure 19 for the 15 cm small SRGS and Figure 20 for the 20 cm small SRGS. A summary of the highest average gamma dose rates in mSv/h obtained from all these parametric studies is provided in Table 8. The computational relative uncertainties(footnote 18, Section 4.1) for all these calculations were <0.2%.

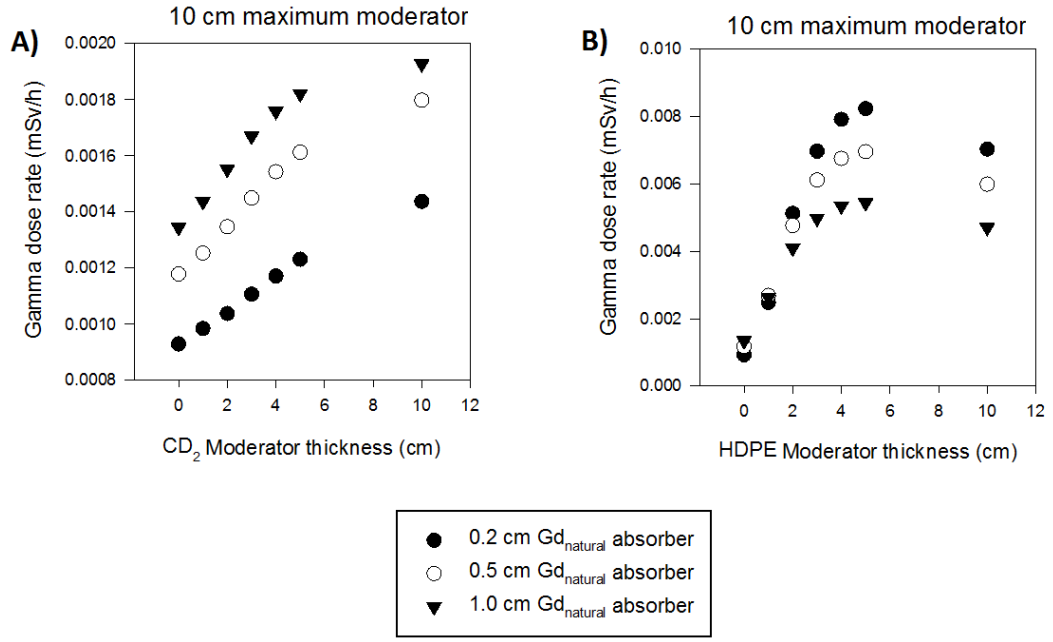

Figure 15 Comparison of average gamma dose rate (mSv/h) *vs.* moderator thickness (cm) for the 10 cm small SRGS, and various $Gd_{natural}$ absorber thicknesses. A) CD_2 moderator; B) HDPE moderator

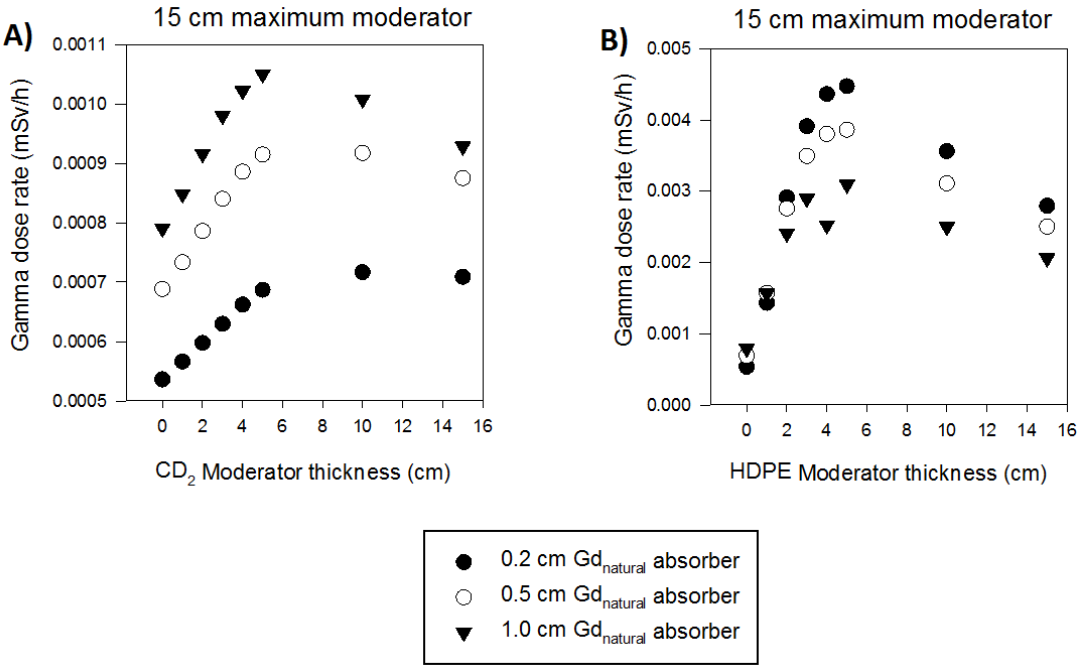

Figure 16 Comparison of average gamma dose rate (mSv/h) *vs.* moderator thickness (cm) for the 15 cm small SRGS, and various $Gd_{natural}$ absorber thicknesses. A) CD_2 moderator; B) HDPE moderator

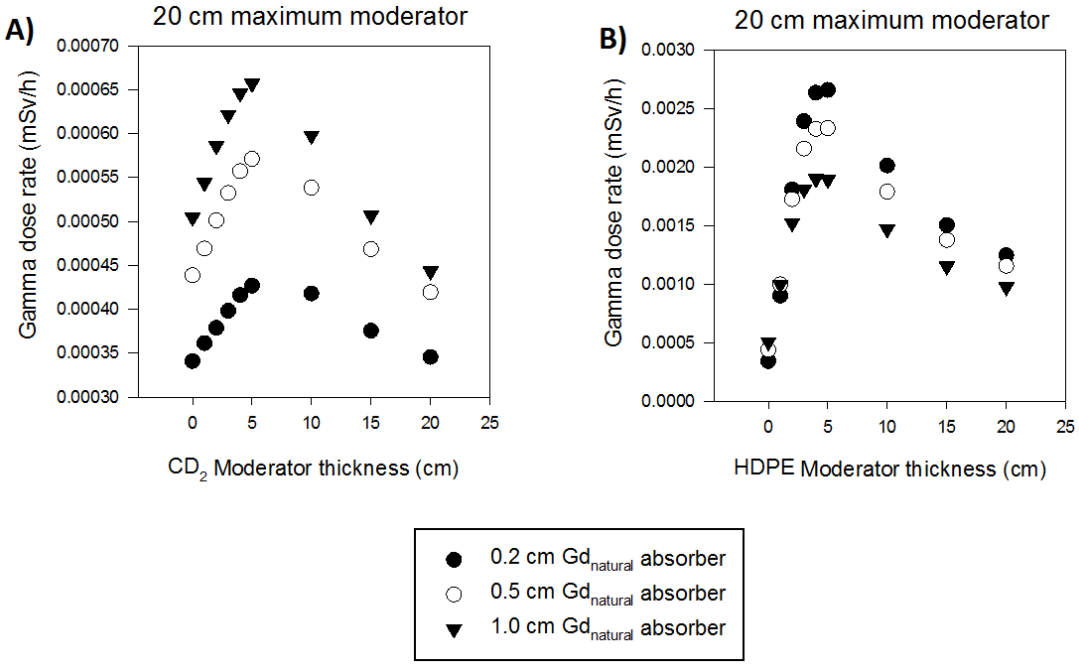

Figure 17 Comparison of average gamma dose rate (mSv/h) *vs.* moderator thickness (cm) for the 20 cm small SRGS, and various $Gd_{natural}$ absorber thicknesses. A) CD_2 moderator; B) HDPE moderator

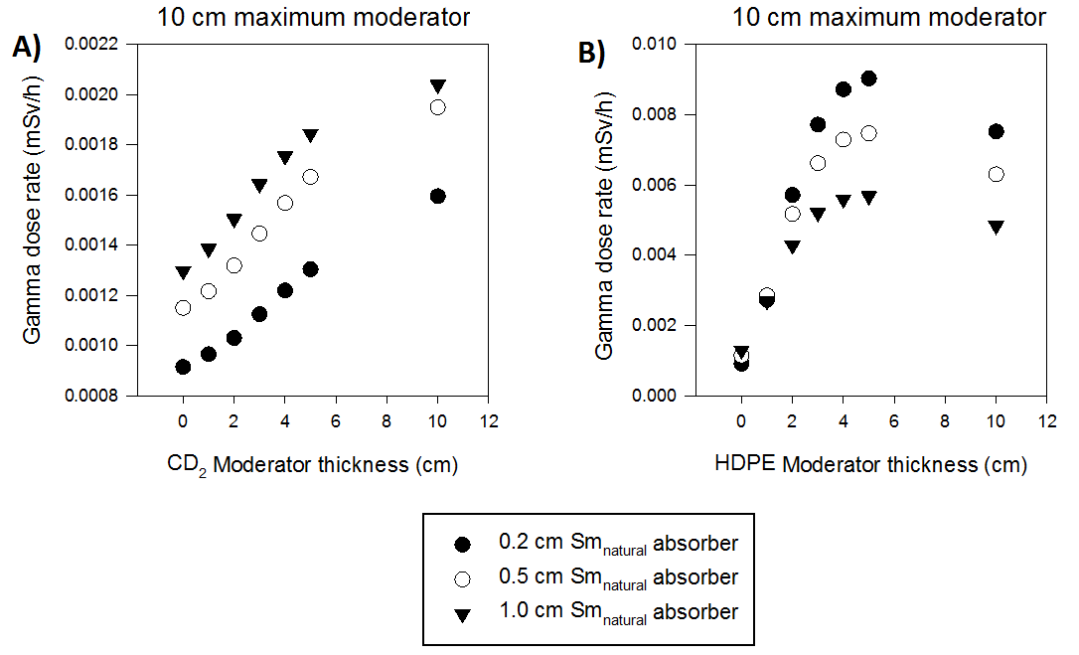

Figure 18 Comparison of average gamma dose rate (mSv/h) *vs.* moderator thickness (cm) for the 10 cm small SRGS, and various $Sm_{natural}$ absorber thicknesses. A) CD_2 moderator; B) HDPE moderator

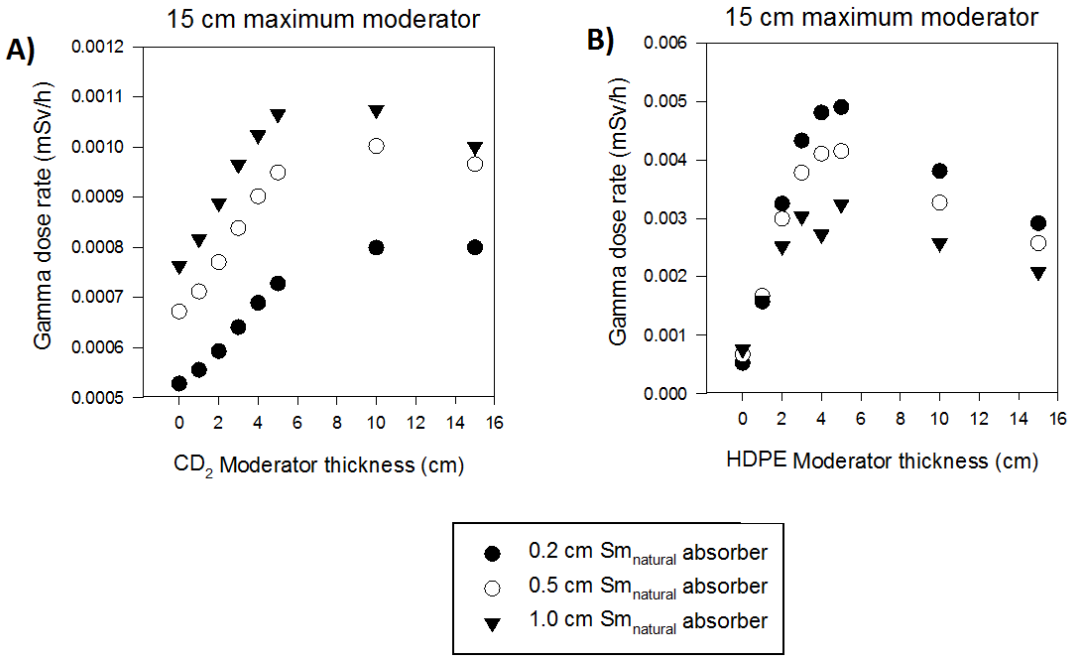

Figure 19 Comparison of average gamma dose rate (mSv/h) *vs.* moderator thickness (cm) for the 15 cm small SRGS, and various $Sm_{natural}$ absorber thicknesses. A) CD_2 moderator; B) HDPE moderator

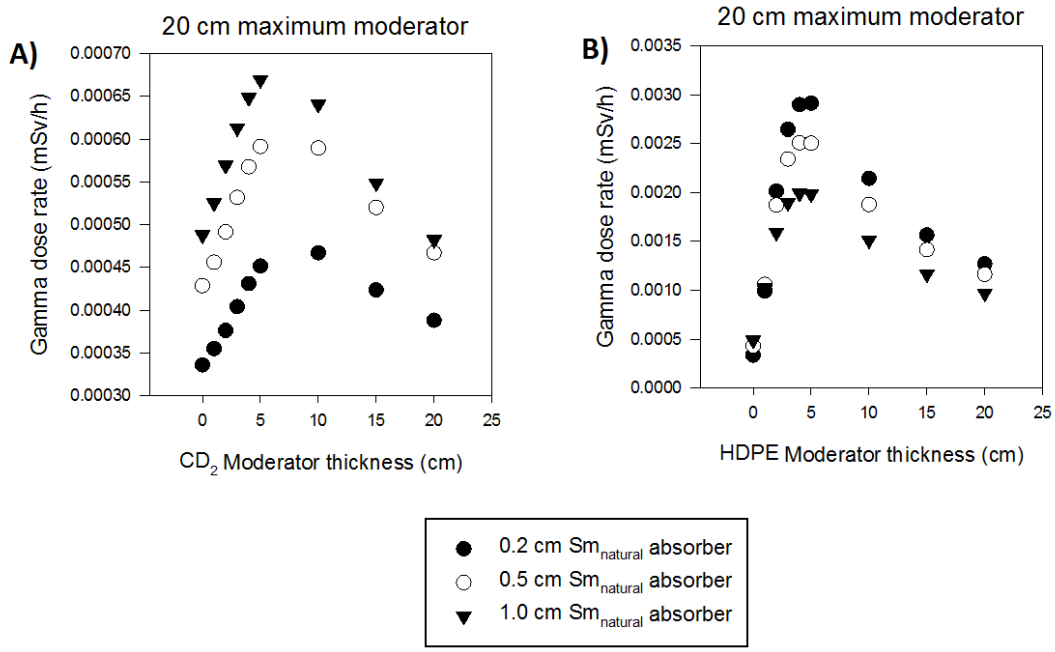

Figure 20 Comparison of average gamma dose rate (mSv/h) *vs.* moderator thickness (cm) for the 20 cm small SRGS, and various $Sm_{natural}$ absorber thicknesses. A) CD_2 moderator; B) HDPE moderator

Table 8 Summary of highest average gamma dose rates (mSv/h) calculated for CD_2 and HDPE moderators and $Gd_{natural}$ and $Sm_{natural}$ absorbers

Max. moderator thickness (cm)	Absorber	Absorber thickness (cm)	Moderator	Moderator thickness (cm)	Average calculated gamma dose rate (mSv/h)
10	$Gd_{natural}$	1.0	CD_2	10	0.002
		0.2	HDPE	5	0.008
	$Sm_{natural}$	1.0	CD_2	10	0.002
		0.2	HDPE	5	0.009
15	$Gd_{natural}$	1.0	CD_2	5	0.001
		0.2	HDPE	5	0.005
	$Sm_{natural}$	1.0	CD_2	5	0.001
		0.2	HDPE	5	0.005
20	$Gd_{natural}$	1.0	CD_2	5	0.001
		0.2	HDPE	5	0.003
	$Sm_{natural}$	1.0	CD_2	5	0.001
		0.2	HDPE	5	0.003

In addition to these parametric studies, a series of mesh tally calculations were performed superimposed on the geometry of the case that resulted in the highest average gamma dose rate for the two moderators. A description of the mesh tally and how it was implemented is provided in Appendix A. The calculated gamma dose rate results for the overall source geometry are illustrated in Figure 21 and Figure 22 for the CD_2 and HDPE moderators, respectively. Also, the calculated gamma dose rate results for a distance of 10 cm away from the YZ face of the source are illustrated in Figure 23 and Figure 24 for the CD_2 and HDPE moderators, respectively. For the mesh tallies, MCNP calculates gamma dose rates averaged over the volume of each mesh cell, as shown and discussed in Appendix A. The computational relative uncertainties associated with these mesh tally results were <0.2%, as provided in the output MCNP files (see also footnote 13, Section 4.1).

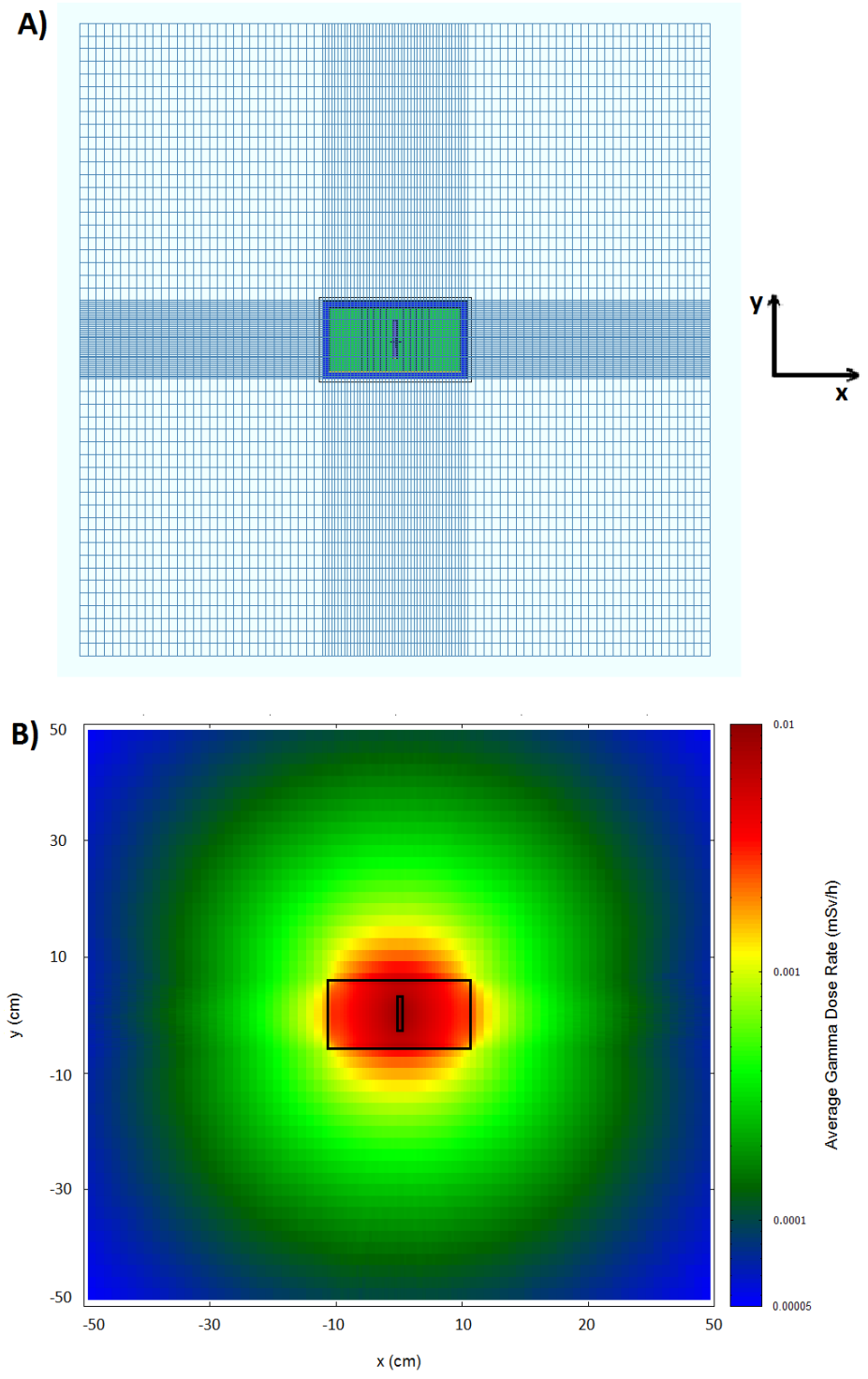

Figure 21 A) XY view of the mesh tally definition for the overall source geometry; B) Average gamma dose rate mesh tally results, using a 1.0 cm $Sm_{natural}$ absorber and 10 cm CD_2 moderator (10 cm small SRGS case).
Mesh tally spans 50 cm on either side of the center of the neutron source.

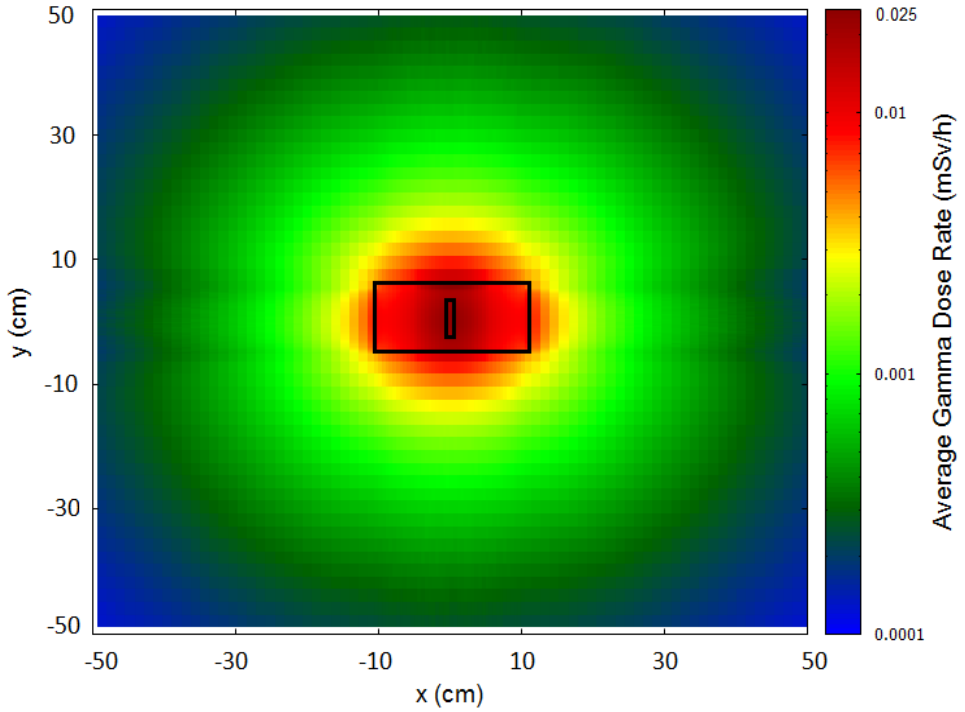

Figure 22 XY view of the average gamma dose rate mesh tally results for the overall source geometry, using a 0.2 cm $Sm_{natural}$ absorber and 5 cm HDPE moderator (10 cm small SRGS case). Mesh tally spans 50 cm on either side of the center of the neutron source. XY view of the mesh tally definition for this source is illustrated in Figure 21A.

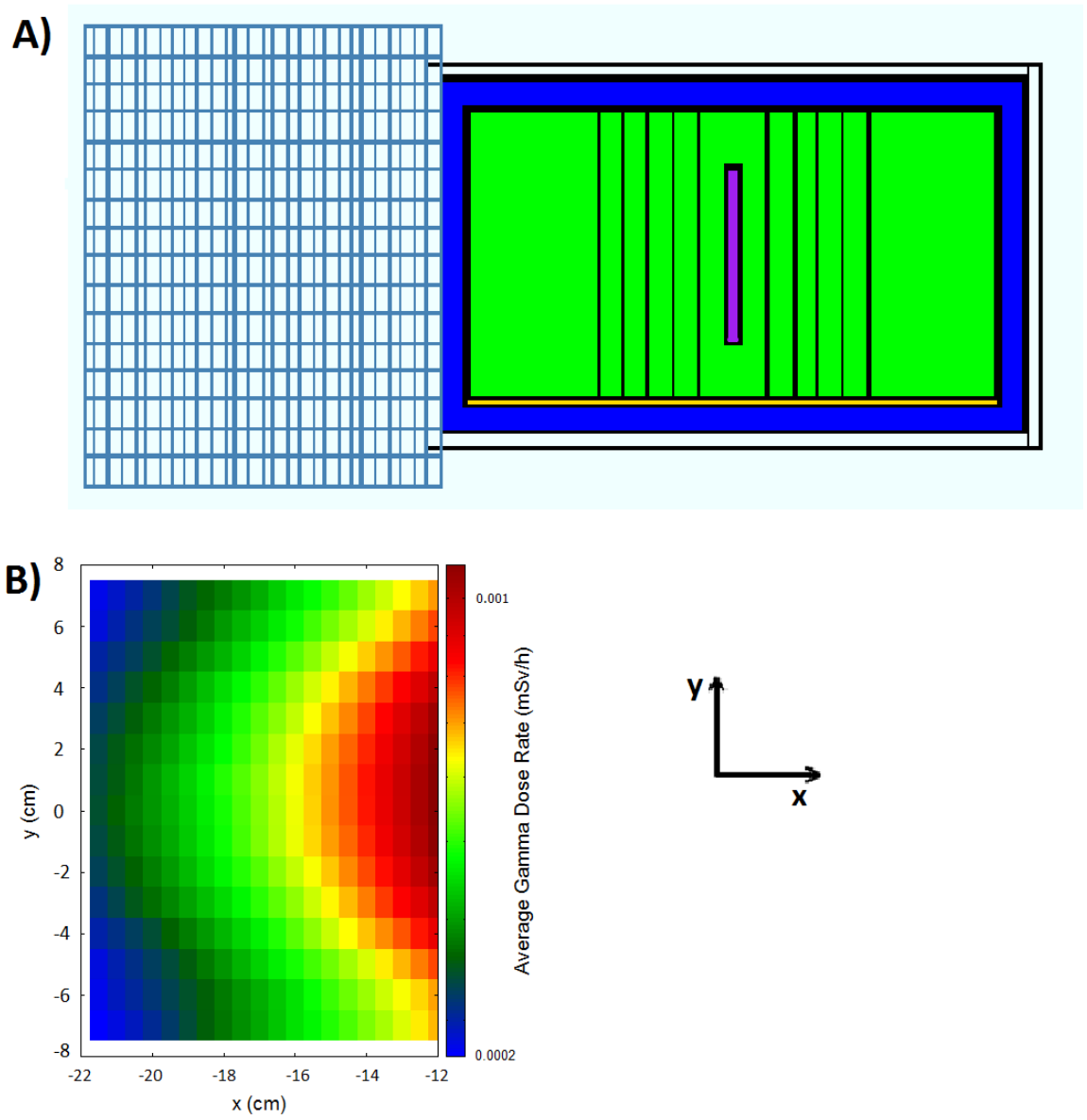

Figure 23 A) XY view of the mesh tally definition a distance of 10 cm away from the YZ face of the source; B) XY view of the average gamma dose rate mesh tally results. These results are for a 1.0 cm $Sm_{natural}$ absorber, 10 cm CD_2 moderator (10 cm small SRGS case).

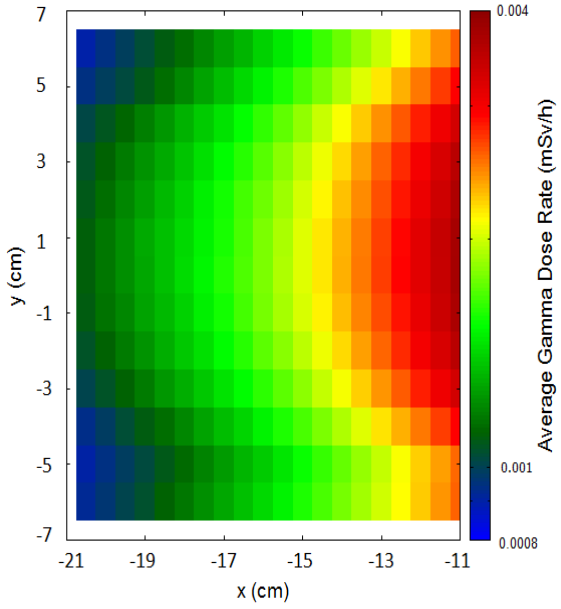

Figure 24 XY view of the average gamma dose rate mesh tally results for a distance of 10 cm away from the YZ face of the source. These results are for a 0.2 cm $Sm_{natural}$ absorber, 5 cm HDPE moderator and maximum source dimension in the x-direction of 20 cm. Example of mesh tally definition and orientation for this source is illustrated in Figure 23A.

4.2.2.1.2 Average Gamma Dose Rates Calculated using the F6 Tally

MCNP simulations were performed to calculate the average gamma dose rates in air region 1 and region 2 using the F6 tally, in mGy/h, to compare these results with those obtained using the F4 tally and the flux-to-dose conversion factors (Section 2.3.1). The $Sm_{natural}$ absorber resulted in higher average gamma dose rates (*e.g.,* 0.009 mSv/h for the 10 cm small SRGS) than the $Gd_{natural}$ absorber (*e.g.*, 0.008 mSv/h for the 10 cm small SRGS) - see Section 4.2.2.1.1, Table 8, thus, only the $Sm_{natural}$ (n, γ)-absorber was used in the parametric study summarized in this section. The results are illustrated in Figure 25 for the 10 cm small SRGS, Figure 26 for the 15 cm small SRGS and Figure 27 for the 20 cm small SRGS. The computational relative uncertainties(footnote 18, Section 4.1) associated with the results reported in these figures were <0.2%.

When comparing gamma doses, the equivalent dose in Sv is equal to the absorbed dose in Gy times a radiation weighing factor (w_r). For gamma radiation and x-rays, this radiation weighting factor is equal to 1 regardless of their energy [21], hence, the equivalent gamma dose in Sv equals the absorbed gamma dose in Gy. Therefore, the average gamma dose rates calculated using the F6 tally (in mGy/h) can be directly compared with those calculated using the flux-to-dose conversion factors applied to the F4 tally, which were summarized in Section 4.2.2.1.1, Figure 18, Figure 19 and Figure 20. The results obtained using the F4 tally and the F6 tally were within 10% of each other. An example of the direct comparison for gamma dose rates calculated using the F6 tally and the F4 tally with flux-to-dose conversion factors applied is illustrated in Figure 28 for the 15 cm small SRGS.

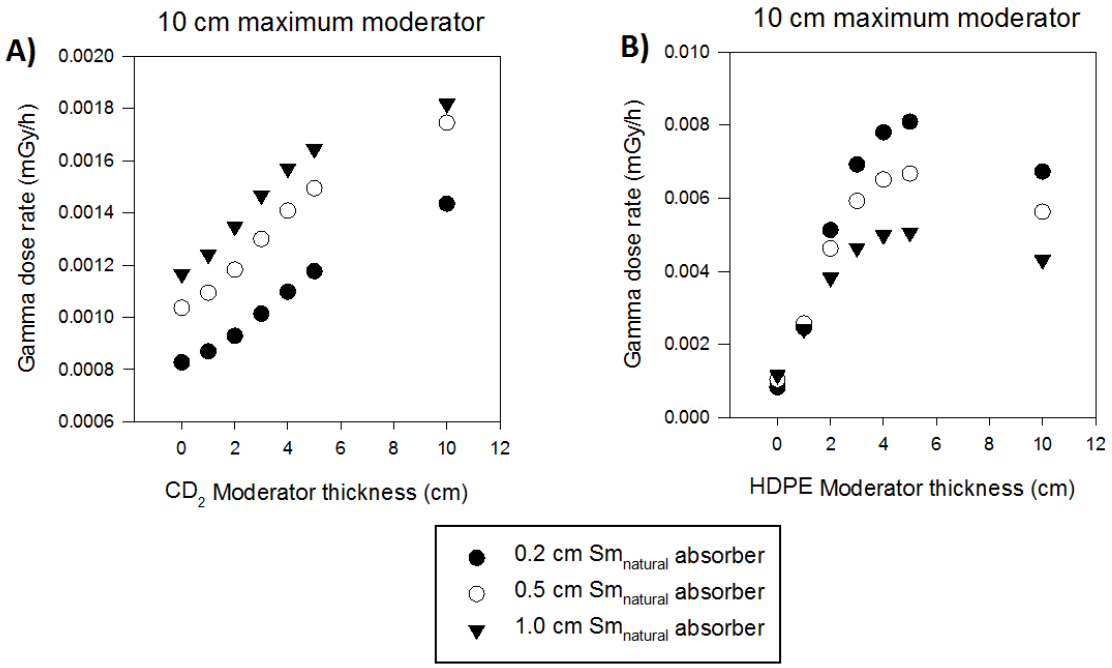

Figure 25 Comparison of average gamma dose rates (mGy/h) calculated using the F6 tally *vs.* moderator thickness (cm) for the 10 cm small SRGS, and various $Sm_{natural}$ absorber thicknesses. A) CD_2 moderator; B) HDPE moderator

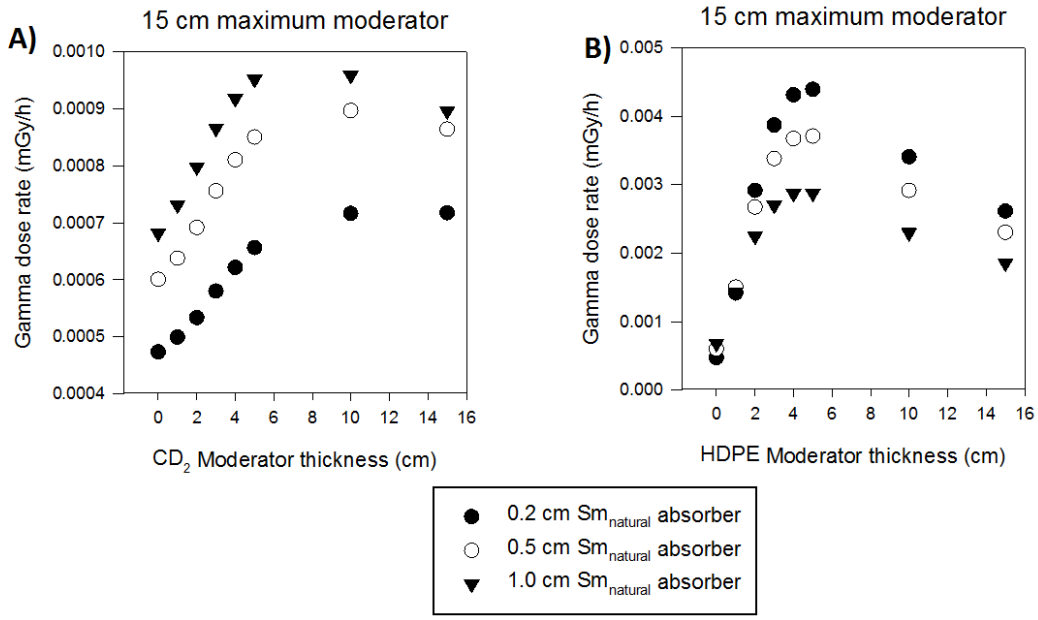

Figure 26 Comparison of average gamma dose rates (mGy/h) calculated using the F6 tally *vs.* moderator thickness (cm) for the 15 cm small SRGS, and various $Sm_{natural}$ absorber thicknesses. A) CD_2 moderator; B) HDPE moderator

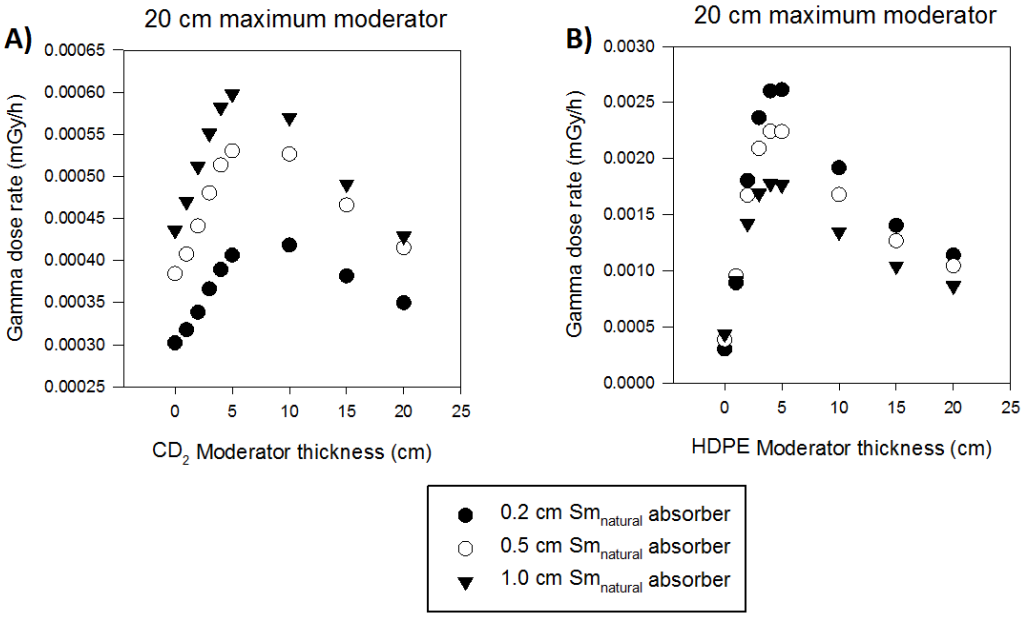

Figure 27 Comparison of average gamma dose rates (mGy/h) calculated using the F6 tally *vs.* moderator thickness (cm) for the 20 cm small SRGS, and various $Sm_{natural}$ absorber thicknesses. A) CD_2 moderator; B) HDPE moderator

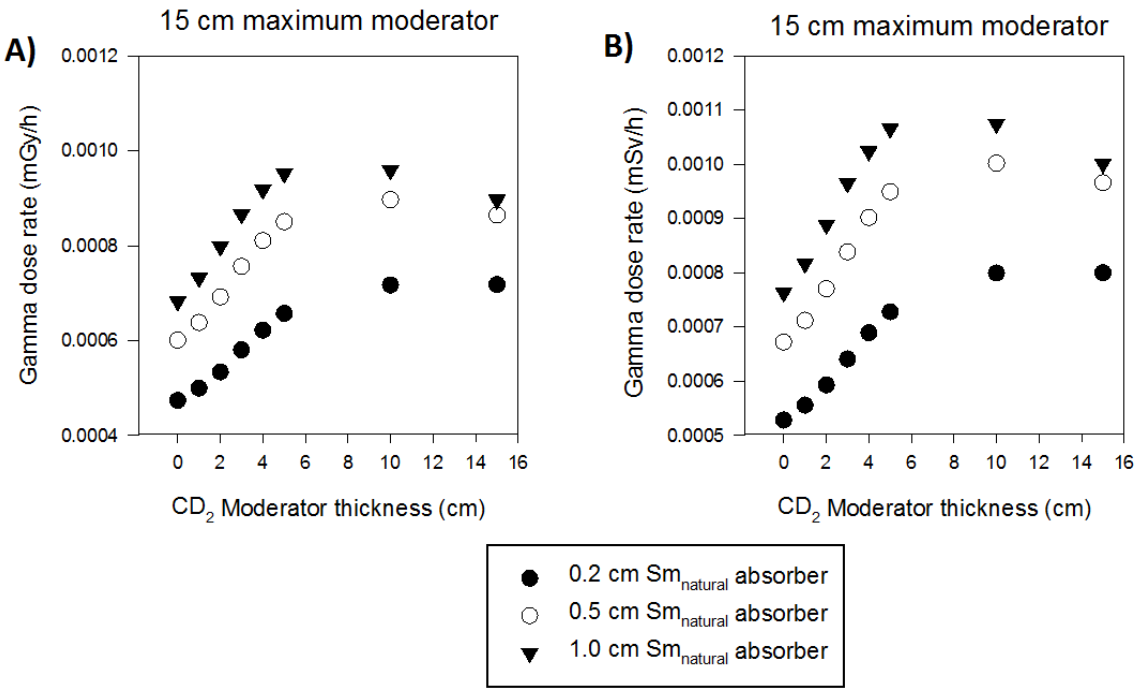

Figure 28 Example of comparison of average gamma dose rates calculated using the F6 tally (A) and the F4 tally with flux-to-dose conversion factors applied (B). Results are illustrated for the 15 cm small SRGS.

4.2.2.1.3 Average Gamma Fluxes Calculated using the F4 Tally

The calculated average gamma fluxes corresponding to the same parametric studies discussed in Section 4.2.2.1.1 are shown in Figure 29, Figure 30 and Figure 31 for the $Gd_{natural}$ absorber and a maximum moderator thickness of 10 cm, 15 cm and 20 cm, respectively, and in Figure 32, Figure 33 and Figure 34 for the $Sm_{natural}$ and a maximum moderator thickness of 10 cm, 15 cm and 20 cm, respectively. The computational relative uncertainties(footnote 18, Section 4.1) associated with the reported results were <0.1%. The maximum values based on the results of these parametric studies are summarized in Table 9.

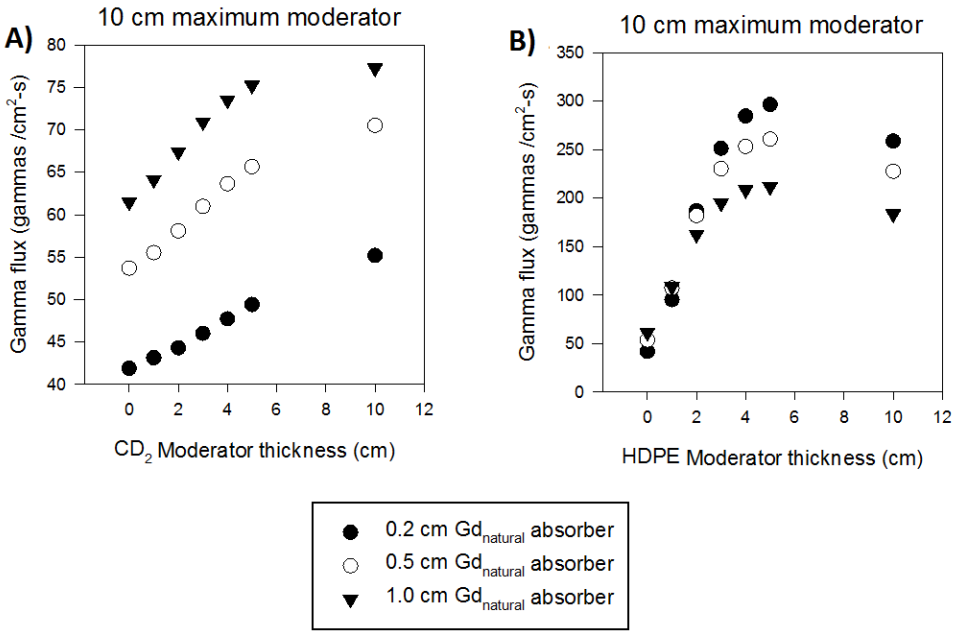

Figure 29 Comparison of average gamma flux (γ/cm^2-s) *vs.* moderator thickness (cm) for the 10 cm small SRGS, and various $Gd_{natural}$ absorber thicknesses. A) CD_2 moderator; B) HDPE moderator

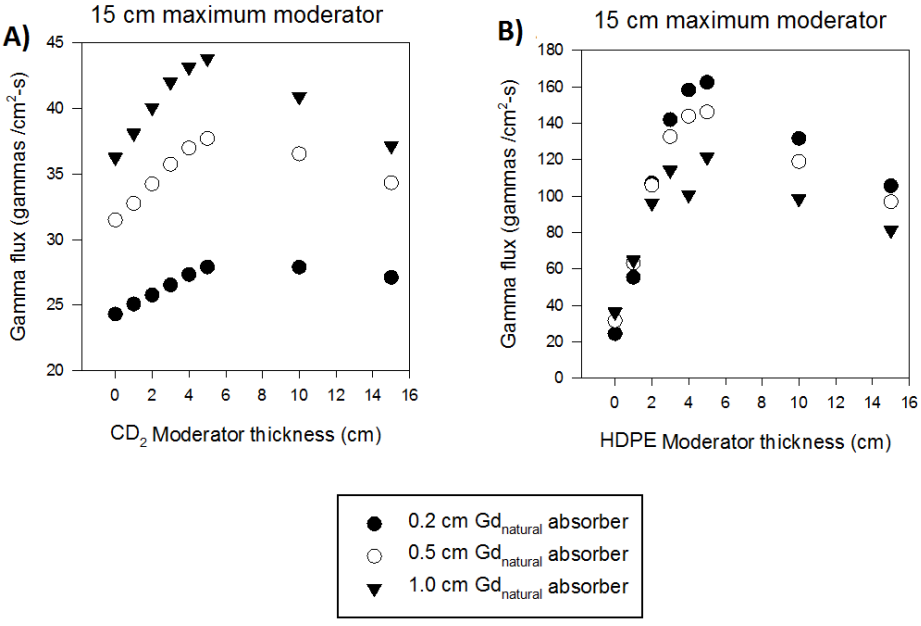

Figure 30 Comparison of average gamma flux (γ/cm^2-s) *vs.* moderator thickness (cm) for the 15 cm small SRGS, and various $Gd_{natural}$ absorber thicknesses. A) CD_2 moderator; B) HDPE moderator

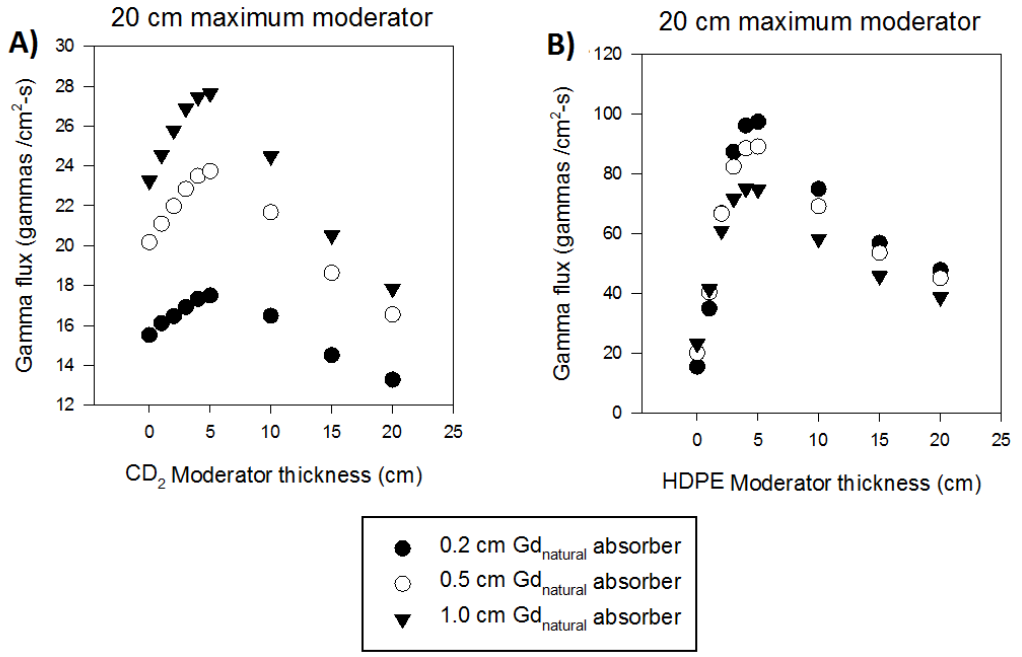

Figure 31 Comparison of average gamma flux (γ/cm^2-s) *vs.* moderator thickness (cm) for the 20 cm small SRGS, and various Gd$_{natural}$ absorber thicknesses. A) CD$_2$ moderator; B) HDPE moderator

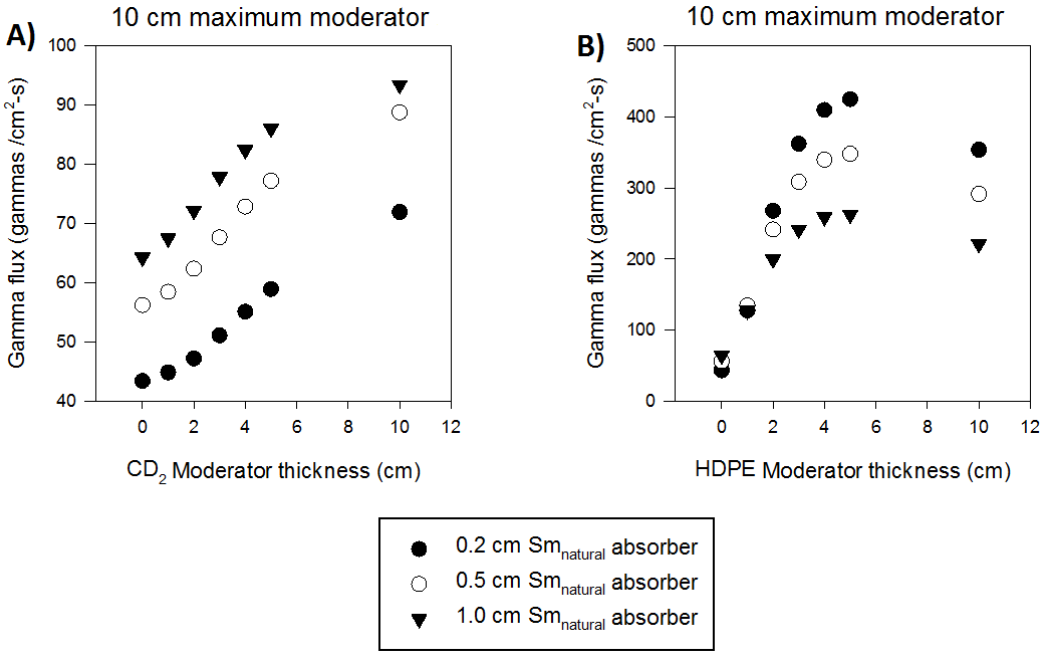

Figure 32 Comparison of average gamma flux (γ/cm^2-s) *vs.* moderator thickness (cm) for the 10 cm small SRGS, and various Sm$_{natural}$ absorber thicknesses. A) CD$_2$ moderator; B) HDPE moderator

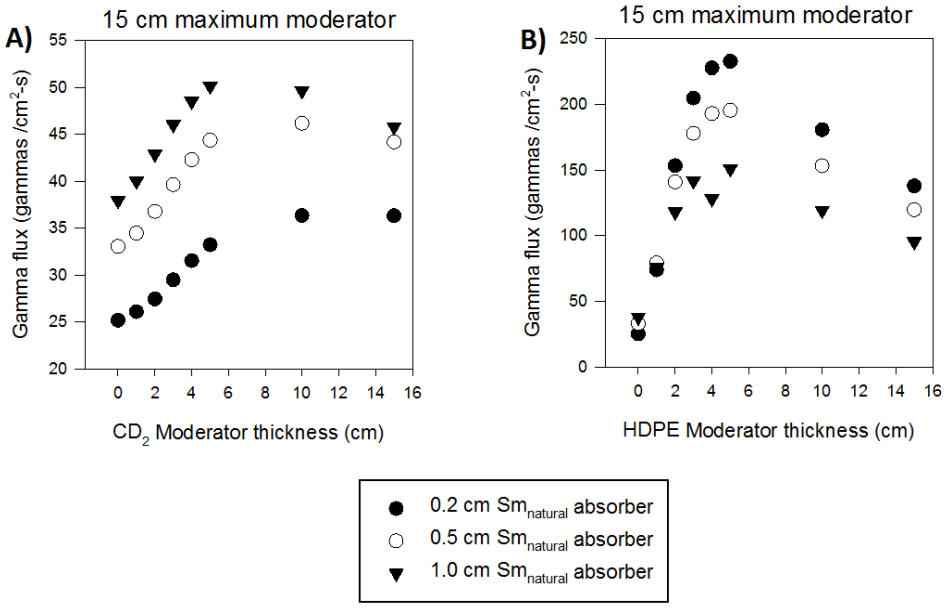

Figure 33 Comparison of average gamma flux (γ/cm^2-s) *vs.* moderator thickness (cm) for the 15 cm small SRGS, and various $Sm_{natural}$ absorber thicknesses. A) CD_2 moderator; B) HDPE moderator

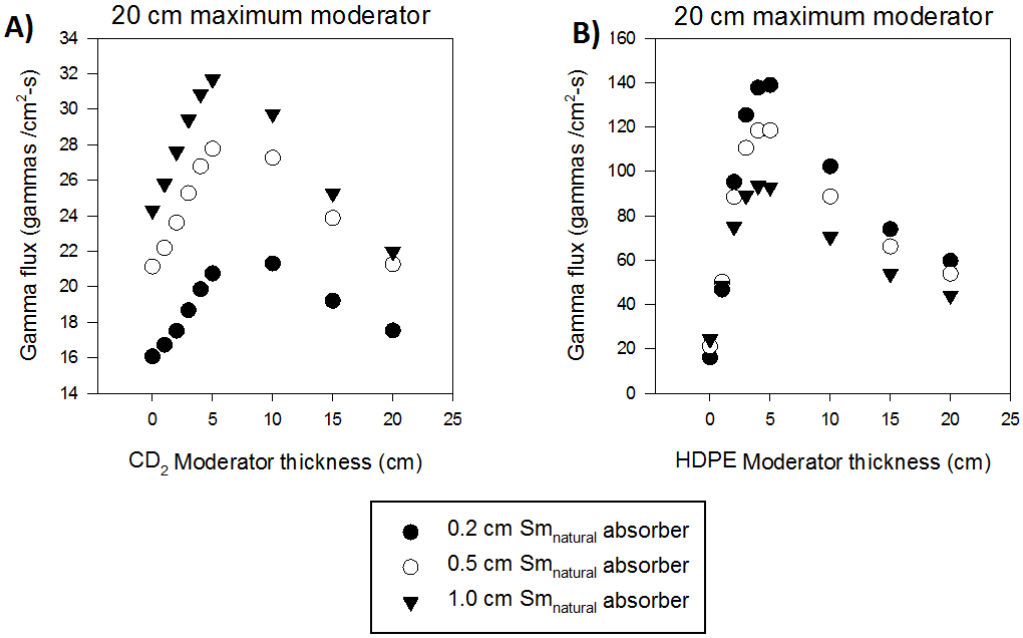

Figure 34 Comparison of average gamma flux (γ/cm^2-s) *vs.* moderator thickness (cm) for the 20 cm small SRGS, and various $Sm_{natural}$ absorber thicknesses. A) CD_2 moderator; B) HDPE moderator

Table 9 Summary of highest average gamma fluxes (γ/cm^2-s) calculated from CD_2 and HDPE moderators and $Gd_{natural}$ and $Sm_{natural}$ absorbers

Max. moderator thickness (cm)	Absorber	Absorber thickness (cm)	Moderator	Moderator thickness (cm)	Average calculated gamma flux (γ / cm^2-s)
10	$Gd_{natural}$	1.0	CD_2	10	77.3
		0.2	HDPE	5	296.5
	$Sm_{natural}$	1.0	CD_2	10	93.4
		0.2	HDPE	5	424.7
15	$Gd_{natural}$	1.0	CD_2	5	43.8
		0.2	HDPE	5	162.5
	$Sm_{natural}$	1.0	CD_2	5	50.1
		0.2	HDPE	5	232.6
20	$Gd_{natural}$	1.0	CD_2	5	27.6
		0.2	HDPE	5	97.5
	$Sm_{natural}$	1.0	CD_2	5	31.7
		0.2	HDPE	5	138.9

A series of mesh tally calculations were performed superimposed on the geometry of the case that resulted in the highest average gamma flux for both moderators. The calculated gamma flux results for the overall source geometry are illustrated in Figure 35 and Figure 36 for the CD_2 and HDPE moderators, respectively. The calculated gamma flux results for a distance of 10 cm away from the YZ face of the source are illustrated in Figure 37 and Figure 38 for the CD_2 and HDPE moderators, respectively. In MCNP, the gamma fluxes were averaged over the volume of each mesh cell, as mentioned in Appendix A. Also, the computational relative uncertainties[(footnote 18, Section 4.1)] associated with these mesh tally results were <0.2%.

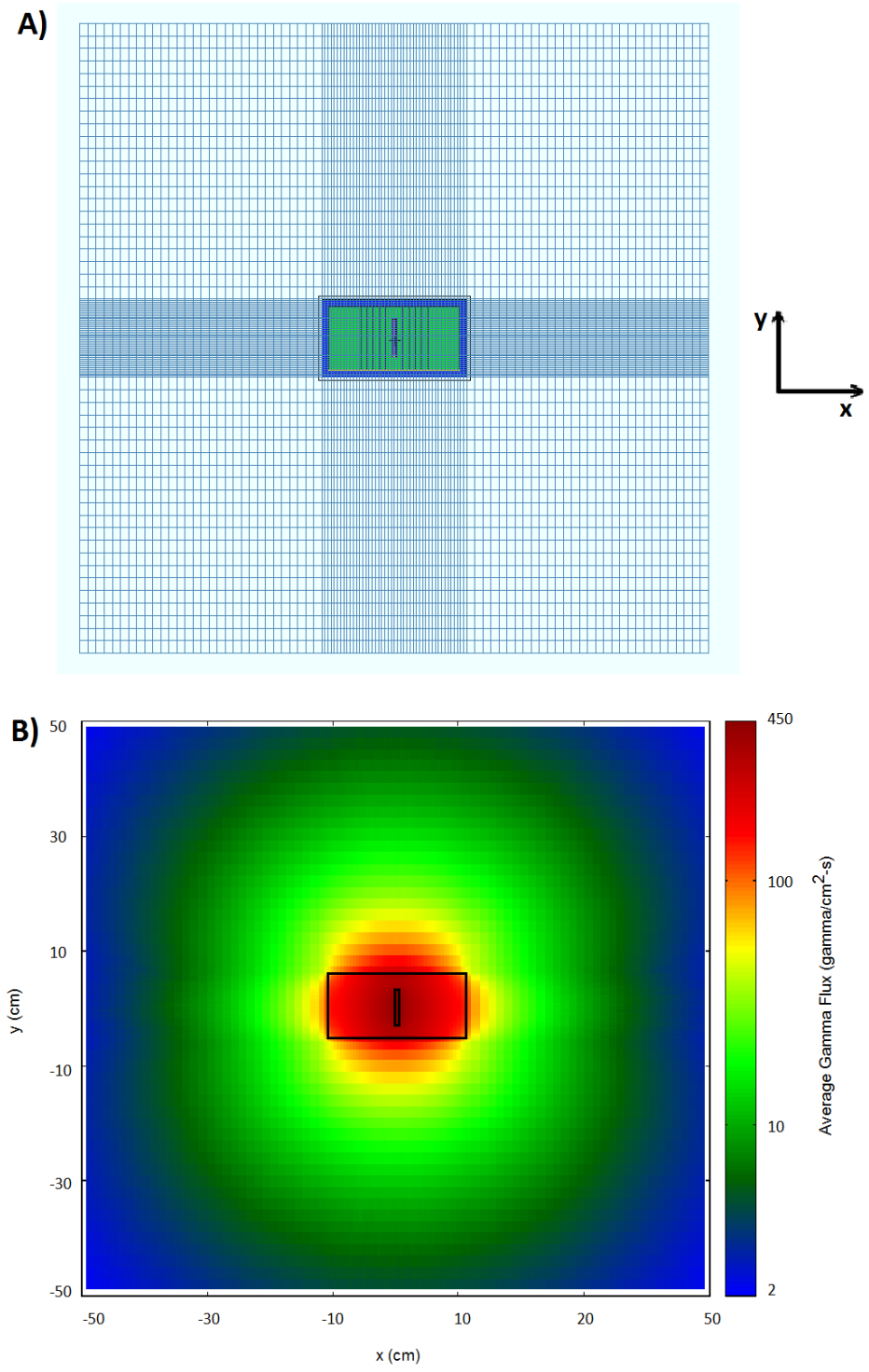

Figure 35 A) XY view of the mesh tally definition for the overall source geometry; B) XY view of the average gamma flux mesh tally results, using a 1.0 cm $Sm_{natural}$ absorber and 10 cm CD_2 moderator (10 cm small SRGS case).
Mesh tally spans 50 cm on either side of the center of the source (*i.e.*, the center of the neutron source).

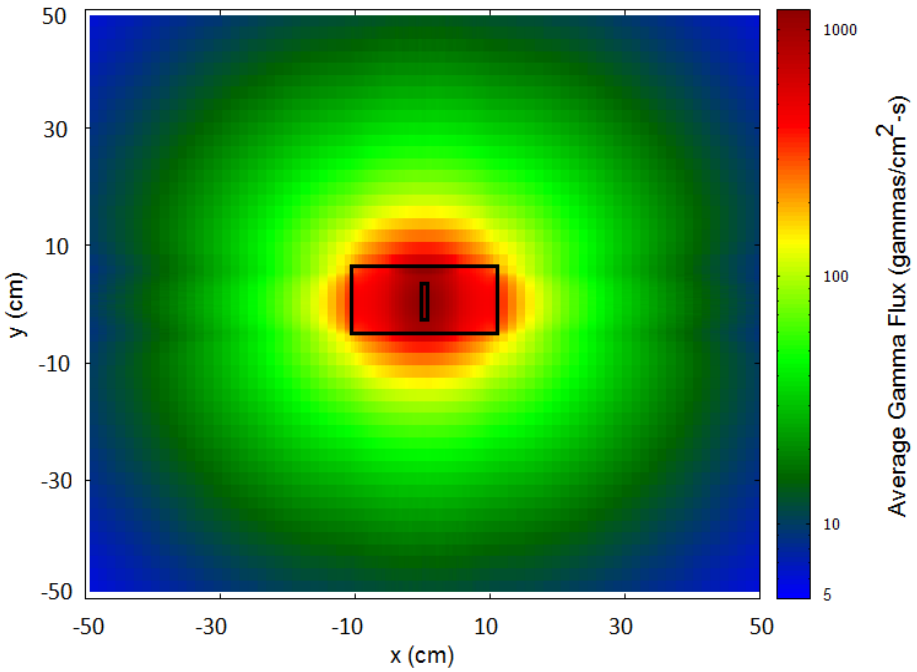

Figure 36 XY view of the average gamma flux mesh tally results for the overall source geometry, using a 0.2 cm $Sm_{natural}$ absorber and 5 cm HDPE moderator (10 cm small SRGS case). Mesh tally spans 50 cm on either side of the center of the source (*i.e.*, the center of the neutron source). Example of mesh tally definition and orientation for this source is illustrated in Figure 35A.

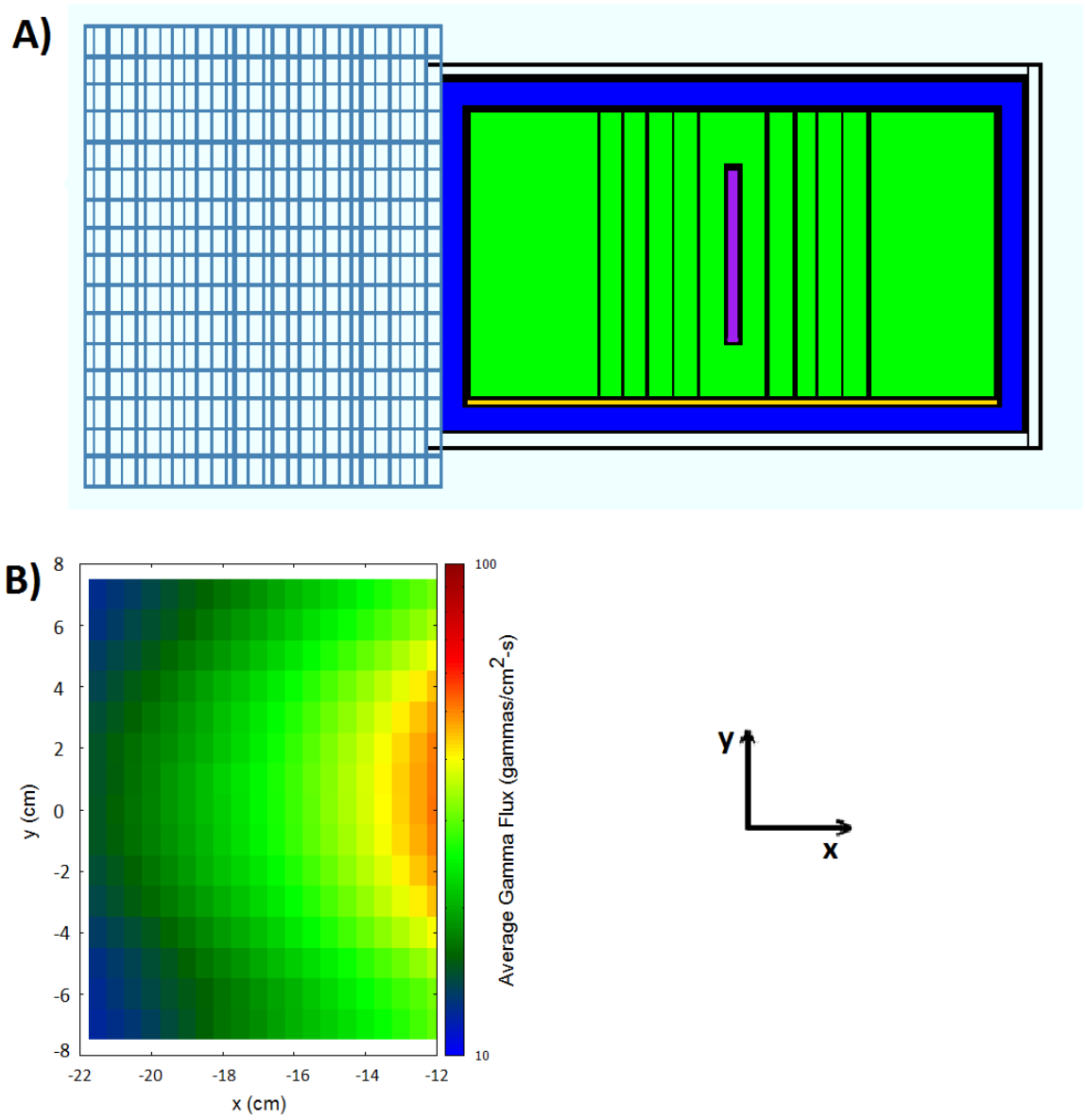

Figure 37 A) XY view of the mesh tally definition for a 10 cm distance away from the YZ face of the SRGS; B) XY view of the average gamma flux mesh tally results. These results are for a 1.0 cm $Sm_{natural}$ absorber, 10 cm CD_2 moderator (10 cm small SRGS case).

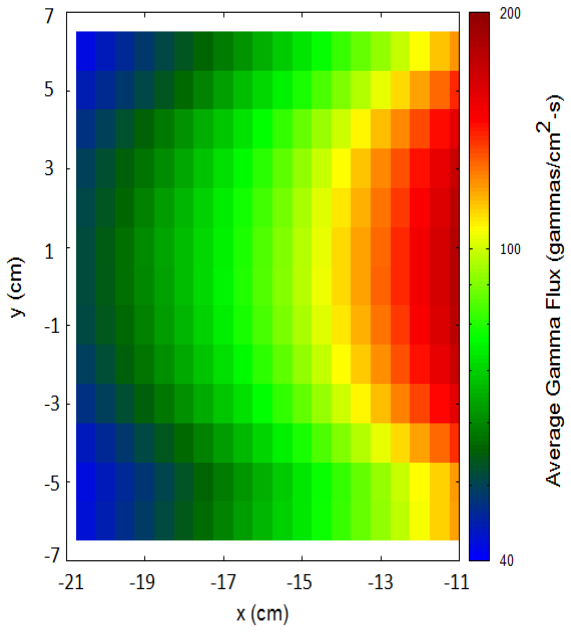

Figure 38 XY view of the average gamma flux mesh tally results for a distance of 10 cm away from the YZ face of the source. These results are for a 0.2 cm $Sm_{natural}$ absorber, 5 cm HDPE moderator (10 cm small SRGS case).
Example of mesh tally definition and orientation for this source is illustrated in Figure 36A.

4.2.2.1.4 Discussion

The results obtained for the various parametric studies summarized in Sections 4.2.2.1.1 to 4.2.2.1.3, show that the shorter the gamma source design, the lower the losses of neutrons and the higher the gamma dose rates and gamma fluxes in air region 1 or region 2 (*i.e.,* the regions of interest, see Figure 9, Section 3.1.2.2). The maximum gamma flux calculated for the10 cm small SRGS, CD_2 moderated, was obtained for a 1 cm thick $Sm_{natural}$ (n, γ)-absorber, at 93.4 γ/cm^2-s, which corresponded to an average gamma dose rate of 0.002 mSv/h. In comparison, for the 15 cm small SRGS (with CD_2 moderator and $Sm_{natural}$ (n, γ)-absorber), the highest calculated average gamma flux was 50.1 γ/cm^2-s, corresponding to an average gamma dose rate of 0.001 mSv/h. This

behaviour was expected because the smaller the source, the lower the number of neutrons that escaped through the XY and XZ faces, contributing to the dose in air region 3, and the higher the fraction of neutrons that reached the absorber close to air region 1 or region 2 (see Figure 9, Section 3.1.2.2). Furthermore, for CD_2, the results were consistent with those discussed in Section 4.2.1, that is, the thicker the (n, γ)-absorber, the higher the average gamma dose rate and gamma flux, because more thermalized neutrons were being absorbed, resulting in more (n, γ) reactions.

The CD_2 moderator parametric studies resulted in higher average gamma fluxes for $Sm_{natural}$ (n, γ)-absorber than $Gd_{natural}$ (n, γ)-absorber:

- 17% (93.4 γ/cm^2-s *vs.* 77.3 γ/cm^2-s) for the 10 cm small SRGS,
- 13% (50.1 γ/cm^2-s *vs.* 43.8 γ/cm^2-s) for the 15 cm small SRGS, and
- 13% (31.7 γ/cm^2-s *vs.* 27.6 γ/cm^2-s), respectively (Table 9, Section 4.2.2.1.3).

However, the calculated average gamma dose rates for both (n, γ)-absorbers were the same: 0.002 mSv/h for the 10 cm small SRGS, 0.001 mSv/h for the 15 cm small SRGS, and 0.001 mSv/h for the 20 cm small SRGS (Table 8, Section 4.2.2.1.1). One possible explanation for why the gamma fluxes are different yet the dose rates are not is because of the differences in the (n, γ) spectra of the two absorbers. The energy deposited in air depends on the energy of the gamma radiation produced by the source. Although the gamma fluxes calculated for $Sm_{natural}$ were higher than those calculated for $Gd_{natural}$, the gamma spectrum resulting from (n, γ) reactions in $Sm_{natural}$ contained a higher percentage of lower energy gammas than those resulting from (n, γ) reactions in $Gd_{natural}$, thus resulting in similar total gamma energy deposition by the two SRGS designs.

For the HDPE moderator and either (n, γ)-absorber, the average gamma flux results obtained for all three small SRGS design were 4 to 5 times higher than those obtained using the CD_2 moderator (*e.g.,* 232.6 γ/cm^2-s using the HDPE moderator *vs.* 50.1 γ/cm^2-s using the CD_2 moderator for the 15 cm small SRGS and $Sm_{natural}$ (n, γ)-absorber, see Table 9, Section 4.2.2.1.3). Also, the average gamma dose rate results were 3 to 5 times higher than those calculated for the CD_2 moderator for both (n, γ)-absorbers (*e.g.,* 0.005 mSv/h using HDPE moderator *vs.* 0.001 mSv/h using CD_2 moderator, for the 15 cm small SRGS and and $Sm_{natural}$ (n, γ)-absorber, see Table 8, Section 4.2.2.1.1). This outcome was expected because the number of collisions required for the high energy neutrons to thermalize is lower for hydrogen (18 collisions) than for deuterium (24 collisions) (Section 2.1.2.3, Table 1). Although hydrogen is better at slowing down neutrons than deuterium (*i.e.,* fewer collisions required to decrease the neutron energy by the same amount), it also has a higher neutron absorption cross-section. When compared with CD_2, which has an estimated moderating ratio of 906, HDPE has a moderating ratio approximately equal to that of light water (72 for HDPE *vs.* 71 for light water, see Table 3, Section 2.1.2.3). The effect of neutron absorption in the moderator on both average gamma dose rate and gamma flux can be observed for the 10 cm small SRGS for both $Gd_{natural}$ and $Sm_{natural}$ (n, γ)-absorbers (see Figure 15 and Figure 18 for the gamma dose rates, and Figure 29 and Figure 32 for the gamma fluxes, for $Gd_{natural}$ and $Sm_{natural}$ (n, γ)-absorbers, respectively). For these parametric studies, the maximum dose rates and fluxes occurred at a moderator thickness of 5 cm when HDPE was used, instead of 10 cm for the cases when CD_2 was used. However, the highest average values for the gamma dose rate and the gamma flux were obtained at an (n, γ)-absorber thickness of 0.2 cm for

the sources that used HDPE as a moderator. One possible explanation is that the self-shielding effects produced by the (n, γ)-absorber region were greater for the HDPE cases than for the CD_2 ones as a result of the neutrons being more thermalized by HDPE than CD_2.

The gamma spectrum resulting from the proposed SRGS design is important for the SPECT gamma camera calibration (Section 2.2.1). The gamma cameras are sensitive to the variations in energies of the gamma source, especially for energies >500 keV, which was observed experimentally in [35]. Figure 39 shows the fraction of total gamma flux *vs.* energy (MeV) for the two small SRGS cases resulting in the highest calculated gamma flux:

- 0.2 cm $Sm_{natural}$ absorber, 5 cm HDPE moderator, 10 cm small SRGS (Figure 39A), and
- 1.0 cm $Sm_{natural}$ absorber, 10 cm CD_2 moderator, 10 cm small SRGS (Figure 39B).

A significant percentage of gammas produced by the proposed source had energies greater than 500 keV (79% for HDPE moderator and 85% for CD_2 moderator), and between 25% - 30% of the gammas had energies between 1 MeV and 2 MeV (Figure 39). Using the proposed SRGS as a flood source for SPECT calibration would lead to high count rates similar to those observed in [35], which are the result of the tail of these high energy photons. Such high count rates would cause the detector gain to be incorrectly calibrated (see also Section 2.2.1). Furthermore, the maximum calculated average gamma flux (424.7 γ/cm^2-s for the 10 cm small SRGS, using HDPE moderator and $Sm_{natural}$ (n, γ)-absorber, Table 9, Section 4.2.2.1.3) is 3 to 4 orders of magnitude smaller than the current ^{57}Co flood sources which would result in a calibration time

increase from minutes to a few days; thus making the proposed SRGS not practical for a SPECT gamma camera flood source.

Finally, the feasibility of the SRGS as a blood irradiator can be determined by comparing the typical dose applied during blood irradiation (20 – 40 Gy, see Section 2.2.2) with the total dose that could be delivered in a reasonable time (*e.g.,* 1 hour) by the proposed SRGS (*i.e.,* 0.009 mSv of γ dose). The dose rates calculated for different SRGS designs can be found in Section 4.2.2.1.1, Table 8. Using the maximum calculated dose rate (*i.e.,* 0.009 mSv/h), the required time for the SRGS to deposit 20 Gy[27] of γ radiation would be ~254 years, thus, the proposed SRGS design is not practically feasible as a blood irradiator because of time constraints.

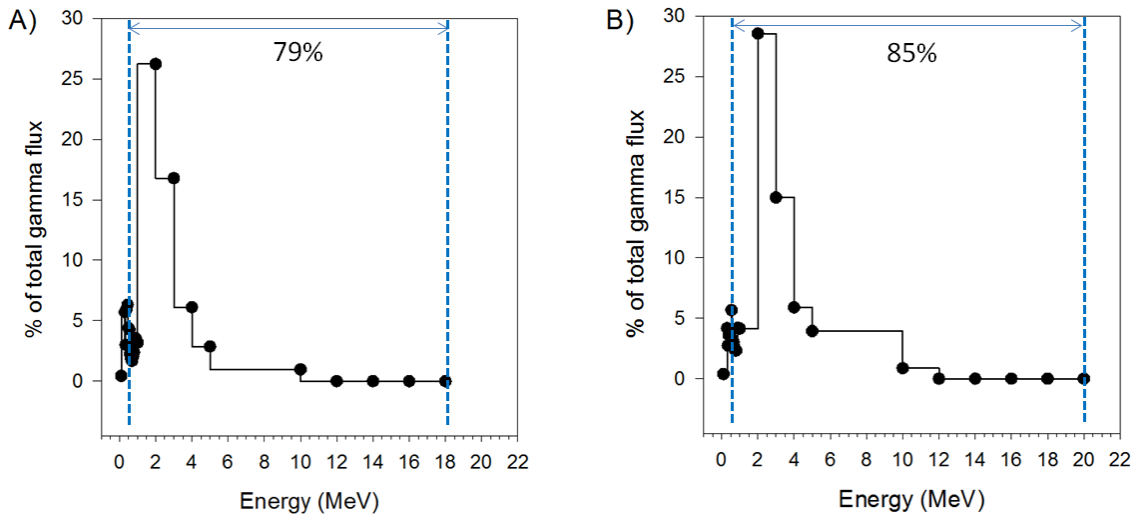

Figure 39 Gamma spectrum corresponding to the models resulting in the maximum average gamma fluxes (*i.e.*, for a 10 cm small SRGS).
A) Percentage of total gamma flux *vs.* energy (MeV) for a 0.2 cm $Sm_{natural}$ absorber and 5 cm HDPE moderator; B) Percentage of total gamma flux *vs.* energy (MeV) for a 1.0 cm $Sm_{natural}$ absorber and 10 cm CD_2 moderator

[27] For gamma radiation, 1 Gy is equivalent to 1 Sv (see Section 4.2.2.1.2); hence, 0.009 mSv/h ≈ 0.009 mGy/h. Therefore, time = 20 Gy / 0.009 mGy/h × 1day / 24 h × 1 year / 365.25 days ≈ 254 years.

4.2.2.2 Calculated Average Neutron Dose Rates and Fluxes

The neutron dose rates and fluxes corresponding to the SRGS designs investigated above have been calculated to look at the neutrons that escape from the source without producing any gamma radiation. The term "neutron escape", as used in this research, refers to both neutrons leakage out of the gamma source, and neutron absorption that does not produce gamma radiation via (n, γ) reactions. Ideally, all neutrons produced by the neutron source and via (n, xn)[(footnote 6, Section 2.1.2.3)] reactions in the SRGS, should be absorbed, resulting in (n, γ) reactions. However, this cannot be realistically achieved as neutrons will always escape from the gamma source.

The average neutron dose rates were calculated using MCNP and the neutron flux-to-dose conversion factors in Section 2.3.1, Table 4, which convert the neutron flux (in n/cm^2-s) directly to equivalent dose rate in rem/h. These factors account for the conversion between flux to absorbed dose rate in Gy/h as well as absorbed dose rate to equivalent dose rate in rem/h (MCNP User Manual [8]). The results in rem/h were then converted to mSv/h using the 100 rem = 1 Sv conversion.

Figure 40, Figure 41 and Figure 42 summarize the average neutron dose rates in mSv/h for the 10 cm small SRGS, 15 cm small SRGS and 20 cm small SRGS, respectively, for the $Sm_{natural}$ (n, γ)-absorber parametric studies using the two different moderators (*i.e.,* CD_2 and HDPE). Figure 43, Figure 44 and Figure 45 summarize the average neutron flux in n/cm^2-s, corresponding to the $Sm_{natural}$ (n, γ)-absorber parametric studies for the two different moderators and three source dimensions. The computational relative uncertainties[(footnote 18, Section 4.1)] associated with the results reported were <0.2%.

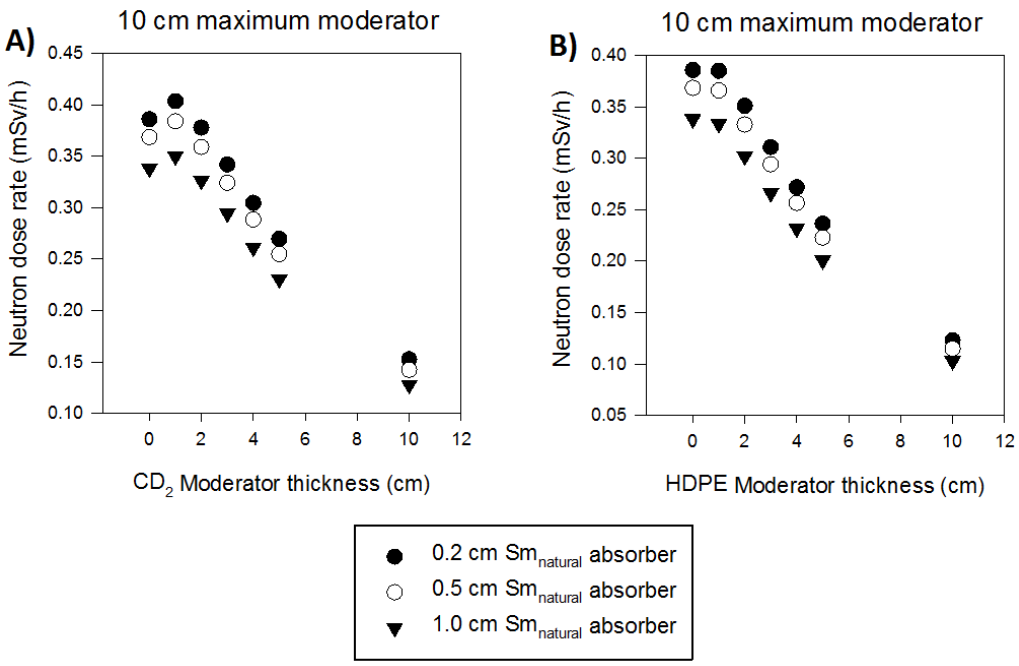

Figure 40 Comparison of average neutron dose rate (mSv/h) *vs.* moderator thickness (cm) for the 10 cm small SRGS, and various $Sm_{natural}$ absorber thicknesses. A) CD_2 moderator; B) HDPE moderator

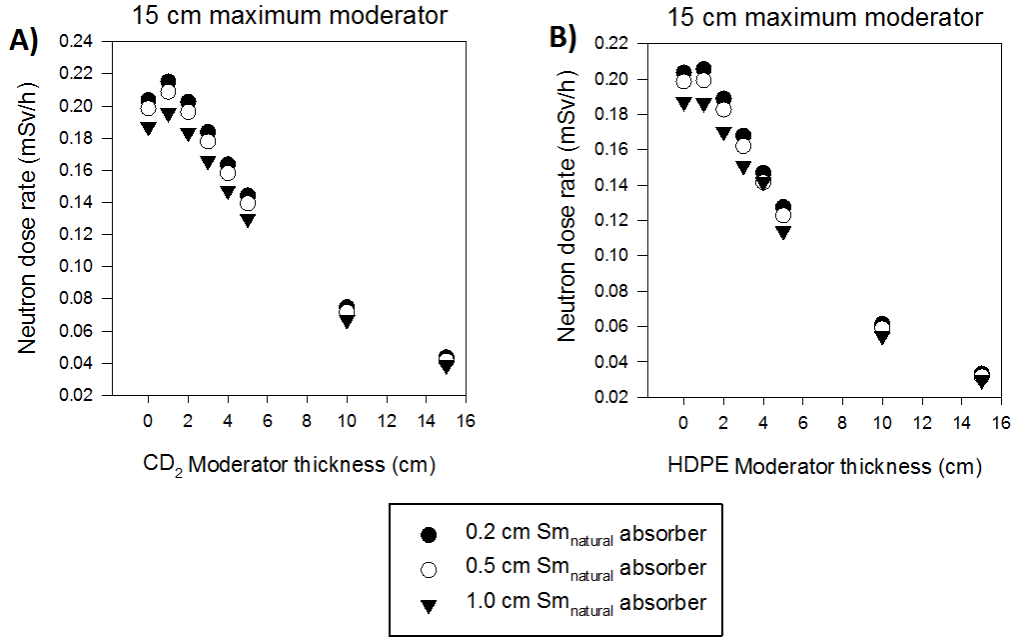

Figure 41 Comparison of average neutron dose rate (mSv/h) *vs.* moderator thickness (cm) for the 15 cm small SRGS, and various $Sm_{natural}$ absorber thicknesses. A) CD_2 moderator; B) HDPE moderator

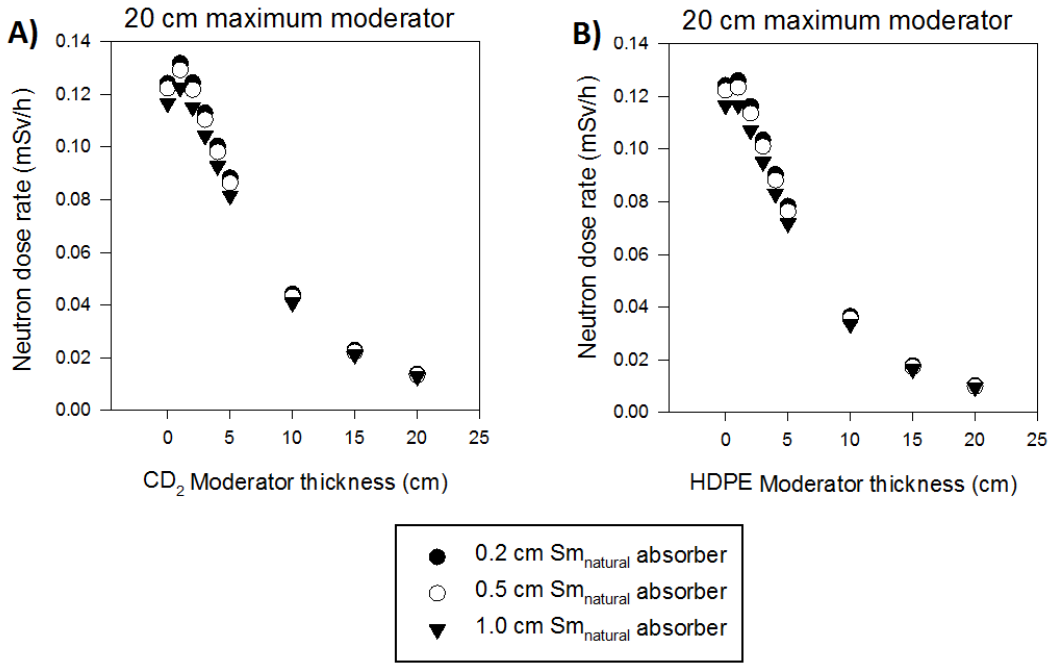

Figure 42 Comparison of average neutron dose rate (mSv/h) *vs.* moderator thickness (cm) for the 20 cm small SRGS, and various $Sm_{natural}$ absorber thicknesses. A) CD_2 moderator; B) HDPE moderator

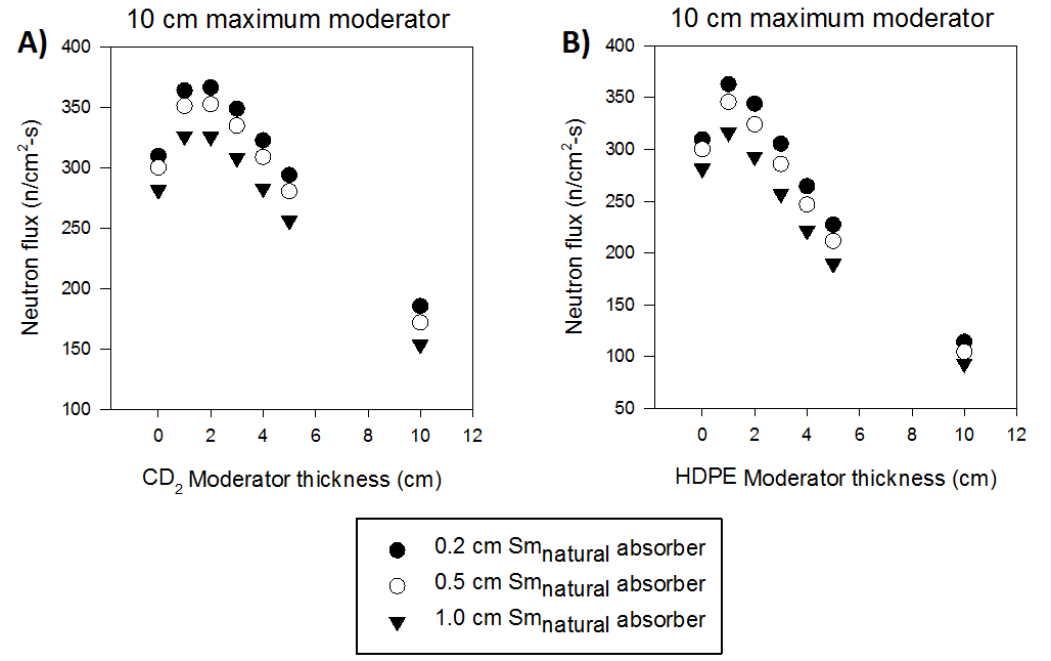

Figure 43 Comparison of average neutron flux (n/cm^2-s) *vs.* moderator thickness (cm) for the 10 cm small SRGS, and various $Sm_{natural}$ absorber thicknesses. A) CD_2 moderator; B) HDPE moderator

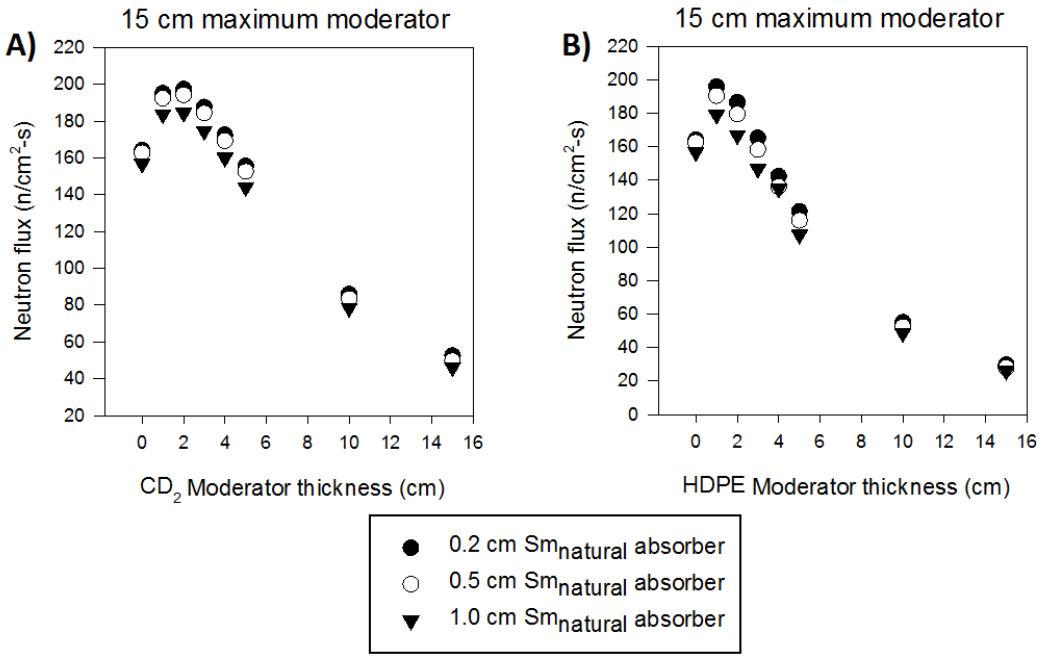

Figure 44 Comparison of average neutron flux (n/cm^2-s) *vs.* moderator thickness (cm) for the 15 cm small SRGS, and various $Sm_{natural}$ absorber thicknesses. A) CD_2 moderator; B) HDPE moderator

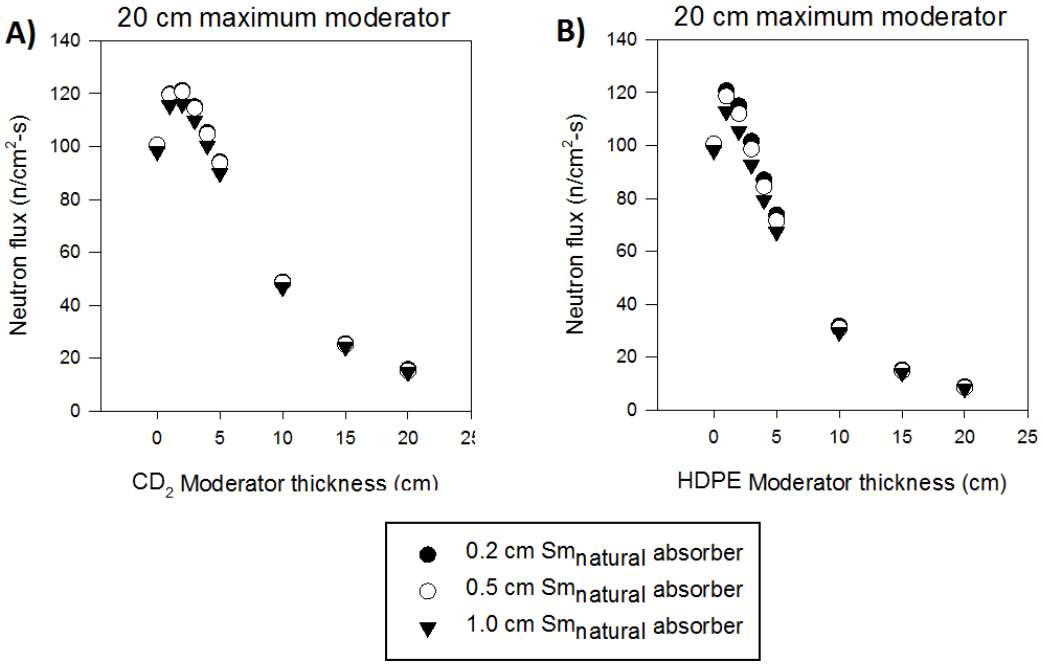

Figure 45 Comparison of average neutron flux (n/cm^2-s) *vs.* moderator thickness (cm)for the 20 cm small SRGS, and various $Sm_{natural}$ absorber thicknesses. A) CD_2 moderator; B) HDPE moderator

Figure 40 to Figure 42 show average neutron dose rates. Gamma dose rates corresponding to the same parametric studies are summarized in Figure 18 to Figure 20, Section 4.2.2.1.1. The calculated average neutron dose rates were approximately 100 to 200 times higher than the calculated gamma dose rates for the CD_2 moderator and ~40 times higher than for the HDPE moderator. The biological effect of neutrons is different than that of gammas. When converting from absorbed dose (in Gy) to equivalent dose in (Sv) the radiation weighing factor (w_R) for neutrons is 5 (for neutrons <10 keV), 10 (for neutrons between 10 keV to 100 keV), 20 (for neutrons between 100 keV and 2 MeV), 10 (for neutrons between 2 MeV and 20 MeV) and 5 (for neutrons >20 MeV) [21]. In comparison, w_R for gammas is 1 (see Section 4.2.2.1.2) [21]. The (α, n) source used in the SRGS has 88% of the neutrons with energies >1 MeV (Figure 8, Section 3.1.2.2), and because of the small SRGS dimensions, the neutrons would escape without causing an (n, γ) reaction. These higher energy neutrons would result in an equivalent dose rate outside the SRGS that is higher than the equivalent gamma dose rate.

The average neutron fluxes were 4 times larger than the gamma fluxes for the CD_2 moderator (*e.g.,* Figure 43A *vs*. Figure 32A, Section 4.2.2.1.3), while the average neutron fluxes for the HDPE moderator were within 15% of each other (*e.g.,* Figure 43B *vs*. Figure 32B, Section 4.2.2.1.3). Two possible explanations for these results are:

- The neutron spectrum reaching the (n, γ)-absorber region is more thermalized when the HDPE moderator is used, thus, increasing the probability of neutrons being absorbed and producing gammas.
- Hydrogen has a higher absorption cross-section compared to deuterium (see Table 2, Section 2.1.2.3), resulting in more neutrons being absorbed in the

moderator region. However, the net effect of using HDPE instead of CD_2 is that the neutrons are moderated faster, increasing their probability of absorption in the (n, γ)-absorber.

4.2.3 Comparing Results for Lead and Carbon Steel Reflector / Shield

Neutrons leakage into air region 3 (*i.e.,* on the y- and z-sides of the SRGS, see Figure 9, Section 3.1.2.2) decreases the gamma production on the YZ faces, which would face the gamma cameras (Figure 2). A number of parametric studies were carried out for the case of a 0.5 cm $Sm_{natural}$ absorber and different CD_2 moderator thicknesses to investigate the impact of a 1.9 cm thick reflector and/or shield around the neutron source, in the y- and z- directions (see Figure 10B, Section 3.1.2.2). Two materials were investigated as part of these parametric studies: carbon steel and lead. These materials provide gamma shielding on the XY and XZ sides of the SRGS (see Figure 9, Section 3.1.2.2), and could also potentially result in some of the neutrons scattering back inside the source instead of leaking out of the modelled system.

The results for these parametric studies are shown in Figure 46 and Figure 47 for the average gamma dose rates (in mSv/h) and gamma flux (in γ/cm^2-s), respectively. Carbon steel resulted in higher average gamma doses and fluxes than lead. Also, the MCNP results showed that, for these designs, gamma radiation was also produced in both the carbon steel and the lead reflector / shield, with average energies of 1.4 MeV to 1.6 MeV. Table 10 summarizes the highest calculated gamma dose rate and gamma dose flux for the carbon steel models in comparison with the corresponding gamma doses and fluxes for the SRGS models reported in Section 4.2.2.1.1 and Section 4.2.2.1.2. Based on

these results, it was concluded that the addition of the carbon steel reflector/shield on the inside of the source (Figure 10, Model B) did not result in additional benefit to the SRGS design in terms of increasing the average gamma dose rate or flux.

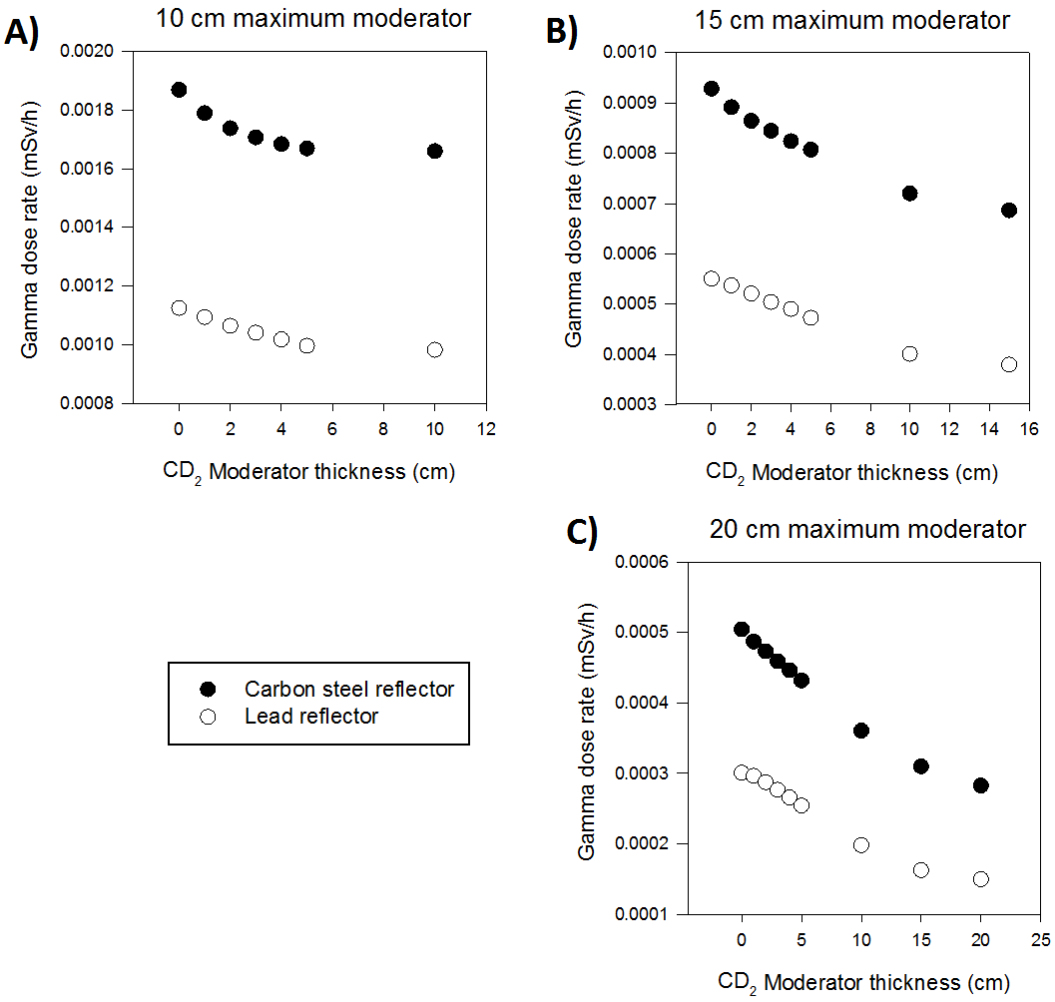

Figure 46 Comparison of average gamma dose rate (mSv/h) *vs.* moderator thickness (cm) for the small SRG source with two different reflector / shielding materials: carbon steel and lead. Results for: A) the 10 cm small SRGS; B) the 15 cm small SRGS; and C) the 20 cm small SRGS.

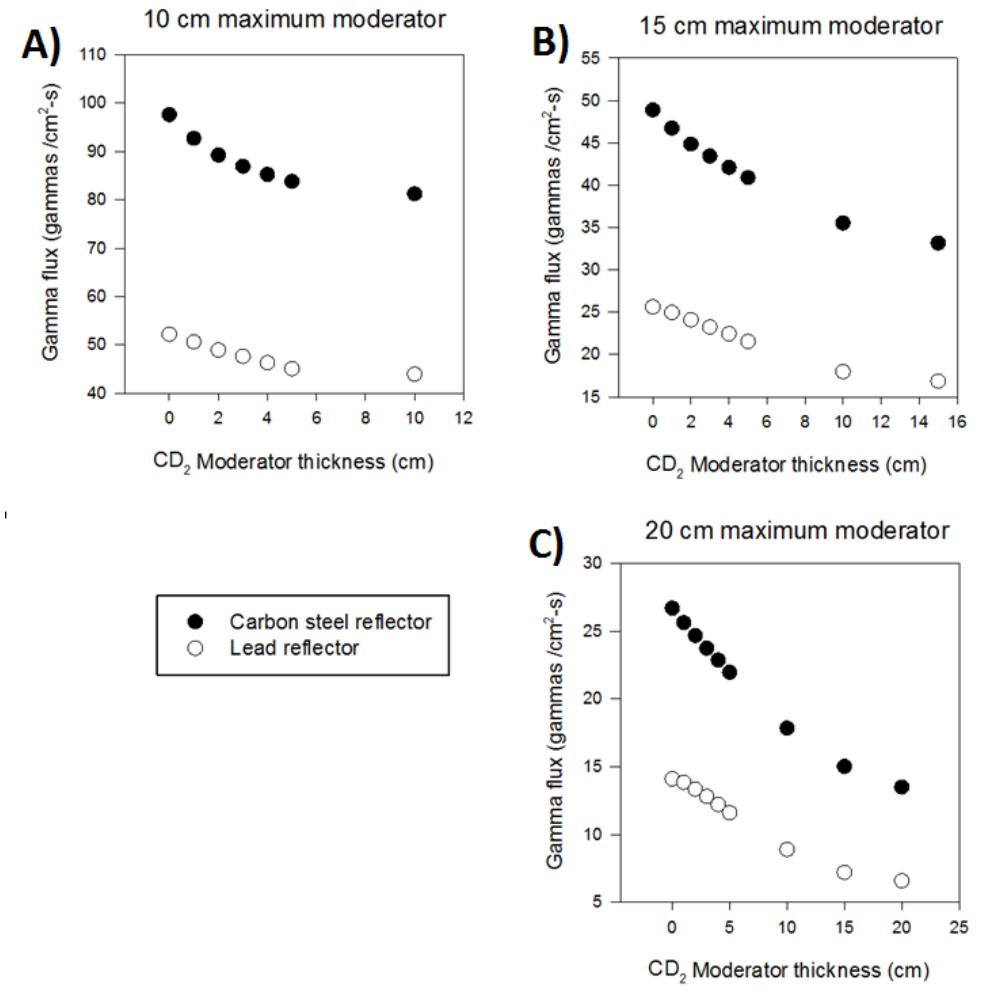

Figure 47 Comparison of average gamma flux (γ/cm^2-s) *vs.* moderator thickness (cm) for the small SRG source with two different reflector / shielding materials: carbon steel and lead. Results for: A) the 10 cm small SRGS; B) the 15 cm small SRGS; and C) the 20 cm small SRGS.

Table 10 Summary of highest average gamma dose rates and gamma fluxes calculated for SRG sources containing a 0.5 cm $Sm_{natural}$ (n, γ)-absorber and CD_2 moderator, with and without the carbon steel reflector / shield

Maximum moderator thickness (cm)	Gamma dose rates (mSv/h)		Gamma fluxes (γ/cm^2-s)	
	Without carbon steel	With carbon steel	Without carbon steel	With carbon steel
10	0.0019	0.0018	88.8	97.6
15	0.0010	0.0009	46.1	48.9
20	0.0006	0.0005	27.8	26.7

5 Chapter: Limitations Associated with the Research Project

The limitations associated with the feasibility study for the two applications discussed can be grouped into three main categories:

1) design limitations;

2) cost limitations; and

3) time-of-use limitations.

In this Chapter, a number of problems associated with each category are presented. Possible solutions and recommendations for future research are discussed in Chapter 6.

5.1 Design Limitations

Three main design limitations for the SRGS have been identified. First, the geometry modelled in this study limits the gamma doses and fluxes produced by the SRGS. The planar geometry chosen for this investigation attempts to emulate the current planar source design (see Figure 2, Section 1.4). However, as it was noted in Chapter 4, a significant number of neutrons are absorbed or lost through the source sides that would not be facing the gamma cameras or the blood bags. This finding is further illustrated in the mesh tally diagrams summarized in Appendix A.2. Adapting the design of the SRGS to decrease this neutron loss is a potential area of further research (see Chapter 6).

Second, the neutron source strength was reduced because of the plated design. The neutron source design used in this research took advantage of mechanical SRNS built by Argonne National Laboratory [47][48] and Sandia National Laboratories [49],

which provided the ability to turn ON and OFF the (α, n) reaction on demand (Section 3.1.1). However, because of the geometry of the source (*i.e.*, two parallel plates, see Figure 7A or Figure 7B, Section 3.1.1), only α particles that move in the direction of the (α, n)-absorber will be absorbed and result in neutron production; α particles moving away from the (α, n)-absorber plate will be lost.

Third, the intent was to create a neutron source based on an α-emitter with a long half-life, which does not produce a significant amount of collateral radiation. This led to the choice of ^{241}Am. This choice of α-emitting radioisotope also impacted the neutron source strength. Chapter 6 provides recommendations that could improve the neutron source strength and these might be considered in future research.

5.2 Cost Limitations

The intended application for the SRGS is to replace current gamma sources used by the medical community, thus, it must be affordable and provide additional benefits (*e.g.,* less frequent replacements, and lower doses to medical personnel when the source is not in use). The estimated cost for the larger proposed SRGS design is 12 - 17 times more costly than a ^{57}Co source, and the gamma flux it generates is 1 - 2 orders of magnitude lower (see Table 6, Section 4.1.1).

5.3 Time-of-Use Limitations

The small SRGS design, introduces significant time limitations: gamma cameras calibration procedures would take a few days, and blood irradiation would take ~254 years (Section 4.2.2.1.4). Reducing the overall gamma source dimensions resulted

in a significant reduction in the gamma flux; the maximum calculated gamma flux for the smaller source was 424.7 γ/cm^2-s, which is ~27 times smaller than the flux calculated for the large SRGS (1.13×10^4 γ/cm^2-s, Section 4.1) and at least 4 orders of magnitude smaller than the flux provided by a ^{57}Co source (Section 4.2.2.1.4). Also, the maximum gamma dose in one hour calculated for the small source (0.009 mSv) was at least 6 orders of magnitude smaller than the required gamma dose for blood irradiation (20 Gy), see Section 4.2.2.1.4. These reductions in the SRGS gamma flux and dose translate into a considerable increase in the length of time that the source would need to be ON for either application, making it impractical from a time-of-use perspective.

6 Chapter: Recommendations to Improve SRGS and Future Research

The neutron source strength is dependent on the design of the neutron source (*e.g.,* homogeneous *vs.* separate α-emitter and (α, n)-absorber regions) and the type of radioisotopes used to design the source (see Section 3.1.1 and Section 3.1.2.1). A recommendation to improve the SRGS is to look at α-emitters that have a shorter half-life than ^{241}Am. Using an α-emitter with a shorter half-life would help increase the neutron source strength by increasing the initial activity of the α source. The higher neutron source strength would lead to an increase in the gamma flux, because more neutrons would be available to interact with the (n, γ)-absorber and produce γ radiation via the (n, γ) reaction. The life-span of a switchable neutrons source based on (α, n) reactions is proportional to the half-life of the α-emitter [9]. For example, a SRGS based on a ^{9}Be (α, n)-absorber and an α-emitter such as ^{210}Po (half-life of 138 days) or ^{242}Cm (half-life of 163 days) would result in a neutron strength of 1.9×10^{7} n/cm^2-s and 1.2×10^{7} n/cm^2-s, respectively, but it would have to be replaced every 5 - 6 months [9]. Furthermore, as it decays, ^{210}Po gives off collateral gammas of 800 keV [9], while ^{242}Cm changes into ^{238}Pu, which gives off collateral gammas between 44 - 766 keV [9]. These high gamma rays would be present even when the source is in the "OFF" state, which would require shielding and special handling procedures to minimize the dose to personnel and follow the ALARA radiation protection principle [7].

Another recommendation would be to investigate different designs for the neutron source. An example of a potential design for the neutron source is to move away from

the planar geometry that was chosen for this study, and look at a spherical geometry, because a concentric sphere design would facilitate the absorption by the (α, n)-absorber of α particles travelling in all directions (see Figure 48). In order to maintain the capability to switch the source ON and OFF, these spherical surfaces can be constructed from multiple pieces that come together like a jigsaw puzzle when they are mechanically actuated (see Figure 48A for the source in the ON position, and Figure 48B for the source in the OFF position). The block containing the α-emitter would be built from multiple blocks that would come apart and move away from the α-absorber. This could be achieved mechanically with an actuator (*e.g.,* pneumatic, electric or magnetic) that would bring the pieces together in the ON position. Furthermore, the design can be replicated to have a series of concentric circles like those illustrated in Figure 48, which would increase the overall source strength. A switchable neutron source, which uses a series of parallel disks that rotate when activated to bring the α-emitting and (α, n)-absorbing materials into contact, has already been demonstrated [9]. This neutron source uses approximately 40 g ^{238}Pu (half-life of 87.8 years) as the α-emitting radioisotope, and it reports an overall source strength of 10^8 neutrons/s [9]. The mass of the ^{238}Pu α-emitting radioisotope is 16 times more than the mass of ^{241}Am that was estimated to be required for the large SRGS investigated in this research (2.5 g, Section 4.1.1).

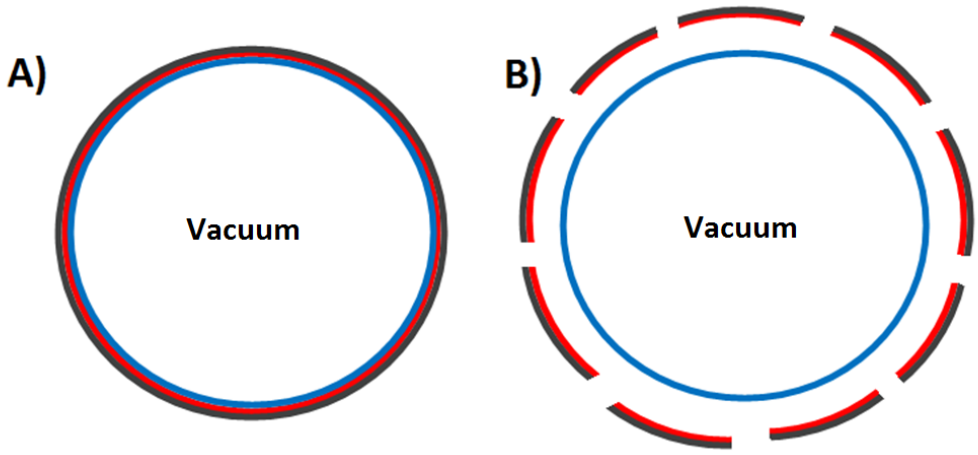

Figure 48 Proposed future design of the SRGS neutron source. A) Source in the ON position; B) Source in the OFF position. Red - α-emitter; Blue - α-absorber; Black - supporting material

Considering other materials both as neutron moderators and neutron absorbers is another recommendation for future research. The results reported in Table 8, Section 4.2.2.1.1 and Table 9, Section 4.2.2.1.3 show that HDPE, a hydrogen-based material, is a better moderator for the current SRGS design than a deuterium-based material, because it slows down neutrons in fewer collisions, bringing their energies closer to the thermal range where the absorption cross-section for $Gd_{natural}$ or $Sm_{natural}$ is higher, thus, increasing the number of (n, γ) reactions in the absorber region. For this reason, other hydrogen-based moderators such as paraffin wax ($C_{13}H_{28}$) may be investigated. Although not hydrogen-based, graphite has been historically used as a moderator and reflector in nuclear reactors, so it could also be investigated as a moderator for the SRGS. Graphite is a solid material that is readily available, it has low thermal neutron absorption cross-section, and can be easily cut and shaped [18].

Future studies could also look into materials such as carbon steel and lead as potential reflectors surrounding the gamma source. Outside the source, different

thicknesses may be used to minimize the gamma radiation produced in the regions that are not facing the SPECT gamma cameras (see Figure 2 and Figure 1), collimate the gamma radiation produced through the other source faces, and attenuate the high energy gamma rays to narrow the gamma spectrum obtained.

Finally, a new application for the SRGS could make the concept investigated in this research feasible. For example, the low levels of radiation could be used to increase the formation of nano-scale hydrogels [59]; thus the SRGS may be used for such an application. The current SRGS design is technically feasible, however, it is not applicable for the two medical applications (*i.e.,* a SPECT gamma camera calibration flood source or a blood irradiator) because these require a high gamma flux and gamma dose rate (see Section 4.2.2.1.4). A nano-scale application may be feasible for the proposed SRGS.

7 Chapter: Conclusions

The objective of this research was to explore the feasibility of the concept of a new switchable radioactive gamma source (SRGS) for two medical applications: a calibration flood source for SPECT gamma cameras and a blood irradiator. To achieve this objective, parametric studies were performed using the Monte Carlo computer code MCNP5 to simulate the interaction of particles with matter, calculate the gamma dose rates and fluxes produced by the SRGS, and compare the calculated values with those corresponding to the two medical applications.

The SRGS was based on a series of (α, n) reactions, followed by (n, γ) reactions. An ^{241}Am-^{9}Be source was chosen for the (α, n) reaction because ^{241}Am has a long half-life (432.2 years), a low spontaneous fission rate and low energy collateral gamma radiation (60 keV) (Section 3.1.2.1). The chosen design of the neutron source was a planar, plated design, with one plate of ^{241}Am and one plate of ^{9}Be that were kept a few millimeters apart in the "OFF" position, and were mechanically brought together in the "ON" position (see Figure 7A). The source strength for this design was estimated using the computer code SOURCES-4C, to be 1.30×10^4 n/cm^2-s (Section 3.1.2.1). This value was used to normalize the MCNP tally results.

The computer code MCNP5 was used to model various planar configurations of the SRGS and calculate the gamma flux in (γ/cm^2-s) and gamma dose rates in (mSv/h) or (mGy/h) for the proposed configurations. Parametric studies were performed to investigate two different (n, γ)-absorbers ($Sm_{natural}$ and $Gd_{natural}$), three different absorber thicknesses (0.2 cm, 0.5 cm, or 1 cm), and three different moderators (D_2O, deuterated

polyethylene - CD_2[footnote 2, Section 1.4), and high density polyethylene - HDPE[footnote 3, Section 1.4)) at moderator thicknesses between 0 cm and 20 cm (Section 3.1.3).

A large neutron source design 40 cm × 40 cm in the y- and z-directions was investigated (Section 4.1). This proposed SRGS is equivalent in surface area to current ^{57}Co calibration flood sources, and it covers the entire SPECT gamma camera. The maximum calculated gamma flux for this source design (1.13×10^4 γ/cm^2-s) was obtained for a 0.2 cm $Sm_{natural}$ (n, γ)-absorber and 20 cm CD_2 moderator. This value is approximately 1 to 2 orders of magnitude lower than the corresponding flux from a standard ^{57}Co calibration flood source, which would result in an increase in the time required to perform the calibration procedure from a few minutes to hours. A cost estimate performed for the large SRGS shows that this design is expensive, costing 12 - 17 times more than a ^{57}Co flood source (Section 4.1.1), the most costly components being the $Sm_{natural}$ (n, γ)-absorber and the CD_2 moderator. Bulk buying of the materials may reduce the costs of a single unit by a factor of 2 or 3, from ~$150,000 to ~$75,000.

Based on these findings, it was concluded that the proposed large source is too expensive as a SPECT gamma camera calibration source, and a number of small SRGS designs were investigated. The SRGS source designs for these studies was based on a neutron source size of 6 cm × 6 cm, which feeds a 10.4 cm × 10.4 cm gamma source to effectively cover a quarter of the gamma camera (Section 3.1). For these studies, different moderating materials, (n, γ)-absorbing materials, and overall SRGS dimensions were investigated to determine the impact on calculated average gamma dose rate and flux.

First, CD_2 and D_2O were compared for the two different (n, γ)-absorbers, $Sm_{natural}$ and $Gd_{natural}$ (Section 4.2.1). The maximum average gamma fluxes for the $Sm_{natural}$ (n, γ)-absorber were calculated to be 23.8 γ/cm^2-s for a 1 cm thick D_2O moderator, and 24.7 γ/cm^2-s for a 2 cm thick CD_2 moderator. The maximum average gamma fluxes for $Gd_{natural}$ (n, γ)-absorber were calculated to be 22.7 γ/cm^2-s for a 1 cm thick D_2O moderator, and 23.3 γ/cm^2-s for a 2 cm thick CD_2 moderator. Based on these results, either (n, γ)-absorber and moderator could be used for a switchable radioactive gamma source. However, all configurations resulted in average gamma fluxes that were significantly lower (at least 4 orders of magnitude) than the gamma fluxes from a ^{57}Co flood source, resulting in a time increase for each calibration procedure from a few minutes to days. Furthermore, the gamma spectrum produced by the SRGS contains a wide range of gamma energies. Current calibration procedures (Section 2.2.1) recommend the use of a calibration gamma source which gives off gammas with energies similar to that used in patient procedures [32]. A wide spectrum of gamma energies, and in particular those with energies >500 keV would confound the calibration of the camera because of their broad energy tail (see Section 2.2.1) that overlaps with the energies of common radioisotopes used in SPECT imaging (*e.g.,* ^{99m}Tc, 140 keV).

Second, parametric studies were performed to calculate the highest average gamma dose rate and gamma flux for different overall gamma source dimensions: 10 cm maximum, 15 cm maximum or 20 cm maximum moderator on either side of the neutron source. These sources have been referred to as the 10 cm small SRGS, 15 cm small SRGS and 20 cm small SRGS. Two moderators were investigated: CD_2 and HDPE. The results obtained 'surprisingly' showed that the smaller SRGS (*i.e.,* 10 cm small SRGS)

produced the highest gamma dose rate and gamma flux for both moderators (Section 4.2.2.1.4). The smaller the source, the lower the number of neutrons that escaped through the XY and XZ faces, contributing to the dose in air region 3 (see Figure 9, Section 3.1.2.2), and the higher the fraction of neutrons that reached the (n, γ)-absorber close to air region 1 or region 2, resulting in more (n, γ) reactions. The maximum gamma dose rate (0.009 mSv/h) and gamma flux (424.7 γ/cm^2-s) were calculated for a 10 cm small SRGS that used 5 cm HDPE moderator and 0.2 cm $Sm_{natural}$ (n, γ)-absorber. For the CD_2 moderator, the maximum values were at least 4 - 5 times smaller (0.002 mSv/h and 93.4 γ/cm^2-s, respectively) and were obtained for 10 cm CD_2 moderator and 1.0 cm $Sm_{natural}$ absorber. These results show that, for the small gamma source geometry, hydrogen-based moderators are slowing down neutrons more efficiently than deuterium-based ones, because they reduced the neutron energy in fewer steps (*i.e.,* 18 collisions versus 24 collisions, Section 2.1.2.3 and Section 4.2.2.1.4). Furthermore, the calculated maximum average gamma flux (*i.e.,* 424.7 γ/cm^2-s) is 3 to 4 orders of magnitude smaller than the current ^{57}Co flood sources, which would result in a calibration time increase from minutes to a few days, thus making the proposed SRGS not practical as a SPECT gamma camera flood source.

The feasibility of the SRGS as a blood irradiator was determined by comparing the doses required for blood irradiation (20 - 40 Gy, Section 2.2.2), with the total dose that would be delivered by the SRGS in a reasonable time (*i.e.,* 0.009 mSv in one hour, Section 4.2.2.1.4). At the maximum calculated dose rate of 0.009 mSv/h, a total of 254 years would be needed to deliver the required blood irradiation gamma dose. Thus,

the proposed small SRGS design is not practically feasible as a blood irradiator, because of time constraints.

In conclusion, this research showed that, although technically feasible, the proposed designs for a switchable radioactive gamma source were not practically feasible for the two medical applications, *i.e.,* a flood source for SPECT gamma camera calibration or a blood irradiator. However, the concept of a gamma source that can be switched ON and OFF on demand and remotely, is appealing and future research may be warranted for nano-scale applications that require smaller gamma fluxes or dose rates (see Chapter 6). Future research may also investigate other source designs, (α, n) materials, hydrogenous materials for neutron moderation, or (n, γ)-absorbing materials.

Appendices

Appendix A MCNP Mesh Tallies Distribution

Mesh tallies were defined in MCNP using the "FMESH" card. This card allowed to superimpose an F4 tally over the defined source geometry and calculate the flux, in particles/cm^2, averaged over each mesh cell defined in the input file. The mesh tally also allowed the user to apply the flux-to-dose conversion factors to the calculated flux tally, to calculate the dose rate averaged over the same mesh cell.

This appendix summarizes the mesh tallies that were created to obtain the corresponding results reported in Section 4.2.2.1.1and Section 4.2.2.1.3. Additional results of the mesh tally calculations were summarized in Appendix A.2.

A.1 Mesh Tally Definitions

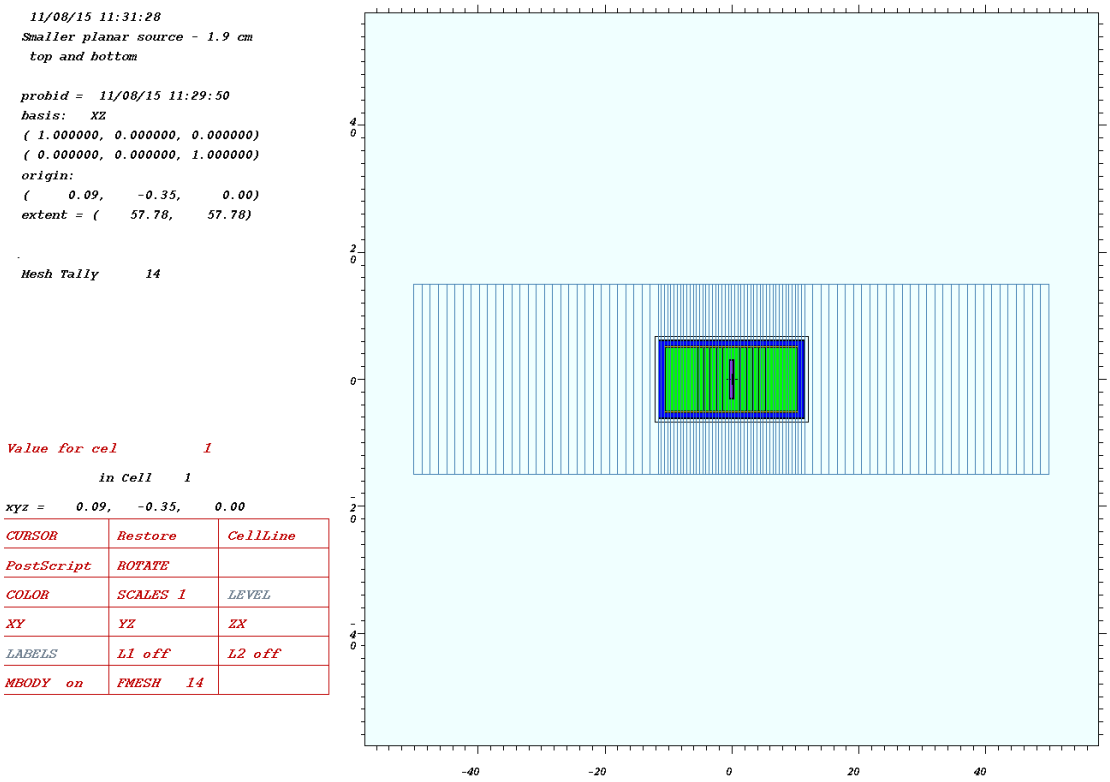

Tally 14 or 24: Mesh tally superimposed to the XZ view of the source. This tally was used to calculate the gamma and/or neutron flux or dose rate for the overall source, for a distance of 50 cm on either side of the origin (*i.e.,* the center of the neutron source). The flux or dose rates were averaged over the entire volume of the each slice shown in this image.

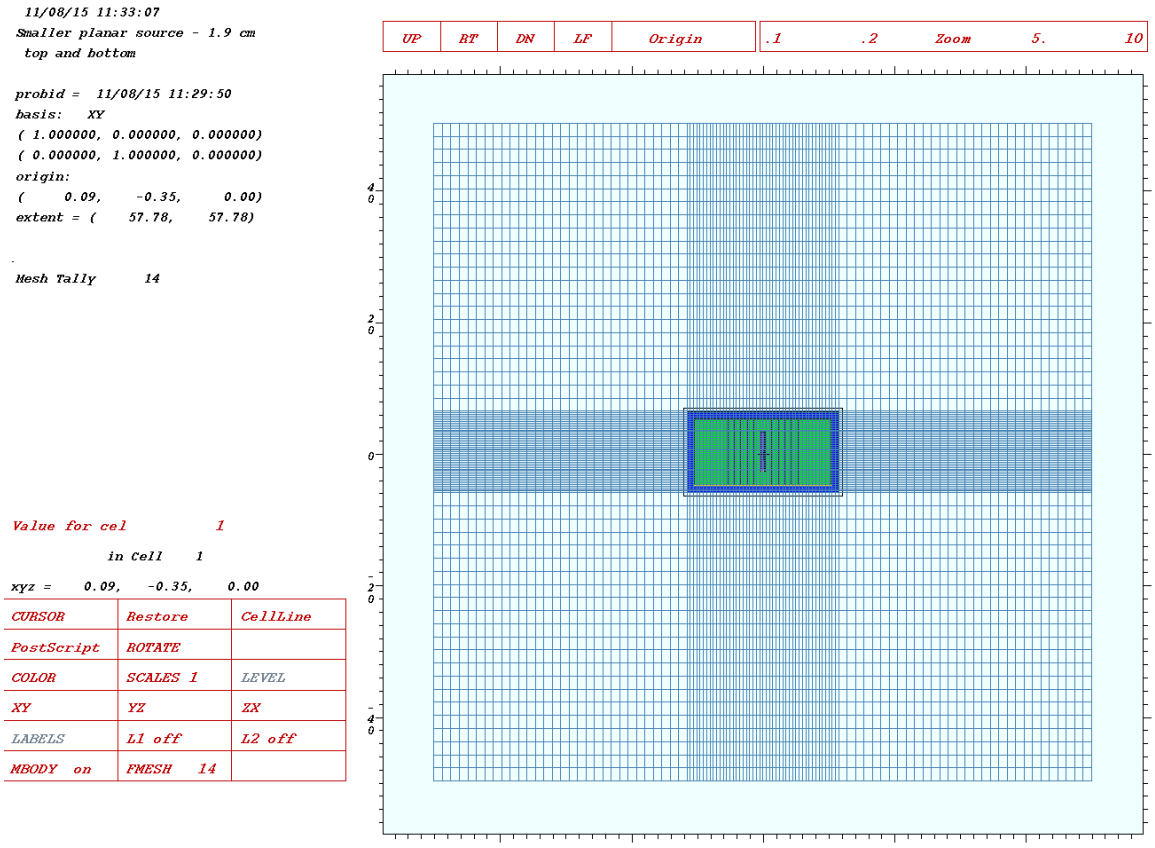

Tally 14 or 24: Mesh tally superimposed to the XY view of the source. This tally was used to calculate the gamma and/or neutron flux or dose rate for the overall source, for a distance of 50 cm on either side of the origin (*i.e.,* the center of the neutron source). The flux or dose rates were averaged over the entire volume of the each cell shown in this image.

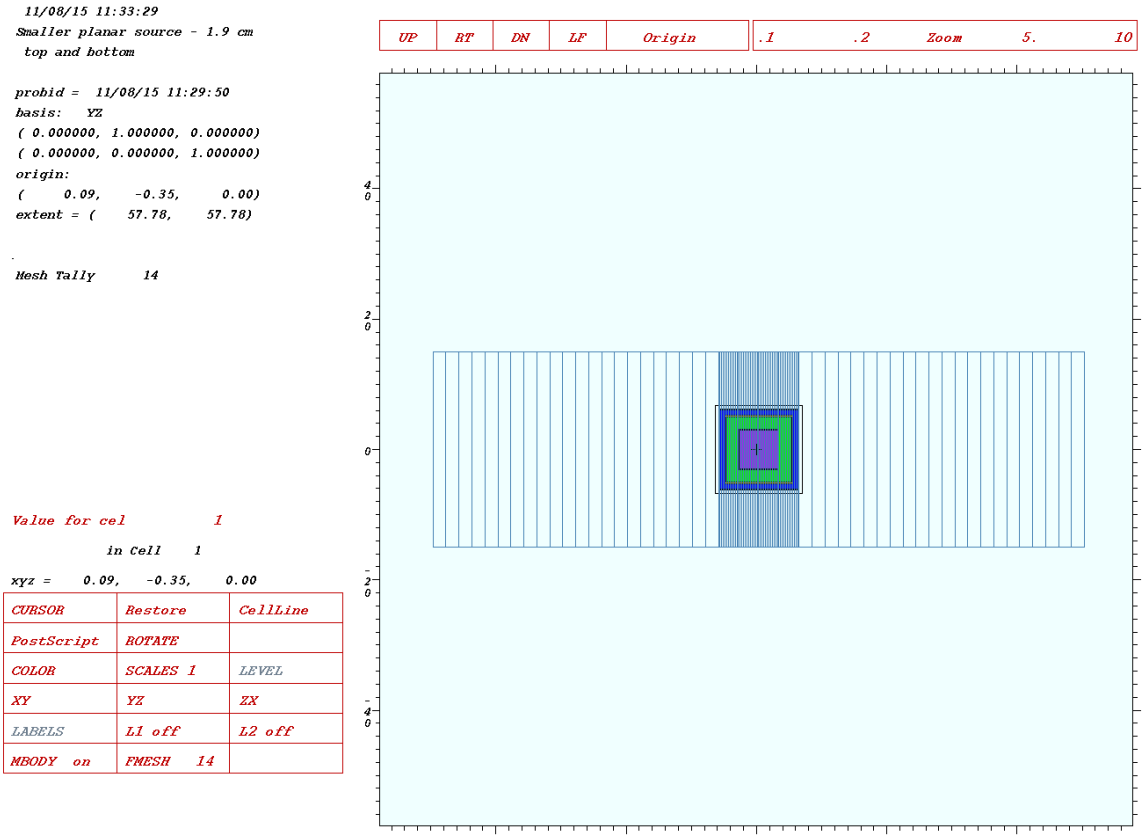

Tally 14 or 24: Mesh tally superimposed to the YZ view of the source. This tally was used to calculate the gamma and/or neutron flux or dose rate for the overall source, for a distance of 50 cm on either side of the origin (*i.e.,* the center of the neutron source). The flux or dose rates were averaged over the entire volume of the each cell shown in this image.

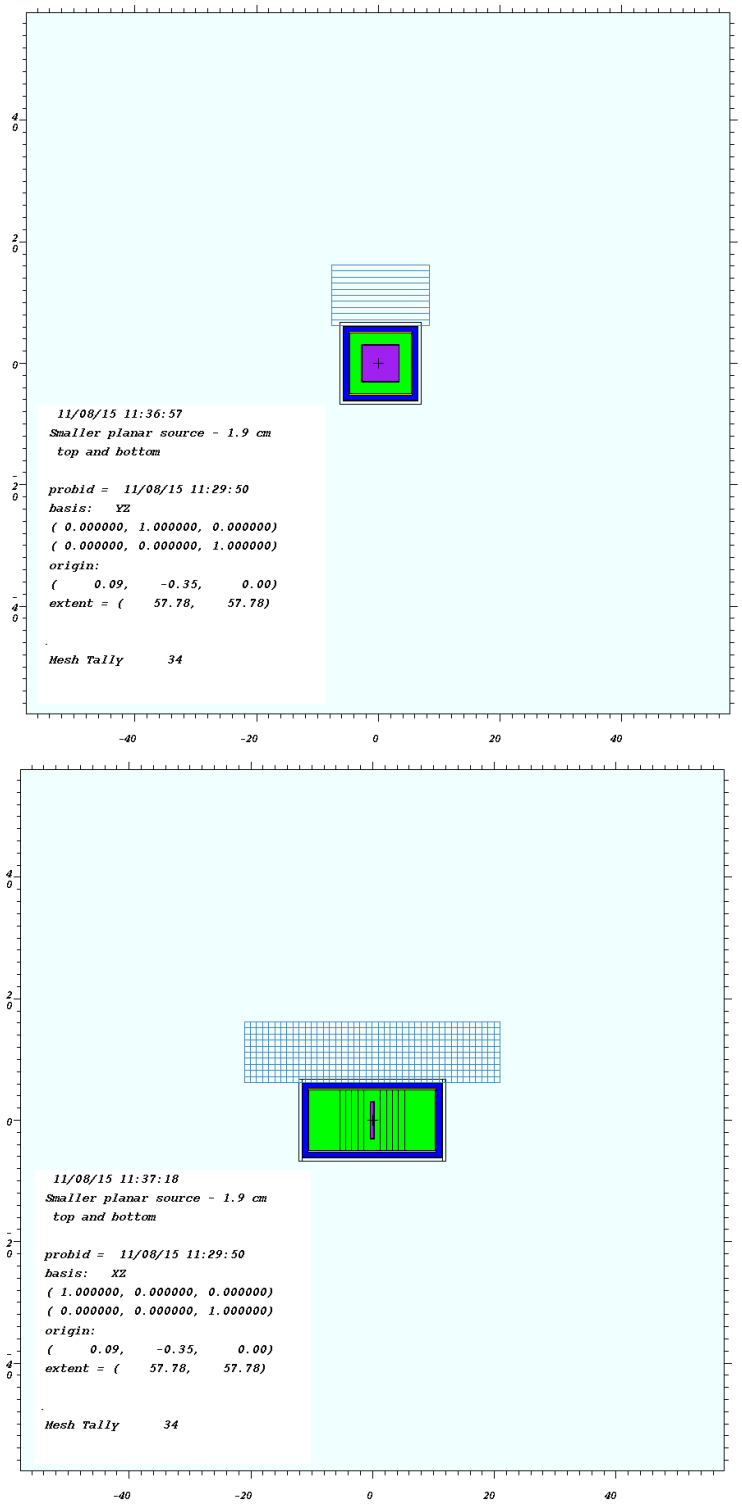

Tally 34 or 44: Mesh tally superimposed to the YZ view of the source (top image) and XZ view of the source (bottom image). This tally was used to calculate the gamma and/or neutron flux or dose rate for the area surrounding the source on the YX face, for a distance of 10 cm away from the source. The values are averaged over the volume of each mesh cell illustrated.

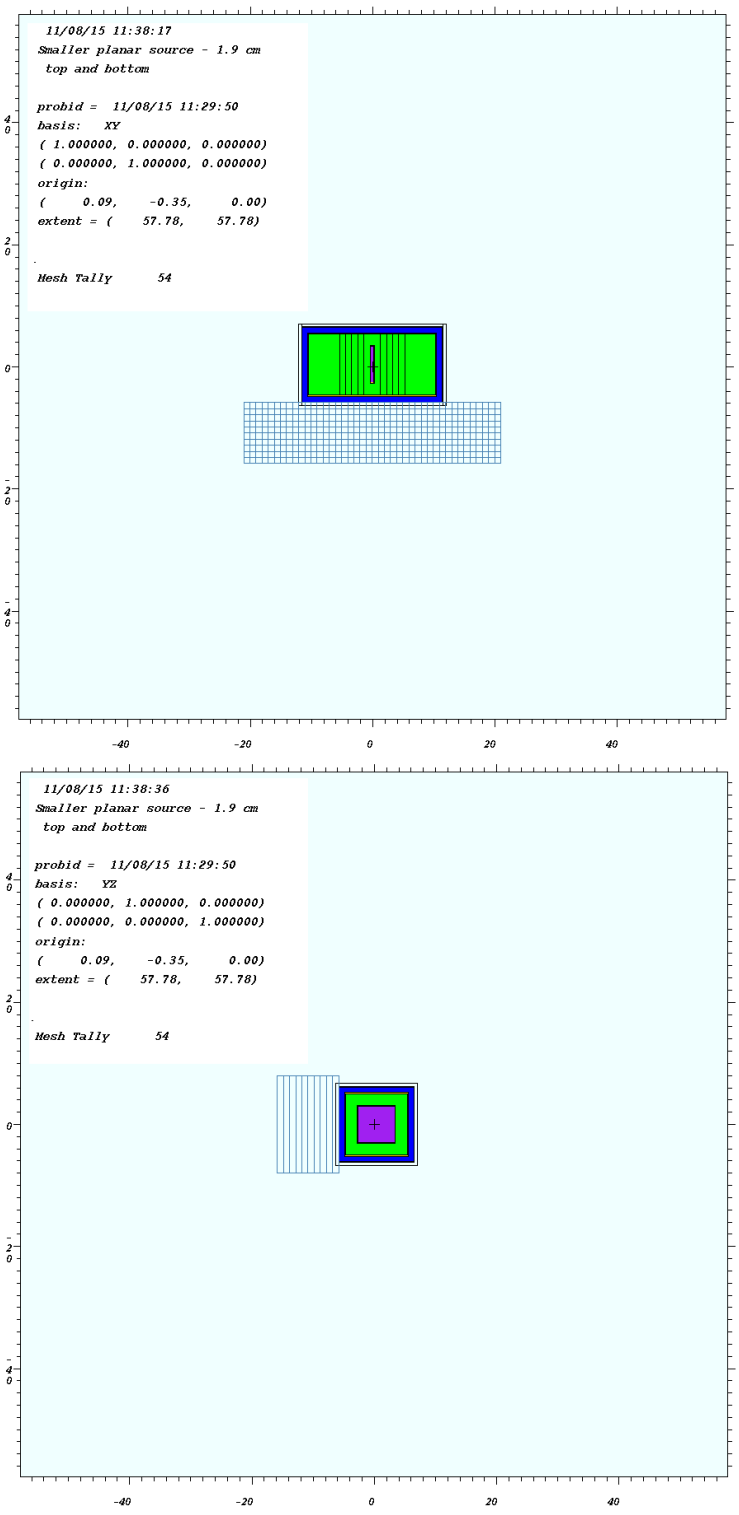

Tally 54 or 64: Mesh tally superimposed to the XY view of the source (top image) and YZ view of the source (bottom image). This tally was used to calculate the gamma and/or neutron flux or dose rate for the area surrounding the source on the XZ face, for a distance of 10 cm away from the source. The values are averaged over the volume of each mesh cell illustrated.

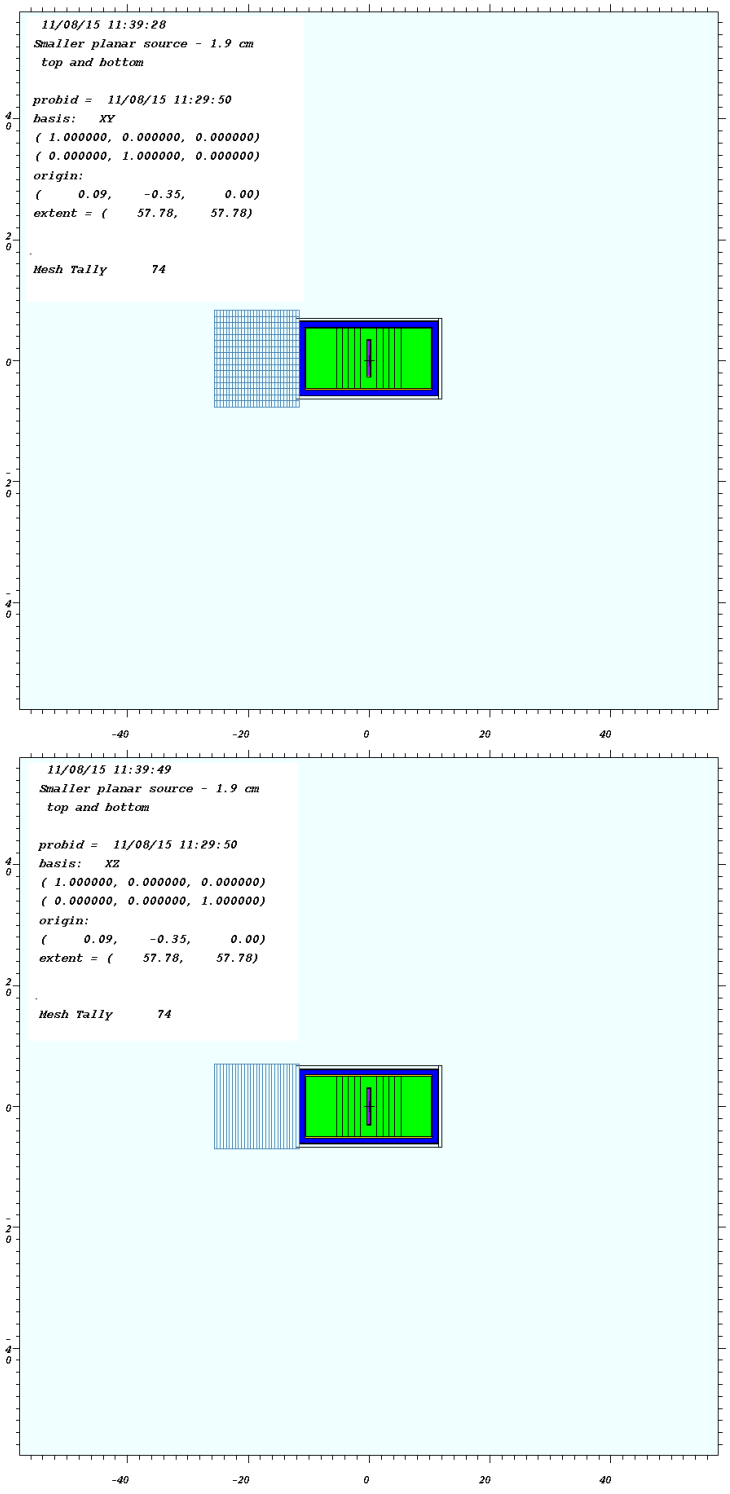

Tally 74 or 84: Mesh tally superimposed to the XY view of the source (top image) and XZ view of the source (bottom image). This tally was used to calculate the gamma and/or neutron flux or dose rate for the area surrounding the source on the YZ face, for a distance of 10 cm away from the source. The values are averaged over the volume of each mesh cell illustrated.

A.2 Additional Flux and Dose Rate Mesh Tally Results

The average flux and dose rate summarized in this section have also been calculated for the two source designs presented in Chapter 4.2.2.1. that resulted in the highest average gamma dose rates and gamma fluxes:

1) 10 cm small SRGS, 1.0 cm $Sm_{natural}$ absorber, 10 cm CD_2 moderator; and

2) 10 cm small SRGS, 0.2 cm $Sm_{natural}$ absorber, 5 cm HDPE moderator.

Mesh tally results are illustrated for both neutron and gamma dose rates and fluxes. Note that the origin (0, 0, 0) of the graphs illustrated in this appendix is referenced to the most lowest (x, y, z) coordinate of the corresponding mesh tally number defined in Appendix A1. For example, in case 1 below, the results correspond to mesh tally 34 defined in Appendix A1, where the plot goes from x=-21 to x=+21 and z=7 to z=17 with respect to the centre of the neutron source.

Case 1: $Sm_{natural}$ absorber, 10 cm CD_2 moderator

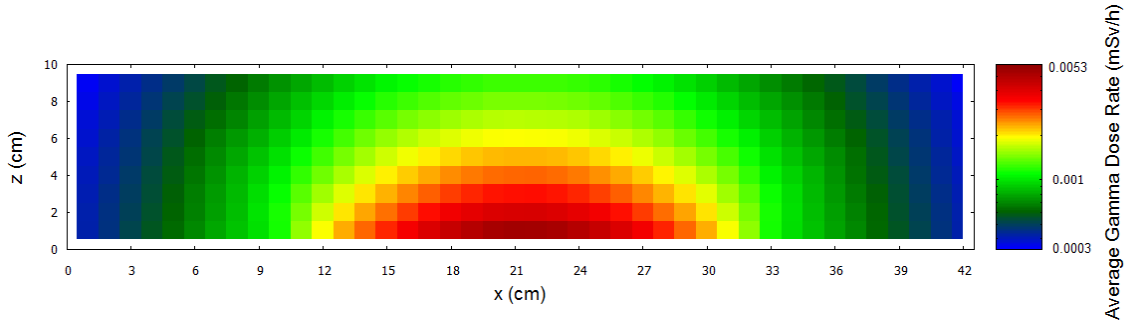

Tally 34: Gamma dose rate mesh tally superimposed to the YX face of the source, for a distance of 10 cm away from the source surface. The values are averaged over the volume of each mesh cell illustrated. The computational relative uncertainty for each cell was lower than 0.2%.

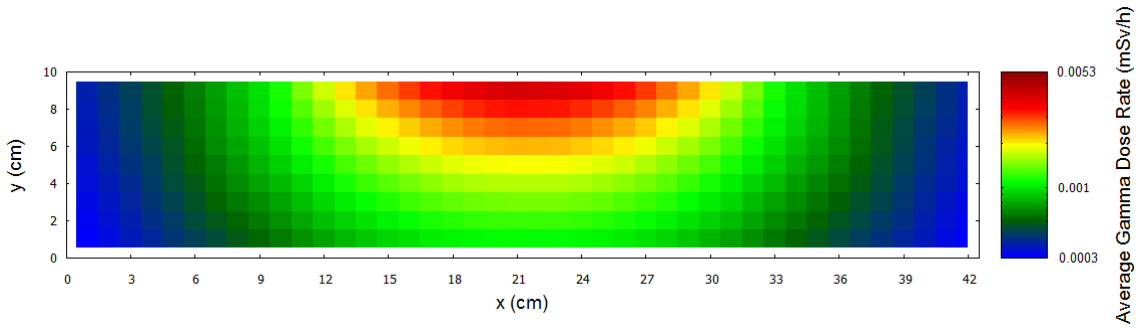

Tally 54: Gamma dose rate mesh tally superimposed to the XZ face of the source, for a distance of 21 cm on either side of the neutron source, and 10 cm away from the source surface. The values are averaged over the volume of each mesh cell illustrated. The computational relative uncertainty for each cell was lower than 0.2%.

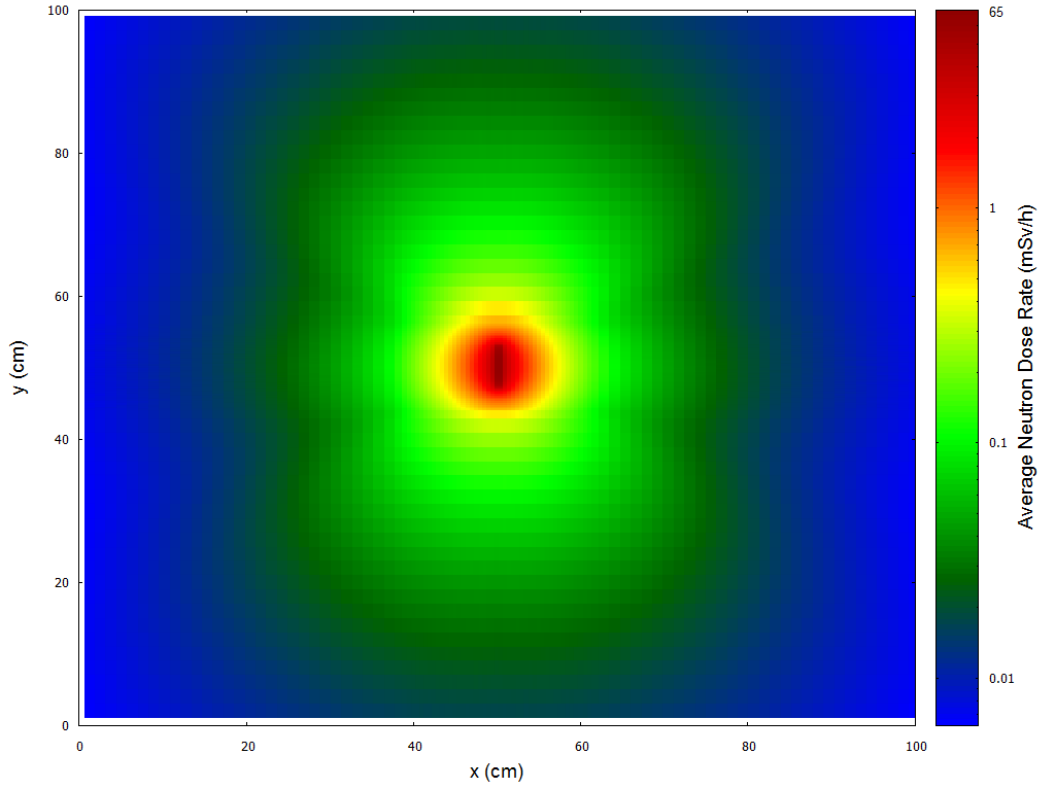

Tally 24: Neutron dose rate mesh tally superimposed to the overall source, for a distance of 50 cm away from the center of the neutron source. The values are averaged over the volume of each mesh cell illustrated. The computational relative uncertainty for each cell was lower than 0.2%.

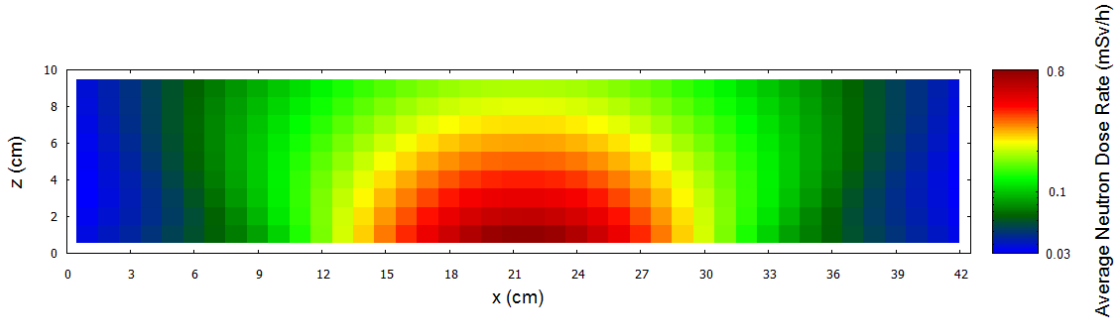

Tally 44: Neutron dose rate mesh tally superimposed to the YX face of the source, for a distance of 10 cm away from the source surface. The values are averaged over the volume of each mesh cell illustrated. The computational relative uncertainty for each cell was lower than 0.2%.

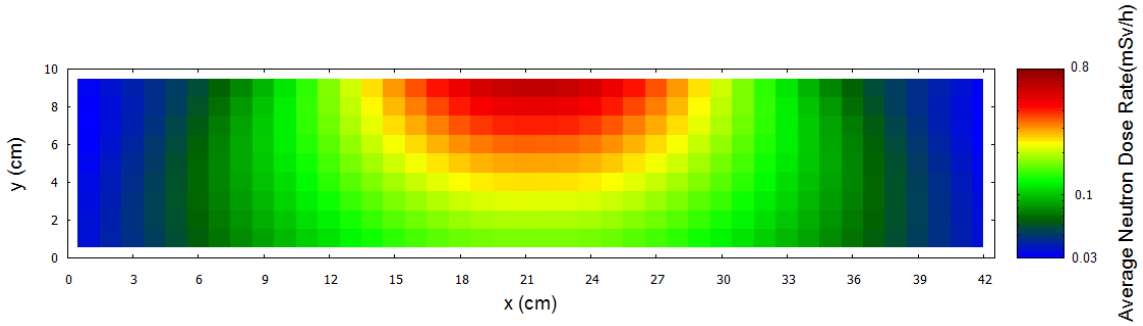

Tally 64: Neutron dose rate mesh tally superimposed to the XZ face of the source, for a distance of 21 cm on either side of the neutron source, and 10 cm away from the source surface. The values are averaged over the volume of each mesh cell illustrated. The computational relative uncertainty for each cell was lower than 0.2%.

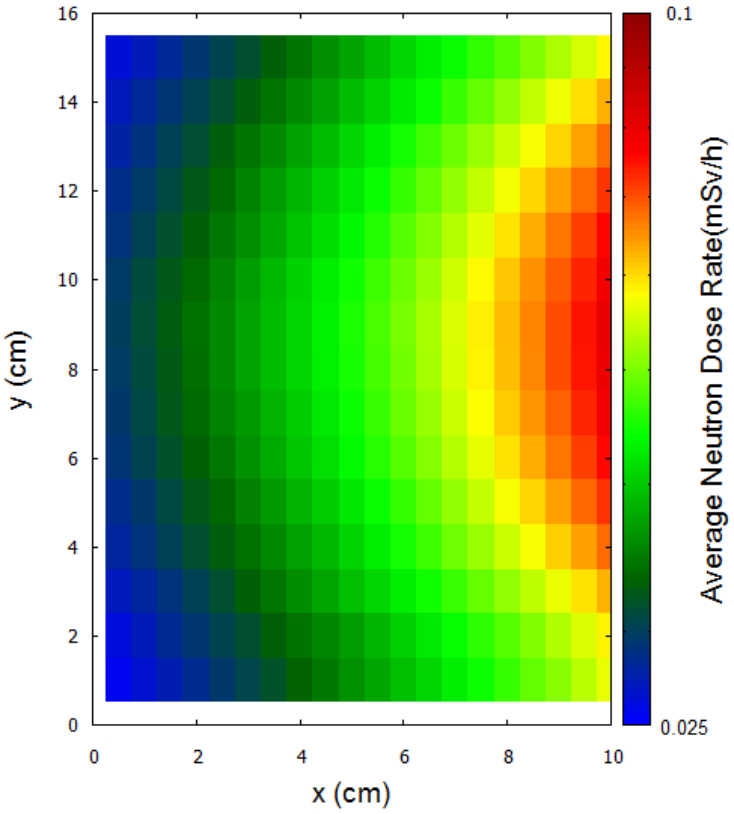

Tally 84: Neutron dose rate mesh tally superimposed to the YZ face of the source, for a distance of 10 cm away from the surface of the source. The values are averaged over the volume of each mesh cell illustrated. The computational relative uncertainty for each cell was lower than 0.2%.

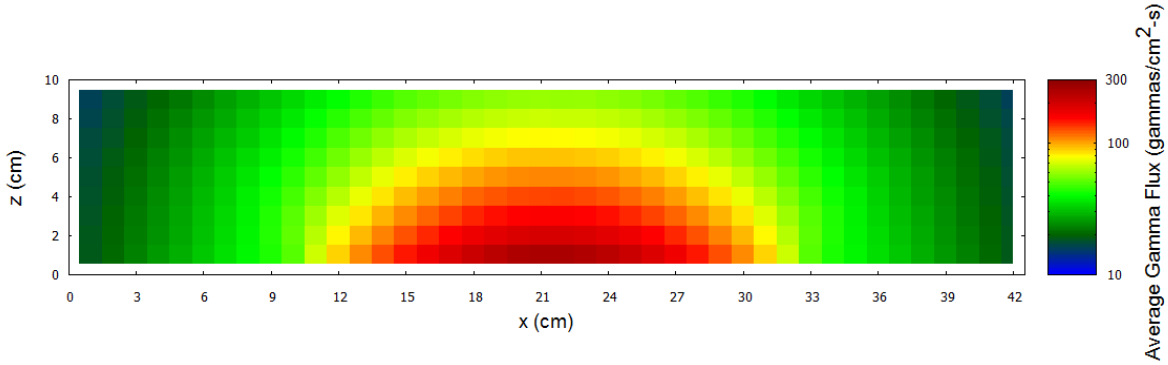

Tally 34: Gamma flux mesh tally superimposed to the YX face of the source, for a distance of 10 cm away from the source surface. The values are averaged over the volume of each mesh cell illustrated. The computational relative uncertainty for each cell was lower than 0.2%.

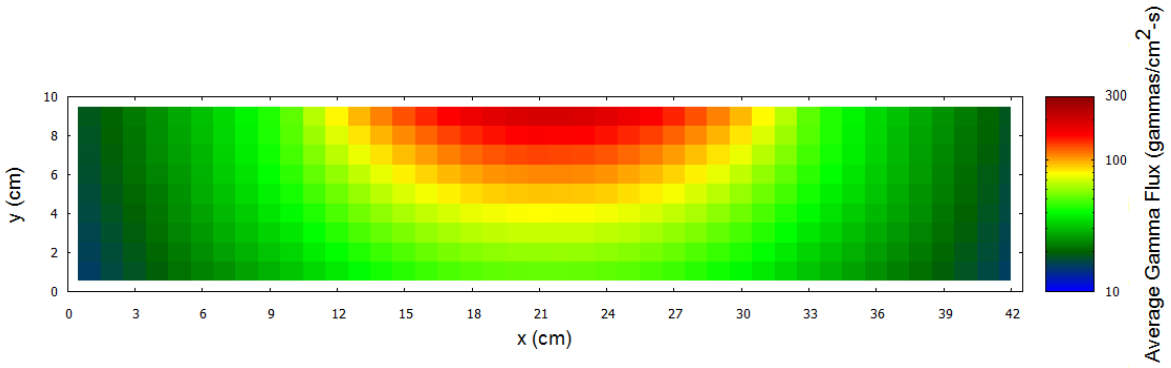

Tally 54: Gamma flux mesh tally superimposed to the XZ face of the source, for a distance of 21 cm on either side of the neutron source, and 10 cm away from the source surface. The values are averaged over the volume of each mesh cell illustrated. The computational relative uncertainty for each cell was lower than 0.2%.

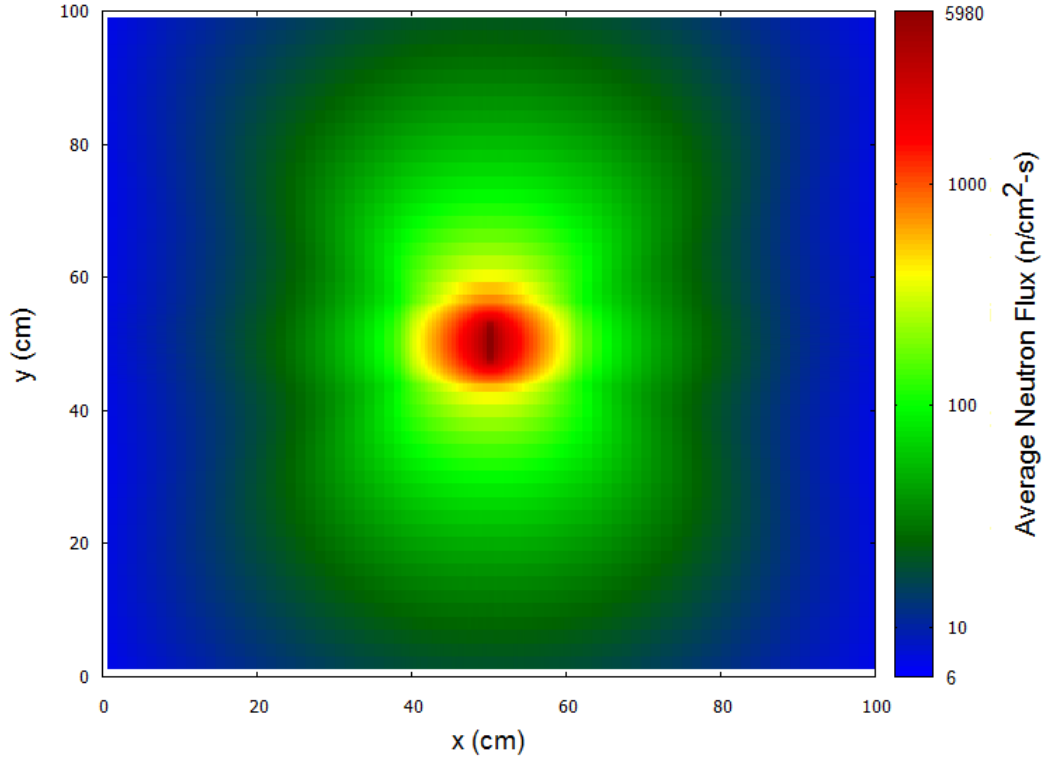

Tally 24: Neutron flux mesh tally superimposed to the overall source, for a distance of 50 cm away from the center of the neutron source. The values are averaged over the volume of each mesh cell illustrated. The computational relative uncertainty for each cell was lower than 0.2%.

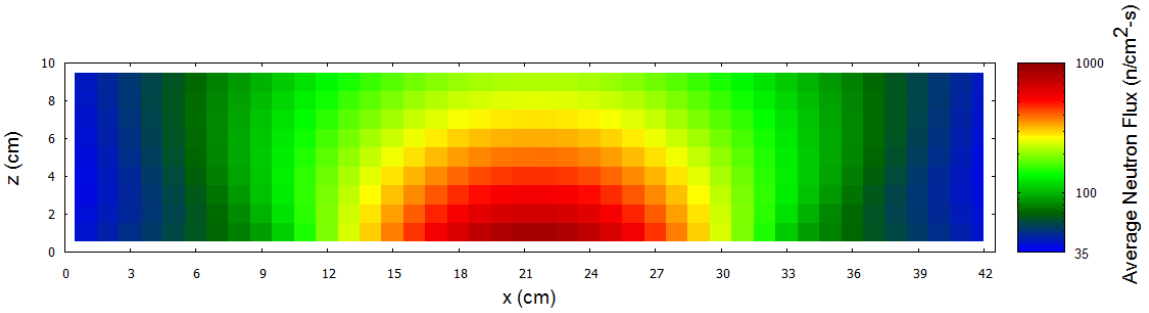

Tally 44: Neutron flux mesh tally superimposed to the YX face of the source, for a distance of 10 cm away from the source surface. The values are averaged over the volume of each mesh cell illustrated. The computational relative uncertainty for each cell was lower than 0.2%.

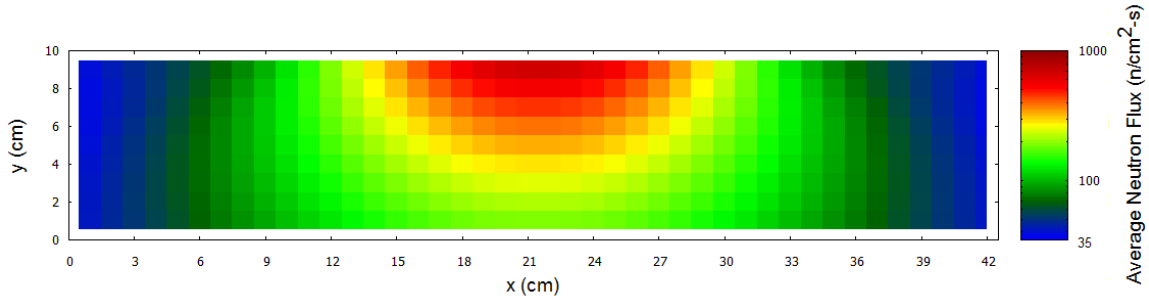

Tally 64: Neutron flux mesh tally superimposed to the XZ face of the source, for a distance of 21 cm on either side of the neutron source, and 10 cm away from the source surface. The values are averaged over the volume of each mesh cell illustrated. The computational relative uncertainty for each cell was lower than 0.2%.

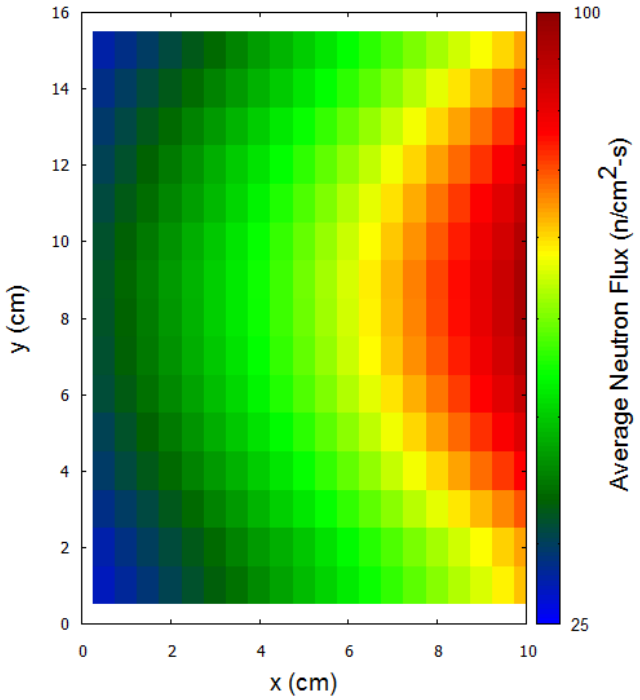

Tally 84: Neutron flux mesh tally superimposed to the YZ face of the source, for a distance of 10 cm away from the surface of the source. The values are averaged over the volume of each mesh cell illustrated. The computational relative uncertainty for each cell was lower than 0.2%.

Case 2: $Sm_{natural}$ absorber, 5 cm HDPE moderator

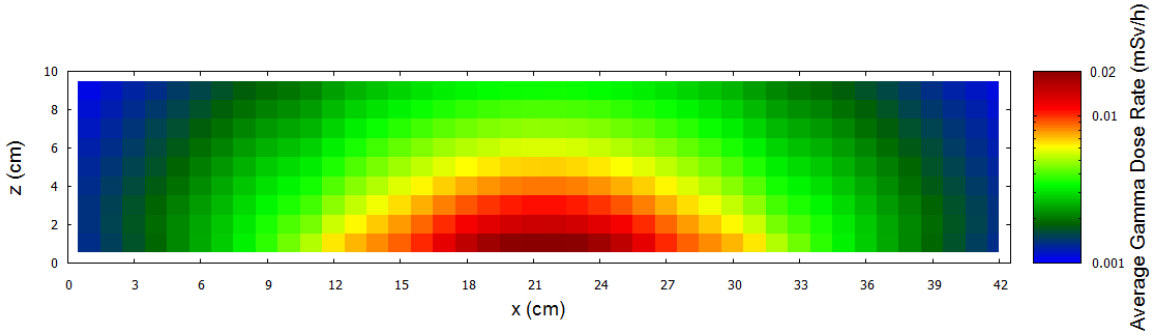

Tally 34: Gamma dose rate mesh tally superimposed to the YX face of the source, for a distance of 10 cm away from the source surface. The values are averaged over the volume of each mesh cell illustrated. The computational relative uncertainty for each cell was lower than 0.2%.

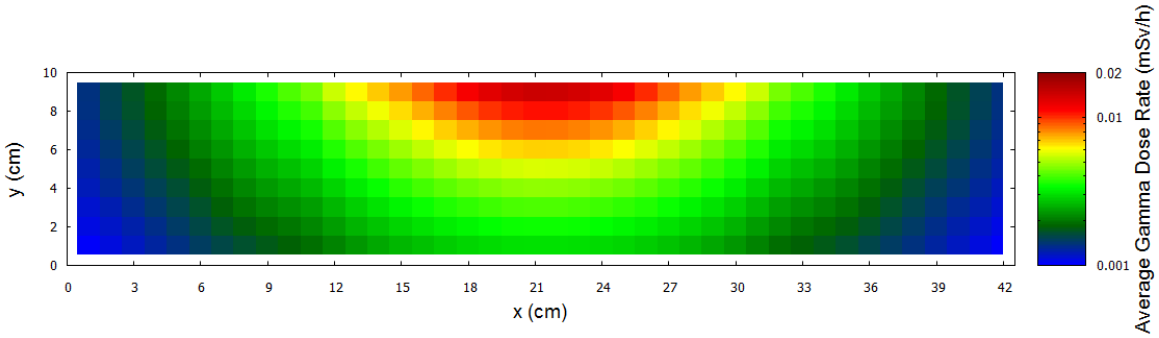

Tally 54: Gamma dose rate mesh tally superimposed to the XZ face of the source, for a distance of 21 cm on either side of the neutron source, and 10 cm away from the source surface. The values are averaged over the volume of each mesh cell illustrated. The computational relative uncertainty for each cell was lower than 0.2%.

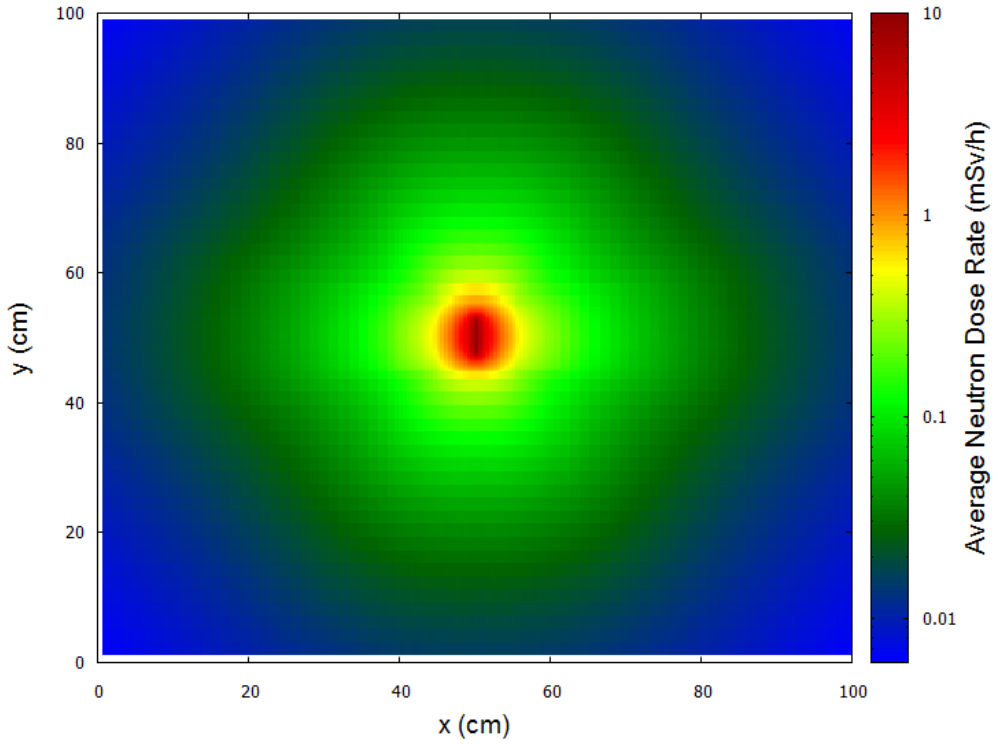

Tally 24: Neutron dose rate mesh tally superimposed to the overall source, for a distance of 50 cm away from the center of the neutron source. The values are averaged over the volume of each mesh cell illustrated. The computational relative uncertainty for each cell was lower than 0.2%.

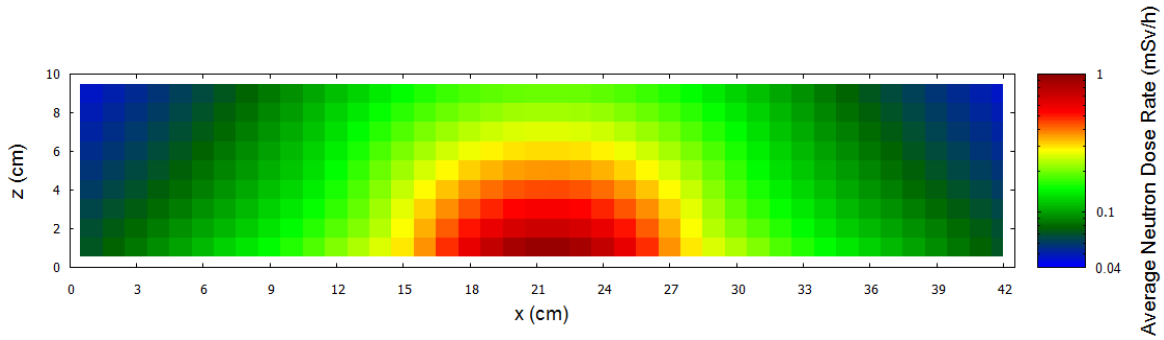

Tally 44: Neutron dose rate mesh tally superimposed to the YX face of the source, for a distance of 10 cm away from the source surface. The values are averaged over the volume of each mesh cell illustrated. The computational relative uncertainty for each cell was lower than 0.2%.

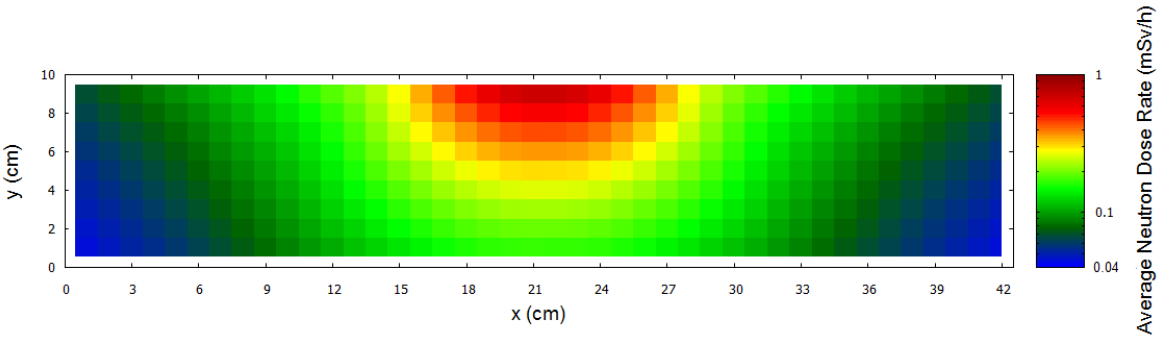

Tally 64: Neutron dose rate mesh tally superimposed to the XZ face of the source, for a distance of 21 cm on either side of the neutron source, and 10 cm away from the source surface. The values are averaged over the volume of each mesh cell illustrated. The computational relative uncertainty for each cell was lower than 0.2%.

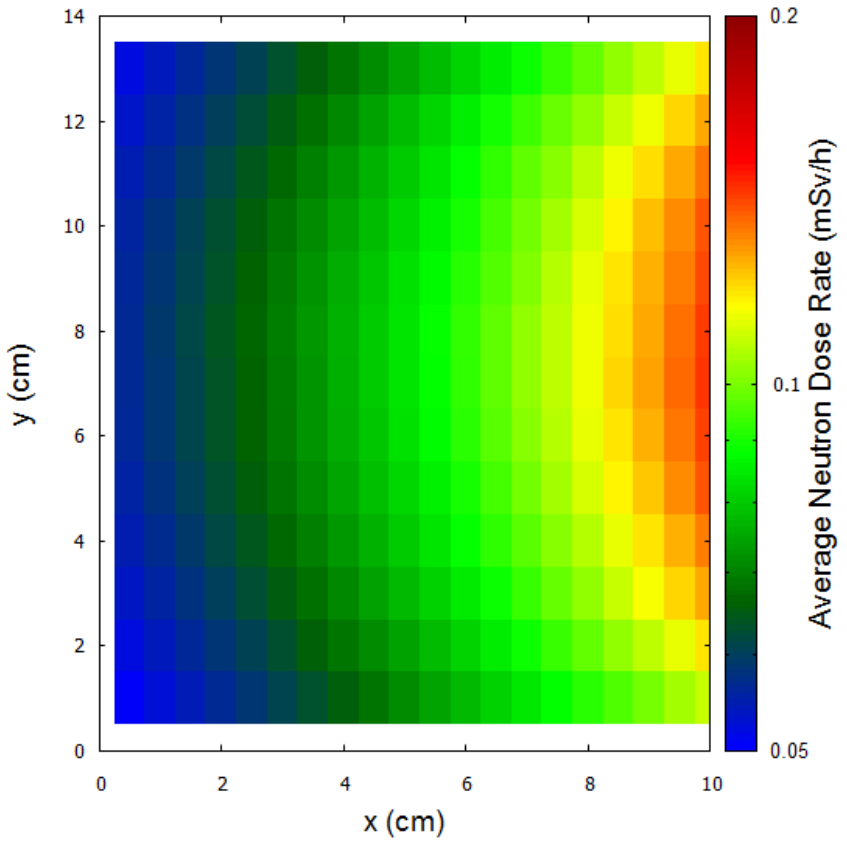

Tally 84: Neutron dose rate mesh tally superimposed to the YZ face of the source, for a distance of 10 cm away from the surface of the source. The values are averaged over the volume of each mesh cell illustrated. The computational relative uncertainty for each cell was lower than 0.2%.

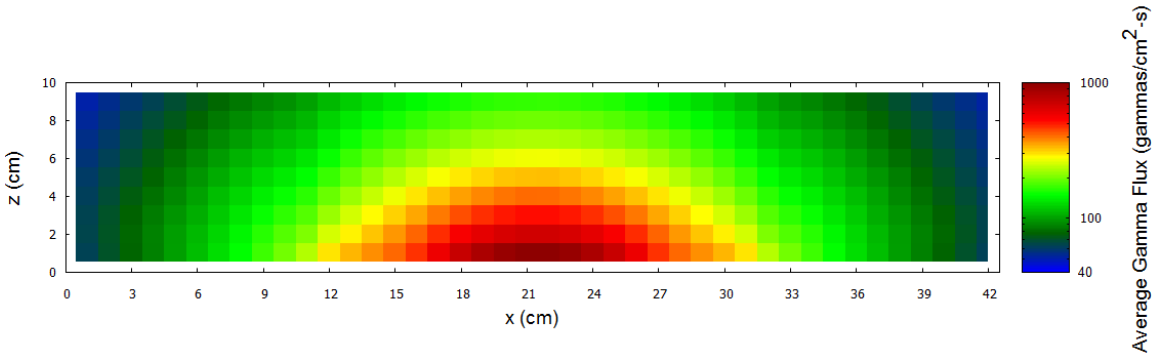

Tally 34: Gamma flux mesh tally superimposed to the YX face of the source, for a distance of 10 cm away from the source surface. The values are averaged over the volume of each mesh cell illustrated. The computational relative uncertainty for each cell was lower than 0.2%.

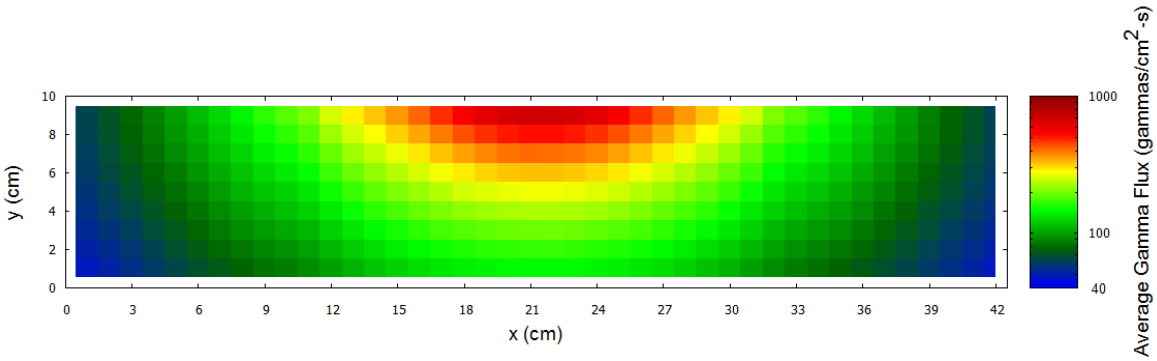

Tally 54: Gamma flux mesh tally superimposed to the XZ face of the source, for a distance of 21 cm on either side of the neutron source, and 10 cm away from the source surface. The values are averaged over the volume of each mesh cell illustrated. The computational relative uncertainty for each cell was lower than 0.2%.

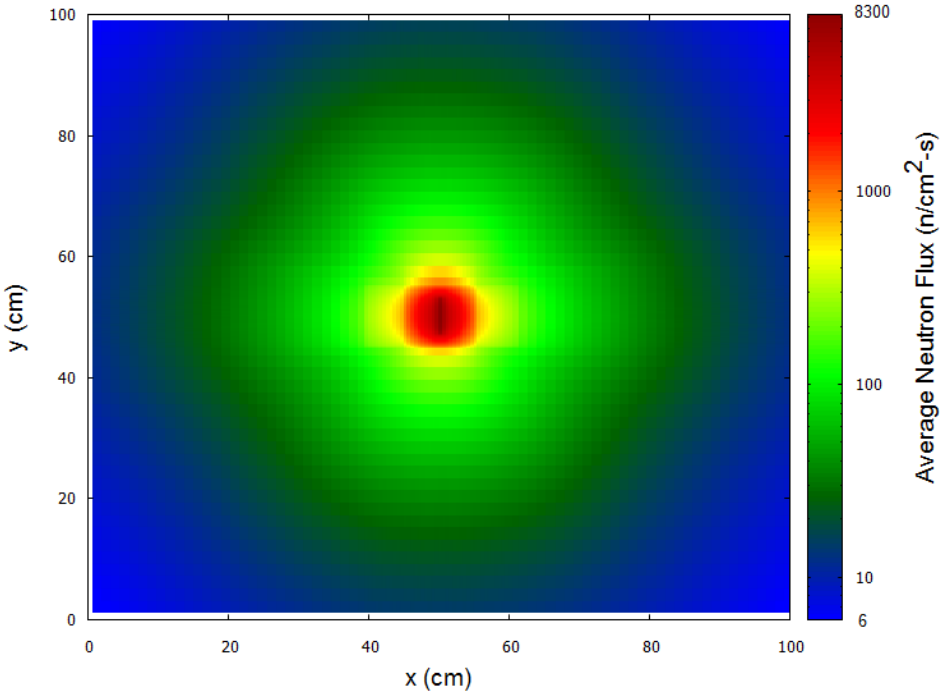

Tally 24: Neutron flux mesh tally superimposed to the overall source, for a distance of 50 cm away from the center of the neutron source. The values are averaged over the volume of each mesh cell illustrated. The computational relative uncertainty for each cell was lower than 0.2%.

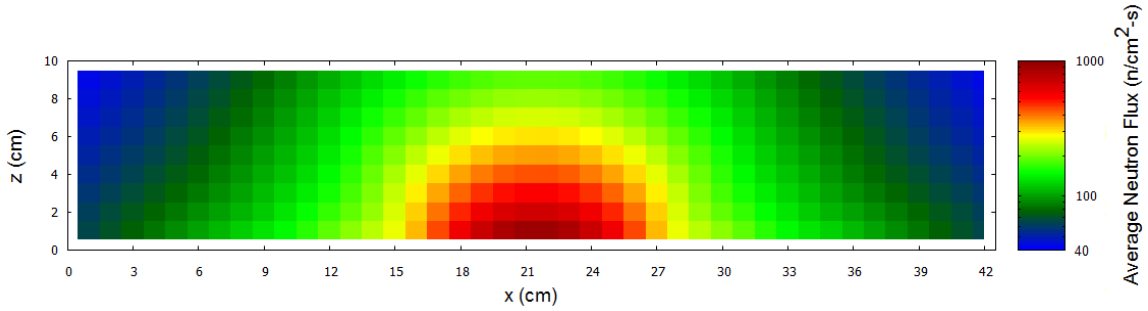

Tally 44: Neutron flux mesh tally superimposed to the YX face of the source, for a distance of 10 cm away from the source surface. The values are averaged over the volume of each mesh cell illustrated. The computational relative uncertainty for each cell was lower than 0.2%.

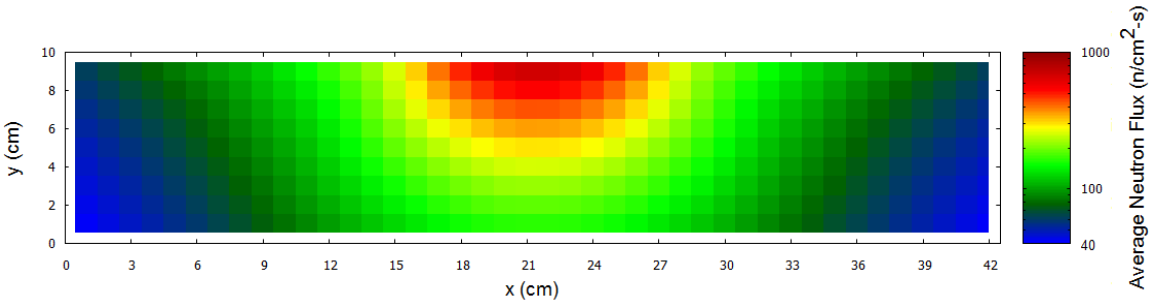

Tally 64: Neutron flux mesh tally superimposed to the XZ face of the source, for a distance of 21 cm on either side of the neutron source, and 10 cm away from the source surface. The values are averaged over the volume of each mesh cell illustrated. The computational relative uncertainty for each cell was lower than 0.2%.

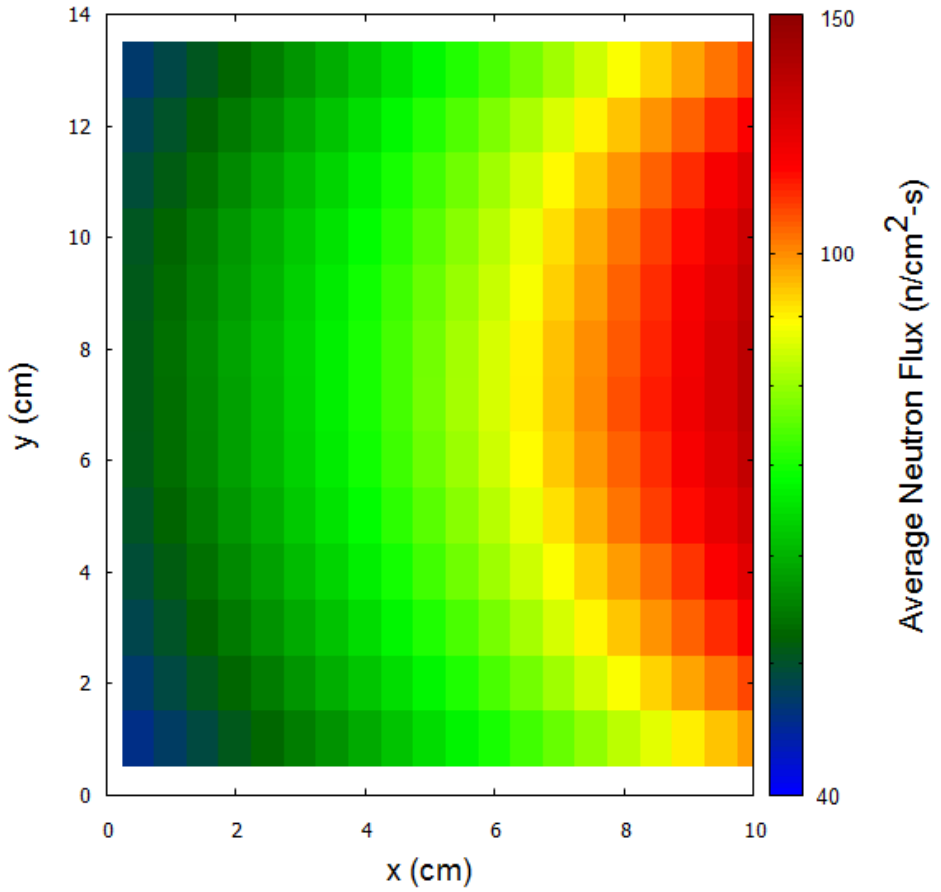

Tally 84: Neutron flux mesh tally superimposed to the YZ face of the source, for a distance of 10 cm away from the surface of the source. The values are averaged over the volume of each mesh cell illustrated. The computational relative uncertainty for each cell was lower than 0.2%.

Appendix B Calculations

B.1 Pair Production Threshold Energy

In pair production, all the energy of the gamma ray is converted into an electron-positron pair and kinetic energy for the pair. The minimum threshold energy required for this process to occur is 1.02 MeV. This value is calculated as follows.

$$E_{gamma} = m_{e^-}c^2 + m_{e^+}c^2 + KE_{e^-} + KE_{e^+}$$

where KE is the kinetic energy of the positron and electron, E_{gamma} is the incident gamma energy, $m_{e^-} = m_{e^+} = 9.10939 \times 10^{-31}$ kg (the rest mass of an electron or a positron), c is the speed of light (2.9979×10^8 m/s).

To calculate the threshold energy, let KE_{e^-} and KE_{e^+} be equal to 0. Therefore,

$$E_{gamma} = m_{e^-}c^2 + m_{e^+}c^2$$

The equation becomes:

$$E_{gamma} = 2 \times (9.10939 \times 10^{-31}\ \text{kg}) \times \left(2.9979 \times 10^8 \frac{\text{m}}{\text{s}}\right)^2$$

$$E_{gamma} = 2 \times 8.1869 \times 10^{-14}\ \text{J}$$

Using the conversion 1 J = 6.242×10^{12} MeV, E_{gamma} = 1.02 MeV.

B.2 Calculating the amount of ^{241}Am required for a large 40 cm × 40 cm neutron source for the SRGS

The total source strength from an ^{241}Am - ^{9}Be 40 cm × 40 cm source was 2.08×10^7 n/s (=1.30×10^4 (n/cm^2-s) × 1600 cm^2).

Step 1. The decay rate of the ^{241}Am source in α per s is calculated as follows:

$$D = \left(\frac{M}{M_{^{241}Am}} \times N_A \times \frac{\ln 2}{T_{\frac{1}{2}}} \right)$$

where M is the required mass of ^{241}Am, $M_{^{241}Am}$ is the atomic mass of ^{241}Am (241.056 g/mol), N_A is Avogado's number (6.022×10^{23} atoms/mole), $T_{1/2}$ is the half-life of ^{241}Am in seconds (1.365×10^{10} s).

Solving the equation we have that $D = 1.268 \times 10^{11} \times M$ (g^{-1} s^{-1})

Step 2. Assume that Be is in a thin shell (thickness Δr) around the ^{241}Am source. The total volume of the shell, V = Δr × A, where A is the area of the shell. The number of Be atoms is defined as

$$N_{Be} = \frac{(\Delta r) \times A \times \rho_{Be}}{M_{Be}} N_A$$

where ρ_{Be} = 1.85 g/cm^3 and M_{Be} = 9.012 g/mole.

Therefore, $N_{Be} = (\Delta r) \times A \times 1.236 \times 10^{23}$ cm^{-3}

Step 3. Total number of reactions per second, R, can be approximated as

$$R = \frac{D}{A} \times \sigma_{(\alpha,n)} N_{Be}$$

where $\sigma_{(\alpha,n)}$ is the absorption cross-section for an α particle of energy 5.48 MeV (*i.e.,* the average α energy resulting from ^{241}Am decay). The $\sigma_{(\alpha,n)}$ value was obtained from the National Nuclear Data Centre Online Database at 524.56 mb = 0.525×10^{-24} cm^2.

$$\therefore \quad R = \frac{D}{A} \times 0.525 \times 10^{-24} \times \Delta r \times A \times 1.236 \times 10^{23}$$

$$R = 1.268 \times 10^{11} \times M \times 0.525 \times 10^{-24} \times \Delta r \times 1.236 \times 10^{23}$$

$$R = 8.228 \times 10^{9} \times M \times \Delta r$$

Assume that the total number of reactions was equal 2.08×10^7 n/s and that Δr was << than the range of alpha particles in ^{9}Be, which was calculated in Section 2.1.2.1 to be 2.17×10^{-3} cm (otherwise the approximation formula for R above would need to account for the shielding effects introduced by the Be). A reasonable value is to assume Δr is 1.0×10^{-3} cm (*i.e.,* half the range). Using this information, the calculate mass of ^{241}Am is 2.5 g.

Appendix C Conference Paper "An MCNP Feasibility for a Switchable Radioactive Gamma Source"

This paper has been presented and published in the Proceedings for the 7th International Conference on Modelling and Simulation in Nuclear Science and Engineering (7ICMSNSE), Ottawa, 2015 October 18 - 21

AN MCNP FEASIBILITY STUDY FOR A SWITCHABLE GAMMA SOURCE

R. Dranga and G.A. McRae
Carleton University, Ottawa, Ontario, Canada
ruxandra.dranga@carleton.ca, glenn.mcRae@carleton.ca

Abstract

Gamma radiation sources are being used for an array of everyday applications, from portal monitors for homeland security to blood sterilization, and as calibration sources in nuclear medicine. This paper presents the preliminary feasibility study of a source that allows the gamma radiation to be turned on and off. The gamma radiation is produced via a sequence of nuclear reactions: an (α, n) reaction, followed by an (n, γ) reaction. Parametric studies in MCNP5 were performed to investigate the effect of different moderators, neutron absorbers, and geometries on the gamma flux and gamma dose produced. The results of the feasibility study are discussed in the context of nuclear medicine applications.

Keywords: MCNP simulation, gamma source design, nuclear medicine applications

1. Introduction

Gamma radiation sources are being used for a wide array of everyday applications, from portal monitors for homeland security [1] to food and blood sterilization [2], and as calibration sources in nuclear medicine [3][4]. Due to their extensive use in a wide array of applications, post September 2001, countries around the world started looking into the possibility of replacing current radiation sources with alternative designs to improve health, safety and security, while maintaining an equivalent performance level of the device [5].

Two main applications of gamma radiation sources provided the motivation behind the current feasibility study: 1) ^{57}Co flood sources used to calibrate gamma cameras used in nuclear imaging devices [3] [4]; and 2) the gamma sources used in self-contained irradiators used primarily for blood irradiation and sterilization processes [5]. In general, the current sources work well, however, a number of disadvantages and limitations were identified, including: 1) frequent replacement of the sources (i.e., ^{57}Co sources need to be replaced every 1-2 years [6], and ^{60}Co sources need to be replaced every 5 years [5]); 2) ^{137}Cs sources, although they have a long shelf-life (i.e., ~30 years), use primarily cesium chloride as the radioactive material, which poses significant hazards to workers, and public safety and security since it is found in powder form and can readily disperse in the environment if not properly contained and dispensed [5]; and 3) the sources are continuously active, that is, the radioactive material continuously emits gamma radiation, therefore, permanent shielding needs to be in place to minimize the dose to personnel, in accord with the ALARA (As Low As Reasonably Achievable) radiation protection principle.

The feasibility of a new gamma source design has been investigated. This new design was proposed to eliminate the need for frequent replacement of the sources, eliminate the use of cesium

chloride as the gamma emitter, aid in the simplification of the storage, transportation and handling procedures, and to reduce the time of radiation exposure and dose received by medical personnel.

The current paper describes the concept behind such a gamma source and summarizes some of the preliminary computational results obtained as part of the feasibility study performed using the Monte Carlo computer code MCNP5 [7]. The goal of this feasibility study was to investigate different geometries for the gamma source, various source materials (for both (α, n) and the (n, γ) reactions), and moderator materials. MCNP modelling of the source was used to calculate the gamma flux and the gamma dose resulting from different source designs.

1.1 General description of proposed design

The basic principle behind the new gamma source design is the production of gamma rays via a sequence of two nuclear reactions: an (α, n) reaction, followed by an (n, γ) reaction. The (α, n) reaction can be switched "ON" and "OFF" manually, thus controlling the production of gamma radiation. The neutrons produced via this reaction are then moderated to maximize their absorption by isotopes that will produce gamma rays, via an (n,γ) reaction.

The feasibility of switchable radioactive neutron sources (or SRNS) has been shown at Argonne National Laboratory [8][9] and at Sandia National Laboratories [10]. The "switchable radioactive gamma source" (SRGS) presented in this paper is based on the SRNS. It is important to note that the computer models investigated in this paper focus on the physics of the system and they do not account for any of the mechanical factors (e.g., the mechanism used for switching the source "ON" or "OF").

2. Modelling Methodology

2.1 Neutron source model

The neutron source is at the heart of the gamma source design. Choosing an appropriate neutron source was a key step. Potential alpha-emitting radioisotopes were chosen based on three criteria: 1) a half life long enough to eliminate the need for frequent replacements (i.e., at least 10 years); 2) be safe to store and transport in the "OFF" state; and 3) the (α, n) reaction must result in a neutron yield which will provide a sufficient gamma flux and dose for the intended application. A neutron source based on ^{241}Am - ^{9}Be satisfies these three criteria according to the information summarized by Hertz et. al [10].

First, ^{241}Am has a half-life of 432.2 years. This long half life eliminates the need for replacement of the gamma source every few years, like, for example, in the case of a ^{57}Co source. Americium-241 is relatively safe when compared with other alpha emitting radioisotopes because of its low number of spontaneous fission events (i.e., 5.38×10^{-7} spontaneous fissions/μs/g [10]) and low energy gamma-ray background (60 keV [12]). Americium-241 decays primarily by alpha emission, with an energy of 5.48 MeV, which, based on the empirical relationship derived by Anderson and Hertz [11], results in an estimated yield for the ^{241}Am - ^{9}Be source of 86 neutrons per 10^6 alpha particles emitted.

MCNP5, version 1.40 was used for the feasibility study, however, it does not have the capability to model the (α, n) reaction. A model neutron source equivalent to a ^{241}Am - ^{9}Be source was developed using literature data for the neutron energy distribution of this (α, n) reaction. The modelled neutron spectrum is illustrated in Figure 1, which is based on data reported by Kluge and Weise [13]. The computer code SOURCES-4C [14] was used to determine the neutron source strength. SOURCES-4C has the capability to calculate the production rate from common (α, n) reactions for a number of different geometric configurations, including the two-region interface, which best represents the SRNS. The calculated neutron strength for the models in the current feasibility study was 1.30×10^4 neutrons / s-cm^2.

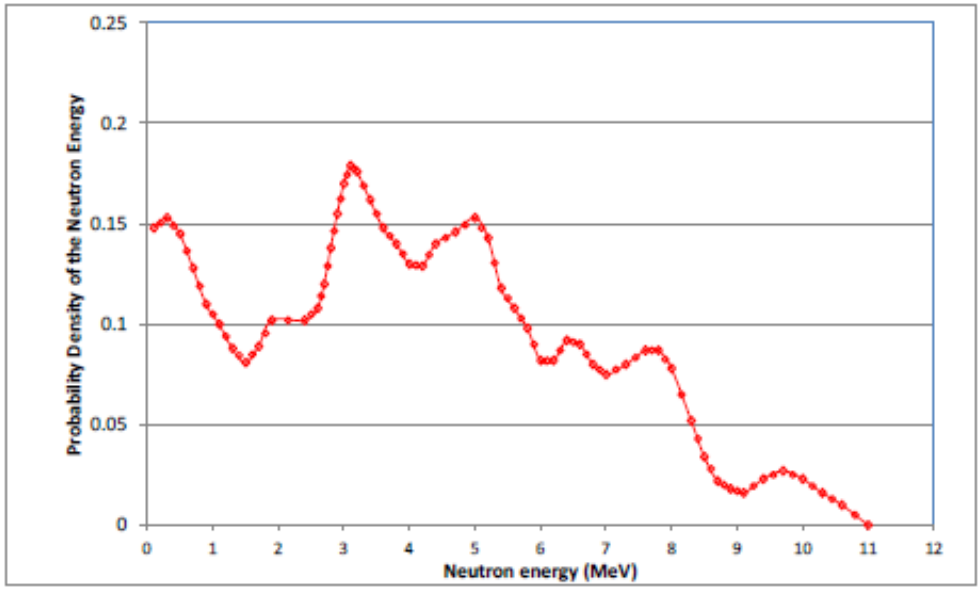

Figure 1 Modelled neutron spectrum for the ^{241}Am - ^{9}Be source

2.2 Gamma Source Models

The neutron source described in Section 2.1 was enclosed in Zircaloy-2 (0.2 cm thick) and surrounded by a neutron moderator of variable thickness. Two neutron moderators were investigated: deuterated polyethylene (CD_2) and heavy water (D_2O). The moderator was enclosed in a Zircaloy-2 shell (0.2 cm thick), which was surrounded by a variable thickness of neutron absorber on the outside. A number of neutron absorbers were investigated (e.g. ^{147}Sm, $Sm_{natural}$ and $Gd_{natural}$). Figure 2 shows an example of an MCNP model for a 40 cm x 40 cm planar source (referred to as the "large source" in this paper), which is equivalent to the size of a standard gamma camera used for Single Photon Emission Computed Tomography (SPECT) imaging. The gamma flux and the dose deposited in the air surrounding the source were calculated for three different regions: (1) the two planar regions in the front and back of the source (see Figure 2A - air region 1 and air region 2); and (2) the air surrounding the source on all other sides (see Figure 2B - air region 3).

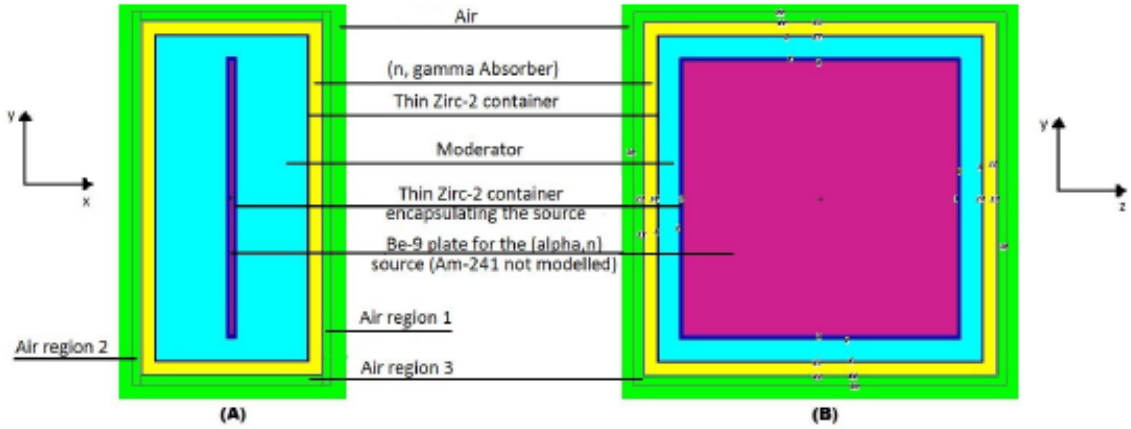

Figure 2 Sample modelled design for the (n, γ) source. (A) X-Y view of a 40 cm x 40 cm source; (B) Z-Y view of the same source.

A 6 cm x 6 cm neutron source (referred to as the "small source" in this paper) was also investigated. As shown in Figure 3 – Model A and Figure 3 – Model B, the neutron source was surrounded by moderator (e.g., CD_2 or D_2O) of thicknesses between 0 cm and 20 cm along the x-direction. The y- and z-dimensions of the Zirc-2 alloy shell containing the moderator and the neutron source were kept constant at either 8 cm x 8 cm or 10 cm x 10 cm. This "smaller" source design (i.e., either 8 cm x 8 cm or 10 cm x 10 cm) would cover one quarter of a standard gamma camera. Also, various absorber thicknesses were investigated to see their effect on the neutron and gamma fluxes and doses obtained outside the source. In addition, a number of models were created using lead as a potential shield / reflector inside the source (see Figure 3 - Model A).

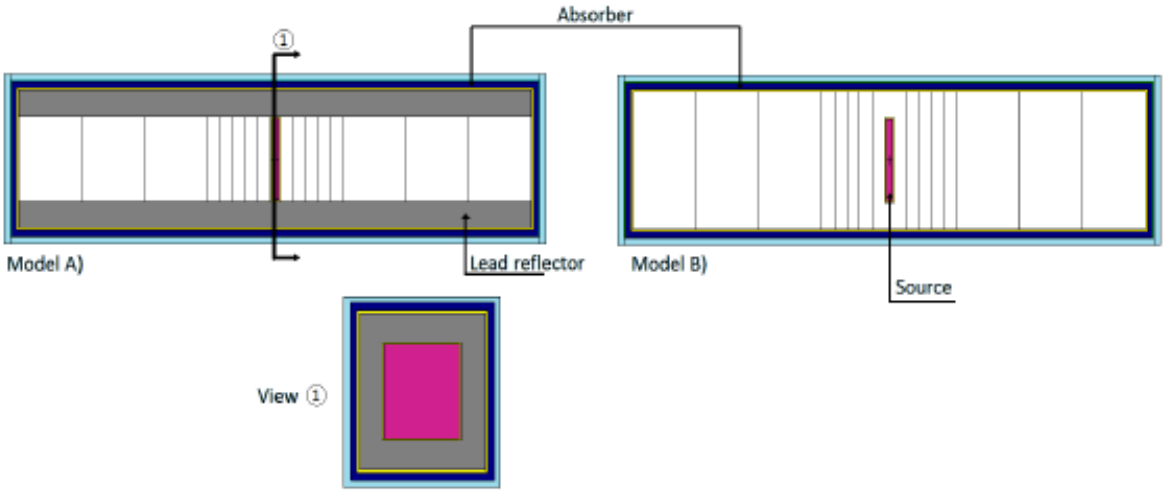

Figure 3 Example of the modelled design for the smaller (n, γ) source. (A) X-Y view of the source with the lead reflector/shield; (B) X-Y view of the similar source without the lead shield.

3. Results and Discussion

Preliminary calculations were performed for the large 40 cm x 40 cm source (the equivalent size of a SPECT gamma camera) using CD_2 as the moderator and ^{149}Sm as the absorber. These calculations resulted in a maximum gamma flux of 2.0 x 10^3 γ /s-cm^2 for a 5 cm thick moderator on each side of the Am/Be source with 0.1 cm ^{149}Sm absorber surrounding the moderator. The cost of this source configuration, considering the main components, i.e., the Am and Be for the (α,n) source, the CD_2 moderator and the ^{149}Sm absorber, was estimated to be at least 100 times more than the cost of current ^{57}Co sources and thus it was not practical.

The technical feasibility of a smaller neutron source (6 cm x 6 cm) was investigated. The results summarized here are from two studies. First the neutron source was surrounded by two different moderators, D_2O or CD_2, and by either $Sm_{natural}$ or $Gd_{natural}$ as absorbers undergoing the (n,γ) reaction. The y- and z-dimensions of the moderator region were kept constant at 8 cm x 8 cm, while the x-dimension was varied between 0 cm and 20 cm on each side of the planar neutron source. Figure 4 shows the gamma fluxes obtained for each moderator parametric study on the Y-Z faces of the source (i.e., air region 1 or 2, Figure 2A). A separate parametric study was performed to investigate the impact of the absorber thickness on the calculated gamma flux: the thicker the absorber the larger is the calculated gamma flux, because more neutrons are absorbed. Increasing the thickness of the moderator led to more neutrons "leaking" out through the side, resulting in increased gamma production in that region (i.e., air region 3, Figure 2A). There was no significant difference observed between the CD_2 and D_2O moderators, which was expected because these moderators have similar properties for this application. For the $Sm_{natural}$, the maximum gamma fluxes calculated were 23.8 gammas/s-cm^2 for a 1 cm thick D_2O moderator and 1 cm absorber, and 24.7 gammas/s-cm^2 for a 2 cm thick CD_2 moderator and 1 cm absorber.

Figure 5 allows a comparison to be made of the gamma output for the (n, γ) absorbers $Sm_{natural}$ and $Gd_{natural}$ using CD_2 as the moderator. As expected, the results show similar trends, because samarium and gadolinium are excellent neutron absorbers. (The absorption cross sections for thermal neutron capture are 49700 barn for $Gd_{natural}$ and 5922 barn for $Sm_{natural}$. [15]) The maximum calculated gamma flux is 24.7 gammas/s-cm^2 for 1 cm $Sm_{natural}$ and 2 cm CD_2 moderator, and 23.2 gammas/s-cm^2 for 1 cm $Gd_{natural}$ and 2 cm CD_2 moderator. These fluxes are orders of magnitude lower than the gamma fluxes resulting from standard 5 mCi or 10 mCi ^{57}Co fixed calibration flood sources [3]. Unfortunately, these calculated fluxes makes this application of the switchable source impractical, because it will significantly increase the calibration times (i.e., from 3-5 min to over a day). Furthermore, the gamma energy range produced by either $Sm_{natural}$ or $Gd_{natural}$ is far from ideal for a flood source. The ideal flood source should have an energy that is similar to that of the isotope used during the medical procedures. For example, ^{99m}Tc, which is the most common isotope used in SPECT imaging, emits 140.5 keV gamma as it decays. The ^{57}Co currently used in calibration procedures emits radiation with two main energies: 122 keV (85.6%) and 136 keV (10.7%), which are sufficiently close to that emitted by ^{99m}Tc [16]. If $Sm_{natural}$ is used as absorber, then the gamma spectrum includes a wide range of gamma energies, from a few keV to as high as 1-2 MeV. Such a wide spectrum of gamma rays could become problematic during calibration procedures for SPECT gamma cameras.

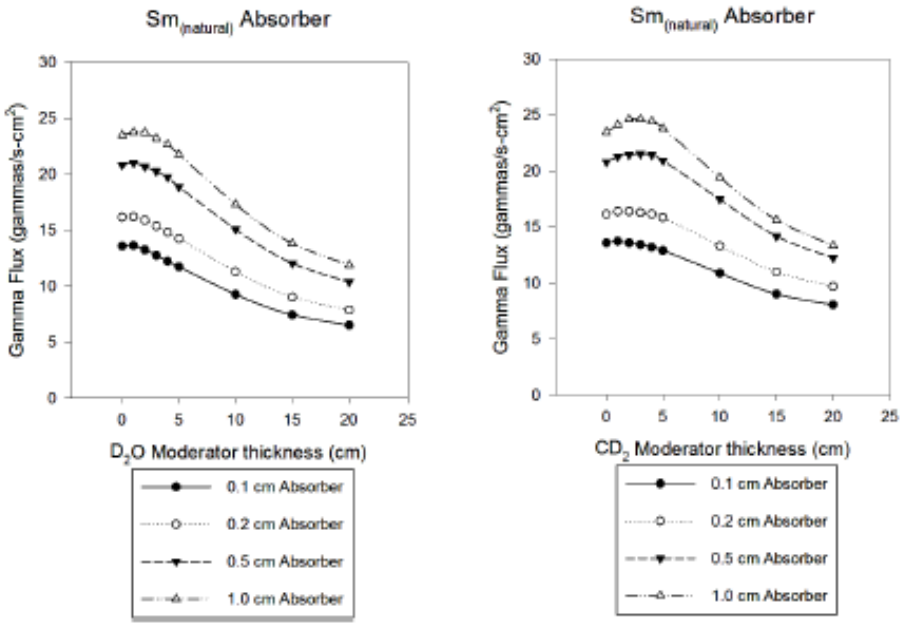

Figure 4 Gamma flux for the small SRG source with CD_2 and D_2O moderators, for varying thicknesses of $Sm_{natural}$ absorber.

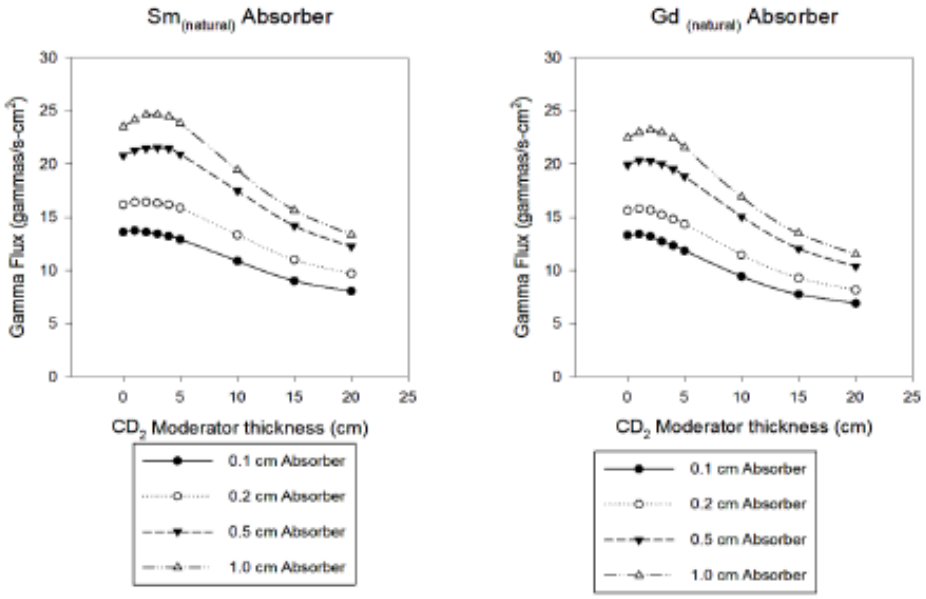

Figure 5 Gamma flux for the small SRG source with $Sm_{natural}$ vs $Gd_{natural}$ using CD_2 as a moderator, for varying thicknesses of absorber

Further studies estimated neutron and gamma fluxes and doses for a CD_2 moderated source using $Gd_{natural}$ as the absorber. The y- and z-dimensions of the moderator region were kept constant at 10 cm x 10 cm, while the x-dimension was varied either between 0 – 15 cm or 0 - 20 cm on either side of the planar neutron source. A parametric study was performed for the configuration

illustrated in Figure 3A, which includes a 1.9 cm thick lead shield surrounding the moderator region. Figures 6 and 7 summarize the results for the calculated gamma fluxes and the corresponding gamma doses outside the planar source (i.e., in air regions 1 and 2, illustrated in Figure 2A). The gamma doses were calculated using the photon flux-to-dose conversion factors from ICRP-21, which were included with MCNP5 [7].

Two sets of parametric studies were performed by varying the thickness of moderator inside each source, while keeping the overall source dimensions unchanged. Figures 6A and 7A illustrate results for moderator thicknesses between 0 cm and 15 cm, with the overall source x, y, and z dimensions, excluding the absorber thickness, of 31.1 cm x 10.4 cm x 10.4 cm. Note that, for moderator thicknesses less than 15 cm, the empty space inside the source was modelled as void. Figures 6B and 7B illustrate results for moderator thicknesses between 0 cm and 20 cm, with overall source x, y, z dimensions, excluding the absorber thickness of 41.1 cm x 10.4 cm x 10.4 cm. The maximum calculated gamma flux for the first set of parametric studies was 37.9 gammas/s-cm^2 (Figure 6A), corresponding to a gamma dose on either side of the planar source of 0.00092 mSv/hr (Figure 7A), for a 5 cm moderator thickness and 0.5 cm of $Gd_{natural}$ absorber. The maximum calculated gamma flux for the second set of parametric studies was 23.9 gammas/s-cm^2 (Figure 6B), corresponding to a gamma dose on either side of the planar source of 0.000571 mSv/hr (Figure 7B), for a moderator thickness of 5 cm and 0.5 cm of $Gd_{natural}$ absorber. The corresponding total gamma dose around the source (i.e., air region 3, Figure 2) is 0.0023 mSv/hr for parametric study (A) and 0.0018 mSv/hr for study (B). The gamma spectrum corresponding to the case resulting in the maximum gamma flux of 37.9 gammas/s-cm^2 (illustrated in Figure 6A) is shown in Figure 8. As noted, a significant percentage of gammas have energies greater than 500 keV, with ~30% of the gammas having energies between 2 MeV and 3 MeV. These high gammas would have a negative impact on the performance of the gamma camera and the electronics, making this design not appropriate as a calibration source.

Similar calculations were performed to estimate the corresponding neutron fluxes and doses for the two different source designs. The results are reported in Figure 9A and Figure 10A for the neutron flux and corresponding neutron dose for a moderator thickness of 15 cm, and Figure 9B and Figure 10B for a neutron flux and corresponding neutron dose for a moderator thickness of 20 cm. The calculated neutron fluxes are at least 5 times larger than the corresponding gamma fluxes, which indicates the neutrons are not sufficiently moderated before they reach the absorber region. As shown in Figure 1, a significant number of neutrons produced via the ^{241}Am - ^{9}Be (α, n) reaction have energies greater than 3 MeV (i.e., a fast spectrum), and in order to take advantage of the large absorption cross section for Gd at low energy, they need to be thermalised (i.e., energies <1 eV). Furthermore, as expected, the flux and dose calculated for the source design with a maximum moderator thickness of 20 cm (i.e., larger overall source dimensions) are lower than those for the source design with a maximum moderator thickness of 15 cm, due to an increased neutron leakage through the sides of the planar source. This effect is consistent for the both gamma and neutron tallies - see Figures 6 and 7 for the gamma flux and dose and Figures 9 and 10 for the neutron fluxes and doses.

The gamma doses calculated here can be compared with the typical doses that are applied to blood bags during the irradiation process used to kill bacteria and prevent transfusion-associated graft versus host disease (TA-GVHD). For such an application, gamma doses between 0.02 - 0.04 kGy (equivalent to 0.02 – 0.04 kSv when looking at gamma radiation) must be applied [6]. The doses calculated for the configurations discussed in this paper are many orders of magnitude smaller than

those intended for blood irradiation, however, this application is more promising than the flood source one because there are no specific constraints on the gamma energies that are required during this procedure, which allows for more choices of isotopes for the (n, γ) reactions. Future studies will focus on investigating other isotopes and configurations that can increase the deposited gamma dose, while reducing the neutron dose.

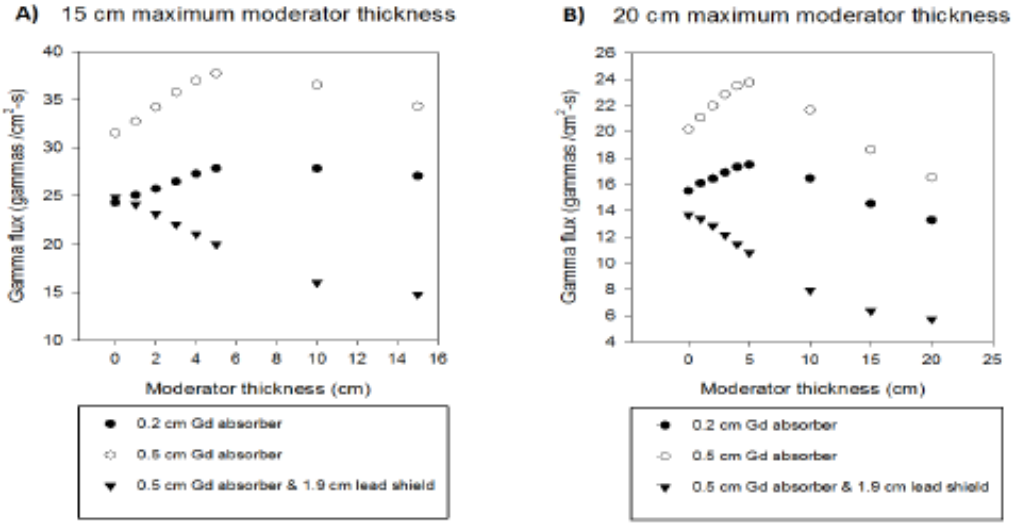

Figure 6 Small SRG source - Gamma flux for $Gd_{natural}$ absorber and CD_2 moderator, for varying thicknesses of absorber. A) Moderator x-, y-, z-dim. 15 x 10 x 10 (cm); B) Moderator x-, y-, z-dim. 20 x 10 x 10 (cm)

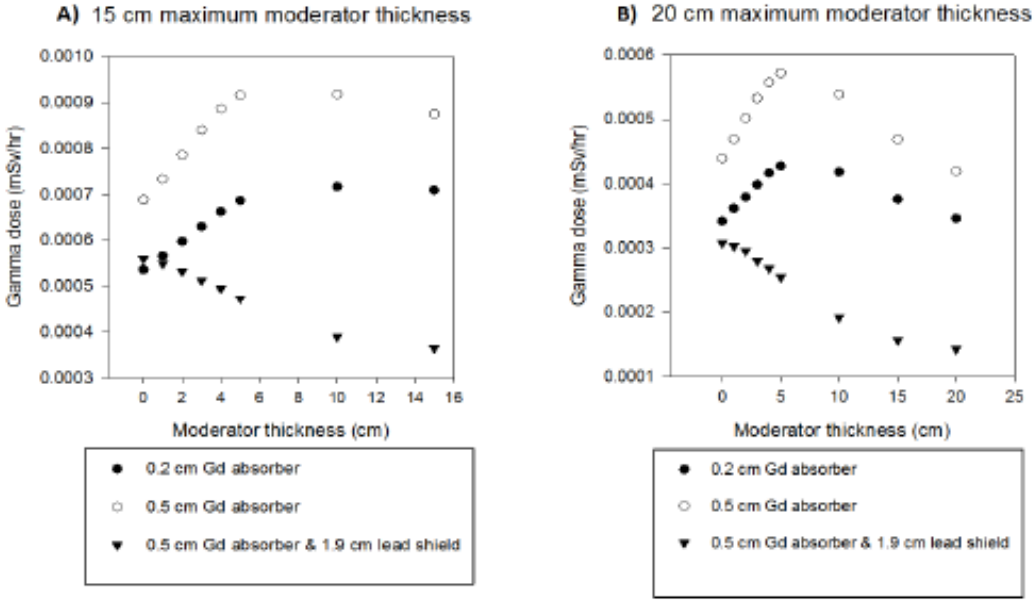

Figure 7 Small SRG source - Gamma dose for $Gd_{natural}$ absorber and CD_2 moderator, for varying thicknesses of absorber. A) Moderator x-, y-, z-dim. 15 x 10 x 10 (cm); B) Moderator x-, y-, z-dim. 20 x 10 x 10 (cm)

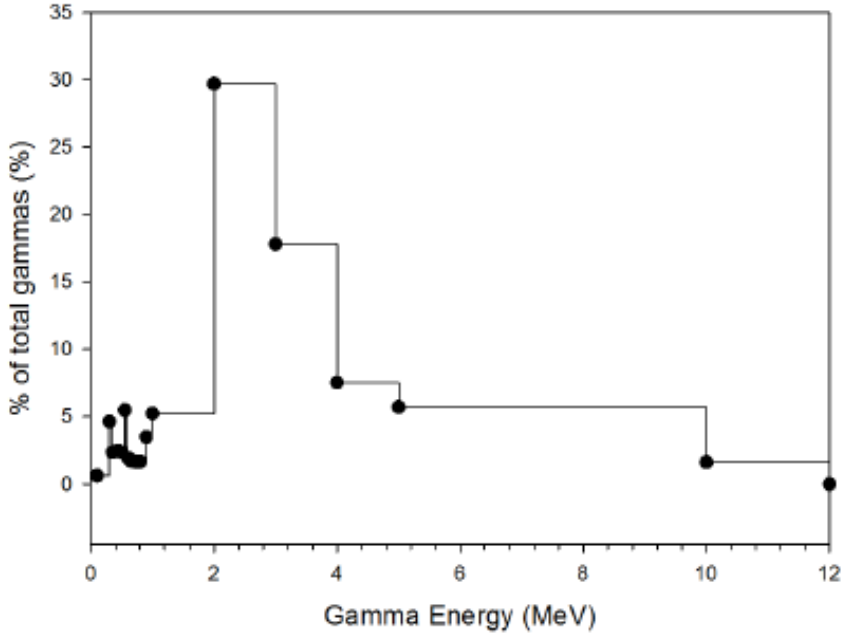

Figure 8 Gamma spectrum corresponding to the source modelled in Figure 6A, at 5 cm moderator thickness and 0.5 cm $Gd_{natural}$ absorber

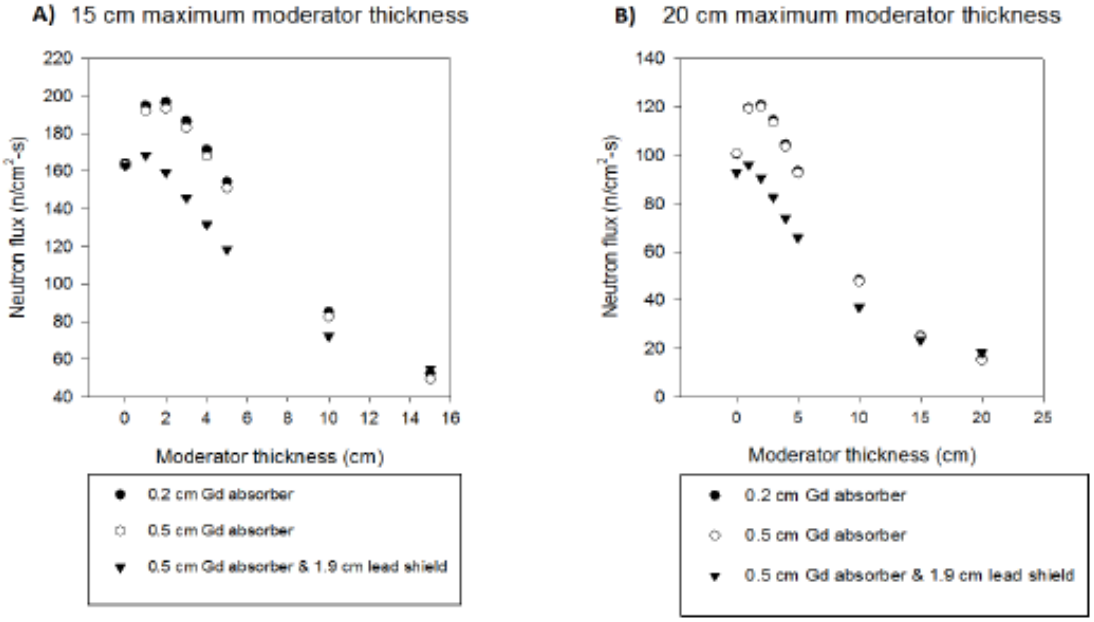

Figure 9 Small SRG source - Neutron flux for $Gd_{natural}$ absorber and CD_2 moderator, for varying thicknesses of absorber. A) Moderator x-, y-, z-dim. 15 x 10 x 10 (cm); B) Moderator x-, y-, z-dim. 20 x 10 x 10 (cm)

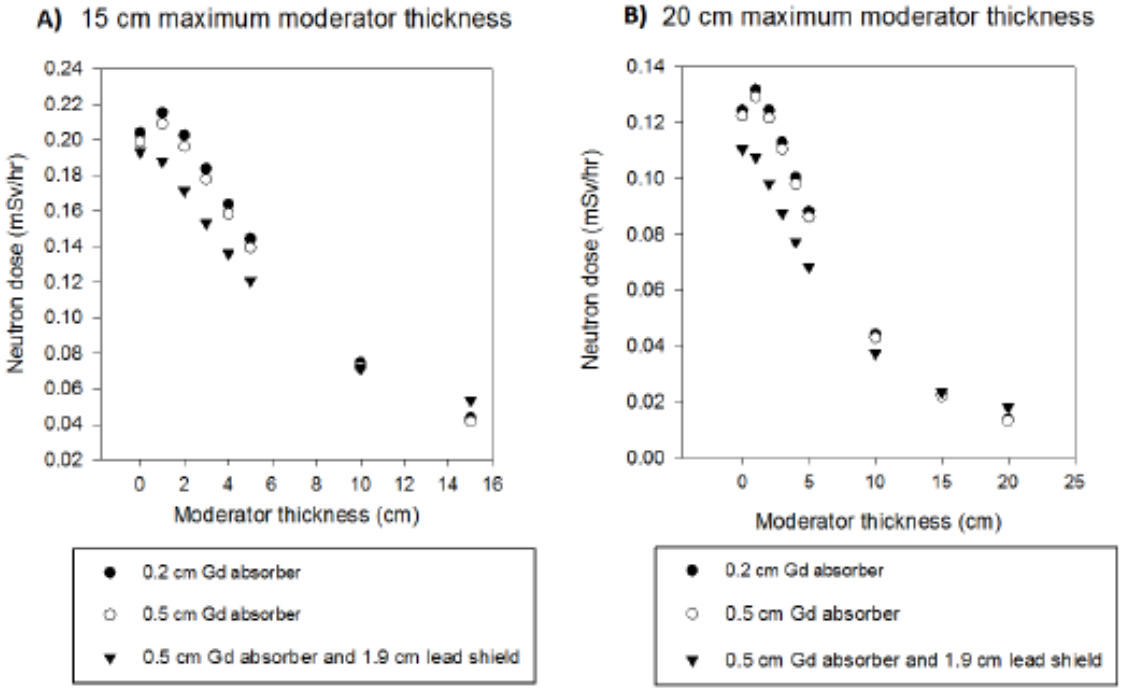

Figure 10 Small SRG source - Neutron dose for $Gd_{natural}$ absorber and CD_2 moderator, for varying thicknesses of absorber. A) Moderator x-, y-, z-dim. 15 x 10 x 10 (cm); B) Moderator x-, y-, z-dim. 20 x 10 x 10 (cm)

4. Conclusions

This paper introduced a switchable radioactive gamma source (SGRS) that can be turned "ON" and "OFF" as required by the user. The feasibility of this source was investigated for two potential applications: 1) a flood source to calibrate gamma cameras used in SPECT imaging; and 2) a self-contained blood irradiator. Preliminary investigation showed that a SGRS would be difficult to apply as a flood source, because 1) the gamma flux produced would be too low to provide a quick calibration of the gamma cameras; and 2) the gamma spectrum would present a wide array of gamma energies (some of which are > 500 keV) that would interfere with the calibration of the gamma cameras. These calibrations require gamma that 1) are close in energy to those of the isotope used during the medical procedure; and 2) have a very narrow energy spectrum. However, preliminary MCNP results show potential promise that a SGRS could be used in a self-contained blood irradiator, as long as the gamma dose deposited around the source is increased and the neutron dose is decreased. Further studies will focus on different absorber isotopes and different source geometries (e.g., a cylindrical source). Furthermore, increasing the strength of the current neutron source will be considered, since a stronger neutron source will help increase the gamma flux and dose for the intended application.

5. References

[1] L. Pibida, M. Unterweger, L. Karam, "Development of gamma-ray emitting test sources for portal monitors", Applied Radiation and Isotopes, Vol 64, 2006, pp. 1271 – 1272

[2] International Atomic Energy Agency, "Gamma Irradiators for Radiation Processing", Industrial Applications and Chemistry Section, 2006 February, http://www-naweb.iaea.org/napc/iachem/Brochure%20on%20gamma%20irradiators.pdf, Accessed online on June 20 2014

[3] M.G. Sayed, "Quality Control in Nuclear Medicine II. Planar and Single Photon Emission Computed Tomographic Gamma Camera Systems, TJNM, Vol. 6, No. 3, 1997, pp. 185 - 189

[4] P. Zanzonico, "Routine Quality Control of Clinical Nuclear Medicine Instrumentation: A Brief Review", Journal of Nuclear Medicine, Vol. 49, No. 7, 2008, pp. 1114 - 1131

[5] Radiation Sources Use and Replacement: Abbreviated Version, Committee on Radiation Sources Use and Replacement, National Research Council, ISBN: 0-309-11015-7, 2008, http://www.nap.edu/catalog/11976.html, Accessed October 18, 2014

[6] M.K. O'Connor, "Quality Control of Scintillation Cameras (Planar and SPECT)", 41st Annual Meeting of the American Association of Physicists in Medicine, Nashville, TN, July 1999, https://www.aapm.org/meetings/99AM/pdf/2741-51264.pdf, Accessed March 10, 2014

[7] Los Alamos National Laboratory, X-5 Monte Carlo Team, "MCNP - A General N-Particle Transport Code, Version 5", Volume II: User's Guide, LA-CP-03-0245, 2003 April

[8] D.L. Bowers, E.A. Rhodes, C.E. Dickerman, "A switchable radioactive neutron source: Proof-of-principle", Journal of Radioanalytical and Nuclear Chemistry, Vol. 233, Issue 1-2, 1998, pp. 161-165

[9] R.E. Boyar, A. DeVolpi, G.S. Stanford, E.A. Rhodes, "Switchable radioactive neutron source device", US Patent Application US 4829191 A, 1989 May[10] K.L. Hertz, N.R. Hilton, J.C. Lund, J.M. Van Scyoc, "Alpha-emitting radioisotopes for switchable neutron generators", Nuclear Instruments and Methods in Physics Research A, Vol. 505, 2004, pp. 41-45

[11] M.E. Anderson, M.R. Hertz, "Thick Target Yields for the ^{9}Be(α,n) Reaction", Nuclear Science and Engineering, Vol. 44, No. 3, 1971, pp. 437-439

[12] E.A. Rhodes, D.L. Bowers, R.E. Boyar, C.E. Dickerman, "Advanced Concept Proof-of-Principle Demonstration: Switchable Radioactive Neutron Source", ANL/ACTV-95/2, 1995

[13] H Kluge, K. Weise, "The Neutron Energy Spectrum of a Am-241/Be (α, n) Source and Resulting Mean Fluence to Dose Equivalent Conversion Factors", Radiation Protection Dosimetry, Vol. 2, No. 2, 1982, pp. 85-93

[14] Los Alamos National Laboratory, "SOURCES-4C: A code for calculating (alpha, n), spontaneous fission, and delayed neutron sources and spectra", LA-UR-02-1839, 2002

[15] NIST Center for Neutron Research, "Neutron Scattering Lengths and Cross Sections", Online resource: http://www.ncnr.nist.gov/resources/n-lengths/list.html, Accessed on September 20 2014

[16] Brookhaven National Laboratory, "Interactive Chart of Nuclides", Online resource http://www.nndc.bnl.gov/nudat2/, Accessed on March 15, 2014

Appendix D Example of Computer Input Files

D.1 Example MCNP Case for Varying the Source Size

Case Description: Maximum 10 cm moderator thickness on either side of the neutron source, moderator CD_2 (5 cm thick), 0.5 cm $Sm_{natural}$ absorber, F4 tally used to calculate fluxes and dose rates

```
Smaller planar source - 1.9 cm top and bottom
C CD2 moderated
C Sm absorber
C Modelled on March 29th, 2015 - calculates gamma doses and flux
C Density values:
C  M1: Am-241, density =12 g/cc
C  M2: Be-9,   density =1.85 g/cc
C  M3: Lead, density = 11.34 g/cc
C  M4: D2O, density = 1.105 g/cc
C  M5: Zircaloy-2, density = 6.55 g/cc
C  M6: Sm-149, density = 7.54 g/cc
C  M7: Air, density = 1.293E-3  g/cc
C  M8: NaI crystal, density = 3.7 g/c
C  M9: CD2 (deuterated polyethylene), den=1.06 g/cc
C  M10: Gd (natural) density = 7.90 g/cc
C  M11: Sm (natural), density = 7.54 g/cc
C  M12: HDPE, density = 0.97 g/cc
C
C  CELL  CARDS
1   2   -1.85   -20          imp:n=1  imp:p=1
2   5   -6.55   -1   20      imp:n=1  imp:p=1
5   9  -1.06   -2   1        imp:n=1   imp:p=1   $   1 cm moderator
6   9  -1.06   -3   2        imp:n=1   imp:p=1   $   2 cm moderator
7   9  -1.06   -4   3        imp:n=1   imp:p=1   $   3 cm moderator
8   9  -1.06   -5   4        imp:n=1   imp:p=1   $   4 cm moderator
9   9  -1.06   -6   5        imp:n=1   imp:p=1   $   5 cm moderator
10  0          -7   6        imp:n=1   imp:p=1   $   10 cm moderator
19   5   -6.55   -10   7         imp:n=1   imp:p=1   $ Zr encapsulation
20  11  -7.54  10  -11      imp:n=1  imp:p=1
21  11  -7.54  11  -12      imp:n=1  imp:p=1
C
C  Air  around  source,  for  tallying
97  7  -1.29E-03  -32  12      imp:n=1  imp:p=1
98  7  -1.29E-03  -30        imp:n=1  imp:p=1
99  7  -1.29E-03  -31        imp:n=1  imp:p=1
C  Overall  room
100  7  -1.29E-03  30  31  32  -50  imp:n=1  imp:p=1
101  0    50        imp:n=0  imp:p=0
C
C  Blank  Line  for  Surface  Cards  section  **********************

CC  SURFACE  CARDS
C
1  box  -0.35  -3.1  -3.1  0.7  0  0  0  6.2  0  0  0  6.2  $  0.1  Zr
20  box  -0.25  -3  -3  0.5  0  0  0  6  0  0  0  6  $  0.5  cm  Be-9
```

```
c
c  Moderator  -  CD2  (deuterated  polyethylene)
2  box  -1.35  -5  -5  2.7  0  0  0  10  0  0  0  10  $  1 cm moderator
3  box  -2.35  -5  -5  4.7  0  0  0  10 0  0  0  10 $  2 cm moderator
4  box  -3.35  -5  -5  6.7  0  0  0  10 0  0  0  10 $  3 cm moderator
5  box  -4.35  -5  -5  8.7  0  0  0  10 0  0  0  10 $  4 cm moderator
6  box  -5.35  -5  -5  10.7  0  0  0  10 0  0  0  10 $  5 cm moderator
7  box  -10.35  -5  -5  20.7  0  0  0  10 0 0  0  10 $  10 cm moderator
c
c  Enclosing  Zr  box  (0.2  cm  thick)  with  (n,gamma)  absorber
10  box  -10.55  -5.2  -5.2  21.1  0  0  0  10.4  0  0  0  10.4
c  absorber  on  the  outside  (  0.5  cm  thick total)
11  box  -10.95  -5.6  -5.6  21.9  0  0  0  11.2  0  0  0  11.2
12  box  -11.05  -5.7  -5.7  22.1  0  0  0  11.4  0  0  0  11.4
C
C  tally  for  air  surrounding  the  source  (  0.5  cm)
30  box  -11.55  -6.2  -6.2  0.5  0  0  0  12.4 0 0  0  12.4  $-X  side
31  box   11.05  -6.2  -6.2  0.5  0  0  0  12.4 0 0  0  12.4  $+X  side
32  box  -11.05  -6.2  -6.2  22.1 0  0  0 12.4  0 0  0  12.4  $ C
C
50 box -200 -200 -150 400 0 0 0 400 0 0 0 450  $ room
C  Blank Line for Physics Cards section **********************

C  Physics cards
mode n p
PHYS:n 40 0 0 0 -1 0 0
C
C  Source
sdef par=1 erg=D1 x=D2 y=D3 z=D4 cel=1
SI1 H .01 0.2 0.4 0.6 0.8 1 1.2 1.4 1.6 1.8 2.15 2.5 2.65 2.75
      2.85 2.95 3.05 3.15 3.3 3.5 3.7 3.9 4.1 4.3 4.55 4.85 5.1
      5.3 5.5 5.7 5.9 6.1 6.3 6.5 6.7 6.9 7.15 7.45 7.7 7.9 8.15
      8.4 8.6 8.8 9 9.25 9.55 9.85 10.15 10.45 10.8
SP1 0 0.0309 0.0306 0.0280 0.0244 0.0216 0.0193 0.0173 0.0174
      0.0196 0.0419 0.0216 0.0117 0.0132 0.0150 0.0167 0.0179
      0.0182 0.0347 0.0318 0.0296 0.0277 0.0266 0.0276 0.0440
      0.0460 0.0304 0.0268 0.0232 0.0211 0.0185 0.0168 0.0179
      0.0187 0.0174 0.0159 0.0239 0.0257 0.0179 0.0169 0.0200
      0.0088 0.0057 0.0041 0.0035 0.0060 0.0077 0.0077 0.0060
      0.0040 0.0021
SI2  -0.25 0.25
SP2   0 1
SI3  -3 3
SP3   0 1
SI4  -3 3
SP4   0 1
C NUMBER OF PARTICLES
NPS 1e8
print
C
C  Measurement cards
C
C Neutron and gamma flux for the last layer of 5 cm of either void or
moderator
F4:n 10
E4   0.1 0.5 1 1.5 2 2.5 3 3.5 4 4.5 5 5.5 6 7 8 9 10 11 14 16
F84:p 10
```

```
E84   0.1 0.3 0.35 0.4 0.45 0.5 0.55 0.6 0.65 0.7 0.75 0.8 0.9
      1 2 3 4 5 10 12 14 16 18 20
C Neutron and gamma fluxes for the air outside the source
F24:n 98
E24   0.1 0.5 1 1.5 2 2.5 3 3.5 4 4.5 5 5.5 6 7 8 9 10 11 14 16
F34:p 98
E34   0.1 0.3 0.35 0.4 0.45 0.5 0.55 0.6 0.65 0.7 0.75 0.8 0.9
      1 2 3 4 5 10 12 14 16 18 20
F44:n 99
E44   0.1 0.5 1 1.5 2 2.5 3 3.5 4 4.5 5 5.5 6 7 8 9 10 11 14 16
F54:p 99
E54   0.1 0.3 0.35 0.4 0.45 0.5 0.55 0.6 0.65 0.7 0.75 0.8 0.9
      1 2 3 4 5 10 12 14 16 18 20
F64:n 97
E64   0.1 0.5 1 1.5 2 2.5 3 3.5 4 4.5 5 5.5 6 7 8 9 10 11 14 16
F74:p 97
E74   0.1 0.3 0.35 0.4 0.45 0.5 0.55 0.6 0.65 0.7 0.75 0.8 0.9
      1 2 3 4 5 10 12 14 16 18 20
F204:p 97
E204  0.1 0.3 0.35 0.4 0.45 0.5 0.55 0.6 0.65 0.7 0.75 0.8 0.9
      1 2 3 4 5 10 12 14 16 18 20
DE204 LOG 0.01 0.015 0.02 0.03 0.04 0.05 0.06 0.08 0.10 0.15 0.2 0.3
          0.4 0.5 0.6 0.8 1.0 1.5 2.0 3.0 4.0 5.0 6.0 8.0 10
DF204 LOG 2.78E-06 1.11E-06 5.88E-07 2.56E-07 1.56E-07 1.20E-07
          1.11E-07 1.20E-07 1.47E-07 2.38E-07 3.45E-07 5.56E-07
          7.69E-07 9.09E-07 1.14E-06 1.47E-06 1.79E-06 2.44E-06
          3.03E-06 4.00E-06 4.76E-06 5.56E-06 6.25E-06 7.69E-06
          9.09E-06
F214:p 98
E214  0.1 0.3 0.35 0.4 0.45 0.5 0.55 0.6 0.65 0.7 0.75 0.8 0.9
      1 2 3 4 5 10 12 14 16 18 20
DE214 LOG 0.01 0.015 0.02 0.03 0.04 0.05 0.06 0.08 0.10 0.15 0.2 0.3
          0.4 0.5 0.6 0.8 1.0 1.5 2.0 3.0 4.0 5.0 6.0 8.0 10
DF214 LOG 2.78E-06 1.11E-06 5.88E-07 2.56E-07 1.56E-07 1.20E-07
          1.11E-07 1.20E-07 1.47E-07 2.38E-07 3.45E-07 5.56E-07
          7.69E-07 9.09E-07 1.14E-06 1.47E-06 1.79E-06 2.44E-06
          3.03E-06 4.00E-06 4.76E-06 5.56E-06 6.25E-06 7.69E-06
          9.09E-06
F224:p 99
E224  0.1 0.3 0.35 0.4 0.45 0.5 0.55 0.6 0.65 0.7 0.75 0.8 0.9
      1 2 3 4 5 10 12 14 16 18 20
DE224 LOG 0.01 0.015 0.02 0.03 0.04 0.05 0.06 0.08 0.10 0.15 0.2 0.3
          0.4 0.5 0.6 0.8 1.0 1.5 2.0 3.0 4.0 5.0 6.0 8.0 10
DF224 LOG 2.78E-06 1.11E-06 5.88E-07 2.56E-07 1.56E-07 1.20E-07
          1.11E-07 1.20E-07 1.47E-07 2.38E-07 3.45E-07 5.56E-07
          7.69E-07 9.09E-07 1.14E-06 1.47E-06 1.79E-06 2.44E-06
          3.03E-06 4.00E-06 4.76E-06 5.56E-06 6.25E-06 7.69E-06
          9.09E-06
F404:n 97
E404 0.1 0.5 1 1.5 2 2.5 3 3.5 4 4.5 5 5.5 6 7 8 9 10 11 14 16  20
DE404 LOG 2.5E-8 1E-7 1E-6 1E-5 1E-4 1E-3 1E-2 1E-1 5E-1 1 2 5 10 20
DF404 LOG 3.85E-6 4.17E-6 4.55E-6 4.35E-6 4.17E-6 3.7E-6 3.57E-6
          2.08E-5 7.14E-5 1.18E-4 1.43E-4 1.47E-4 1.47E-4 1.54E-4
F414:n 98
E414 0.1 0.5 1 1.5 2 2.5 3 3.5 4 4.5 5 5.5 6 7 8 9 10 11 14 16  20
DE414 LOG 2.5E-8 1E-7 1E-6 1E-5 1E-4 1E-3 1E-2 1E-1 5E-1 1 2 5 10 20
DF414 LOG 3.85E-6 4.17E-6 4.55E-6 4.35E-6 4.17E-6 3.7E-6 3.57E-6
```

```
          2.08E-5 7.14E-5 1.18E-4 1.43E-4 1.47E-4 1.47E-4 1.54E-4
F424:n 99
E424 0.1 0.5 1 1.5 2 2.5 3 3.5 4 4.5 5 5.5 6 7 8 9 10 11 14 16 20
DE424 LOG 2.5E-8 1E-7 1E-6 1E-5 1E-4 1E-3 1E-2 1E-1 5E-1 1 2 5 10 20
DF424 LOG 3.85E-6 4.17E-6 4.55E-6 4.35E-6 4.17E-6 3.7E-6 3.57E-6
          2.08E-5 7.14E-5 1.18E-4 1.43E-4 1.47E-4 1.47E-4 1.54E-4
C
C  MATERIALS CARDS
C Am-241, density = 12 g/cc
M1 95241 1
C
C Be-9, density = 1.85 g/cc
M2 4009.10c -100
C
C Lead, density = 11.34 g/cc
M3 82208.10c -100
C
C D2O, density =1.105 g/cc at 293.6 K, purity = 99.8%
c M4   1001.10c   -2.238177e-4
c      1002.10c   -2.007695e-1
c      8016.10c   -7.985217e-1
c      8017.10c   -4.849243e-4
C
C Zircaloy-2, density = 6.55 g/cc at 293.6 K
M5   50112.10c     -0.014065   $ Sn     1.45wt%
     50114.10c     -0.009425
     50115.10c     -0.00493
     50116.10c     -0.210685
     50117.10c     -0.11136
     50118.10c     -0.351335
     50119.10c     -0.124555
     50120.10c     -0.472555
     50122.10c     -0.067135
     50124.10c     -0.083955
c  Fe     0.135wt%
     26054.10c     -0.00783
     26056.10c     -0.123822
     26057.10c     -0.00297
     26058.10c     -0.000378
c  Cr     0.105wt%
     24050.10c     -0.00456225
     24052.10c     -0.08797845
     24053.10c     -0.00997605
     24054.10c     -0.00248325
c  Ni     0.055wt%
     28058.10c     -0.03744235
     28060.10c     -0.01442265
     28061.10c     -0.000627
     28062.10c     -0.0019987
     28064.10c     -0.0005093
c  N      0.006wt%
     7014.10c     -0.00597804
     7015.10c     -0.00002196
c  Zr      98.249wt%
     40090.10c     -50.5491105
     40091.10c     -11.0235378
     40092.10c     -16.8497035
```

```
     40094.10c     -17.0756762
     40096.10c     -2.750972
C
C  Sm-149 Absorber, density=7.54 g/cc
M6   62149.10c  -100
C
C  Air, including Argonne, density = 1.293E-3
M7   7014.10c     -78.084
     8016.10c     -20.9476
     18040.10c    -0.9684
C
C  NaI crystal, no Tl, density = 3.7 g/cc
M8   11023.10c   -15.337
     53127.10c   -84.663
C
C  CD2, density = 1.06 g/cc
M9   1002.10c    -25.115
     6000.10c    -74.885
C
C  Gd, natural abundance, density = 7.90 g/cc
M10  64152.10c -0.2
     64154.10c -2.18
     64155.10c -14.8
     64156.10c -20.47
     64157.10c -15.65
     64158.10c -24.84
     64160.10c -21.86
C  Sm, natural abundance, density = 7.54 g/cc
M11  62144.10c   -3.1
     62147.10c   -15.0
     62148.10c   -11.3
     62149.10c   -13.8
     62150.10c   -7.4
     62152.10c   -26.7
     62154.10c   -22.7
C  high density polyethylene, density = 0.97 g/cc
M12  1001.10c   -14.372
     6000.10c   -85.628
```

D.2 Mesh Tally Example MCNP Input File

Case Description: Definition of Mesh Tallies for Dose Rate Calculations (extract from input files). Material compositions were defined as in the input file example above.

```
C   Mesh Tally averaged over the entire height
FMESH14:p  origin -50 -50 -15
         IMesh -11.55 11.55 50
         IINTS 30 46 30
         JMESH -6.2 6.2 50
         JINTS 22 48 22
         KMESH 15
         KINTS 1
```

```
         EMESH 0.1 0.3 0.35 0.4 0.45 0.5 0.55 0.6 0.65 0.7 0.75 0.8 0.9
               1 2 3 4 5 10 12 14 16 18 20
         OUT ij
DE14 0.01 0.015 0.02 0.03 0.04 0.05 0.06 0.08 0.10 0.15 0.2 0.3
          0.4 0.5 0.6 0.8 1.0 1.5 2.0 3.0 4.0 5.0 6.0 8.0 10
DF14 2.78E-06 1.11E-06 5.88E-07 2.56E-07 1.56E-07 1.20E-07
        1.11E-07 1.20E-07 1.47E-07 2.38E-07 3.45E-07 5.56E-07
        7.69E-07 9.09E-07 1.14E-06 1.47E-06 1.79E-06 2.44E-06
        3.03E-06 4.00E-06 4.76E-06 5.56E-06 6.25E-06 7.69E-06
        9.09E-06
C
FMESH24:n  origin -50 -50 -15
         IMesh -11.55 11.55 50
         IINTS 30 46 30
         JMESH -6.2 6.2 50
         JINTS 22 48 22
         KMESH 15
         KINTS 1
         EMESH 0.1 0.5 1 1.5 2 2.5 3 3.5 4 4.5 5 5.5 6 7 8 9 10 11 14
16  20
         OUT ij
DE24 2.5E-8 1E-7 1E-6 1E-5 1E-4 1E-3 1E-2 1E-1 5E-1 1 2 5 10 20
DF24 3.85E-6 4.17E-6 4.55E-6 4.35E-6 4.17E-6 3.7E-6 3.57E-6
        2.08E-5 7.14E-5 1.18E-4 1.43E-4 1.47E-4 1.47E-4 1.54E-4
C
C   Mesh Tally X-Z top of source
FMESH34:p  origin -21 -8 6.2
         IMesh 21
         IINTS 42
         JMESH 8
         JINTS 1
         KMESH 16.2
         KINTS 10
         EMESH 0.1 0.3 0.35 0.4 0.45 0.5 0.55 0.6 0.65 0.7 0.75 0.8 0.9
               1 2 3 4 5 10 12 14 16 18 20
         OUT ik
DE34 0.01 0.015 0.02 0.03 0.04 0.05 0.06 0.08 0.10 0.15 0.2 0.3
          0.4 0.5 0.6 0.8 1.0 1.5 2.0 3.0 4.0 5.0 6.0 8.0 10
DF34 2.78E-06 1.11E-06 5.88E-07 2.56E-07 1.56E-07 1.20E-07
        1.11E-07 1.20E-07 1.47E-07 2.38E-07 3.45E-07 5.56E-07
        7.69E-07 9.09E-07 1.14E-06 1.47E-06 1.79E-06 2.44E-06
        3.03E-06 4.00E-06 4.76E-06 5.56E-06 6.25E-06 7.69E-06
        9.09E-06
C
FMESH44:n  origin -21 -8 6.2
         IMesh 21
         IINTS 42
         JMESH 8
         JINTS 1
         KMESH 16.2
         KINTS 10
         EMESH 0.1 0.5 1 1.5 2 2.5 3 3.5 4 4.5 5 5.5 6 7 8 9 10 11 14
16  20
         OUT ik
DE44 2.5E-8 1E-7 1E-6 1E-5 1E-4 1E-3 1E-2 1E-1 5E-1 1 2 5 10 20
DF44 3.85E-6 4.17E-6 4.55E-6 4.35E-6 4.17E-6 3.7E-6 3.57E-6
        2.08E-5 7.14E-5 1.18E-4 1.43E-4 1.47E-4 1.47E-4 1.54E-4
```

```
C
C   Mesh Tally X-Y front of source
FMESH54:p  origin -21 -16.2 -8
         IMesh 21
         IINTS 42
         JMESH -6.2
         JINTS 10
         KMESH 8
         KINTS 1
         EMESH 0.1 0.3 0.35 0.4 0.45 0.5 0.55 0.6 0.65 0.7 0.75 0.8 0.9
               1 2 3 4 5 10 12 14 16 18 20
         OUT ij
DE54 0.01 0.015 0.02 0.03 0.04 0.05 0.06 0.08 0.10 0.15 0.2 0.3
          0.4 0.5 0.6 0.8 1.0 1.5 2.0 3.0 4.0 5.0 6.0 8.0 10
DF54 2.78E-06 1.11E-06 5.88E-07 2.56E-07 1.56E-07 1.20E-07
        1.11E-07 1.20E-07 1.47E-07 2.38E-07 3.45E-07 5.56E-07
        7.69E-07 9.09E-07 1.14E-06 1.47E-06 1.79E-06 2.44E-06
        3.03E-06 4.00E-06 4.76E-06 5.56E-06 6.25E-06 7.69E-06
        9.09E-06
C
FMESH64:n  origin -21 -16.2 -8
         IMesh 21
         IINTS 42
         JMESH -6.2
         JINTS 10
         KMESH 8
         KINTS 1
         EMESH 0.1 0.5 1 1.5 2 2.5 3 3.5 4 4.5 5 5.5 6 7 8 9 10 11 14
16  20
         OUT ij
DE64 2.5E-8 1E-7 1E-6 1E-5 1E-4 1E-3 1E-2 1E-1 5E-1 1 2 5 10 20
DF64 3.85E-6 4.17E-6 4.55E-6 4.35E-6 4.17E-6 3.7E-6 3.57E-6
        2.08E-5 7.14E-5 1.18E-4 1.43E-4 1.47E-4 1.47E-4 1.54E-4
C
C C   Mesh Tally X-Y side of source (flat with source)
FMESH74:p  origin -25.55 -8 -7
         IMesh -11.55
         IINTS 28
         JMESH 8
         JINTS 16
         KMESH 7
         KINTS 1
         EMESH 0.1 0.3 0.35 0.4 0.45 0.5 0.55 0.6 0.65 0.7 0.75 0.8 0.9
               1 2 3 4 5 10 12 14 16 18 20
         OUT ij
DE74 0.01 0.015 0.02 0.03 0.04 0.05 0.06 0.08 0.10 0.15 0.2 0.3
          0.4 0.5 0.6 0.8 1.0 1.5 2.0 3.0 4.0 5.0 6.0 8.0 10
DF74 2.78E-06 1.11E-06 5.88E-07 2.56E-07 1.56E-07 1.20E-07
        1.11E-07 1.20E-07 1.47E-07 2.38E-07 3.45E-07 5.56E-07
        7.69E-07 9.09E-07 1.14E-06 1.47E-06 1.79E-06 2.44E-06
        3.03E-06 4.00E-06 4.76E-06 5.56E-06 6.25E-06 7.69E-06
        9.09E-06
C
FMESH84:n  origin -25.55 -8 -7
         IMesh -11.55
         IINTS 28
         JMESH 8
```

```
         JINTS 16
         KMESH 7
         KINTS 1
         EMESH 0.1 0.5 1 1.5 2 2.5 3 3.5 4 4.5 5 5.5 6 7 8 9 10 11 14
16  20
         OUT ij
DE84 2.5E-8 1E-7 1E-6 1E-5 1E-4 1E-3 1E-2 1E-1 5E-1 1 2 5 10 20
DF84 3.85E-6 4.17E-6 4.55E-6 4.35E-6 4.17E-6 3.7E-6 3.57E-6
       2.08E-5 7.14E-5 1.18E-4 1.43E-4 1.47E-4 1.47E-4 1.54E-4
```

D.3 SOURCES-4C Input File

```
Am-241/Be source - Interface
2 2 1
1 0 6.50 0.000001
  95 1.00
52
1
  952410 1.00
Target composed of 9Be
1 0
  4 1.0
210 11.0 0.0
1 4000
  40090 1.0
```

This input deck was used to run SOURCES-4C and calculate the neutron source strength for the ^{241}Am-^{9}Be source modelled in this research. The following is an explanation of each row in this input file:

`Am-241/Be source - Interface:` Title of the problem (α-emitter)

`2 2 1:` Specifies that this is an interface problem, and it calculates the source strength and neutron spectrum

`1 0 6.50 0.000001:` The α-emitter consists of one isotope (1), solid-stopping cross-sections are used instead of gas ones for the α-source side (0). A total of 52-groups linearly interpolated between 6.50 MeV and 0.000001 MeV are used at the interface between the α-emitter and the α-absorber, neutron-emitter. 52-groups were chosen as per example provided in the user manual for SOURCES-4C.

`95 1.00:` Atomic number of the α-emitter ($_{95}$Am) and the fraction of all atoms (1.00)

`52:` 52 α-energy groups used at the interface between the two materials (i.e., the α-emitter and the α-absorber, neutron-emitter).

`1:` One source nuclide is evaluated (i.e., only ^{241}Am)

`952410 1.00` The α-emitting isotope is only ^{241}Am

`Target composed of 9Be:` Title of the problem (α-absorber, neutron-emitter)

`1 0:` The target has only one α-absorber nuclide (1), and it solid-stopping cross-sections are used instead of gas ones for the α-absorbing side (0)

`4 1.0:` Atomic number of the α-absorber neutron-emitter ($_4$Be), and the fraction of all atoms (1.0)

`210 11.0 0.0:` Number of particle energy groups (210), linearly interpolated between maximum energy (11 MeV) and minimum energy (0 MeV)

`1 4000:` Number of target nuclides (1) and the number of α-particle energy groups used in the calculation (4000)

`40090 1.0:` Target nuclide (^{9}Be), and fraction of all atoms on the target side (1)

References

[1] L. Pibida, M. Unterweger, L. Karam, "Development of gamma-ray emitting test sources for portal monitors", Applied Radiation and Isotopes, Vol 64, 2006, pp. 1271 – 1272

[2] International Atomic Energy Agency, "Gamma Irradiators for Radiation Processing", Industrial Applications and Chemistry Section, 2006 February, http://www-naweb.iaea.org/napc/iachem/Brochure%20on%20gamma%20irradiators.pdf, Accessed June 20, 2014

[3] M.G. Sayed, "Quality Control in Nuclear Medicine II. Planar and Single Photon Emission Computed Tomographic Gamma Camera Systems, TJNM, Vol. 6, No. 3, 1997, pp. 185 - 189

[4] P. Zanzonico, "Routine Quality Control of Clinical Nuclear Medicine Instrumentation: A Brief Review", Journal of Nuclear Medicine, Vol. 49, No. 7, 2008, pp. 1114 - 1131

[5] Radiation Sources Use and Replacement: Abbreviated Version, Committee on Radiation Sources Use and Replacement, National Research Council, ISBN: 0-309-11015-7, 2008, http://www.nap.edu/catalog/11976.html, Accessed October 18, 2014

[6] M.K. O'Connor, "Quality Control of Scintillation Cameras (Planar and SPECT)", 41st Annual Meeting of the American Association of Physicists in Medicine, Nashville, TN, July 1999, https://www.aapm.org/meetings/99AM/pdf/2741-51264.pdf, Accessed March 10, 2014

[7] International Commission on Radiological Protection, ICRP, "The 2007 Recommendations of the International Commission on Radiological Protection", ICRP Publication 103, ann. ICRP 37 (2-4), 2007

[8] Los Alamos National Laboratory, X-5 Monte Carlo Team, "MCNP - A General N-Particle Transport Code, Version 5", Volume II: User's Guide, LA-CP-03-0245, 2003 April

[9] E.A. Rhodes, D.L. Bowers, R.E. Boyar, C.E. Dickerman, "Advanced Concept Proof-of-Principle Demonstration: Switchable Radioactive Neutron Source", ANL/ACTV-95/2, 1995

[10] R.D. Jefferson, R.E., Goans, P.B. Blain, S.H.L. Thomas, "Diagnosis and Treatment of Polonium Poisoning", Clinical Toxicology, Vol. 47, Issue 5, 2009, pp. 379 - 392

[11] Material Safety Data Sheet, ExxonMobil, "High Density Polyethylene", Revision Date: 24 Feb 2012, Available online at http://www.erotomold.com/documents/ExxonMobil-Polyethylene-Resin-HDPE-8660-MSDS.pdf, Accessed November 25, 2015

[12] H. Cember, "Introduction to Health Physics", 3rd edition, McGraw-Hill, ISBN 0-07-10546108, 1996

[13] R. Chandra, "Nuclear Medicine Physics - The Basics", 7th Edition, Lippincott Williams & Wilkins, ISBN 978-1-4511-0941-2, 2011

[14] National Nuclear Data Center, Brookhaven National Laboratory, “Interactive Chart of Nuclides”, Online resource http://www.nndc.bnl.gov/nudat2/, Accessed March 15, 2014

[15] S.R. Cherry, J.A. Sorenson, M.E. Phelps, "Physics in Nuclear Medicine", 3rd Edition, Saunders, ISBN: 978-0-7216-8341-6, 2003

[16] S.N. Ahmed, "Physics and Engineering of Radiation Detection", 1st Edition, Academic Press, ISBN 978-0-12-045581-2, 2007

[17] J.R. Lamarsh, A.J. Baratta, "Introduction to Nuclear Engineering", 3rd Edition, Prentice-Hall, ISBN: 0-201-82498-1, 2001

[18] R. Stephenson, "Introduction to Nuclear Engineering", McGraw-Hill Book Company, New York, 1954

[19] NIST Center for Neutron Research, “Neutron Scattering Lengths and Cross Sections”, Online resource: http://www.ncnr.nist.gov/resources/n-lengths/list.html, Accessed September 20 2014

[20] A.R. Foster, R.L. Wright, Jr., "Basic Nuclear Engineering", 3rd Edition, Allyn and Bacon Inc., ISBN 0-205-05697-0, 1977

[21] J.E. Turner, "Atoms, Radiation and Radiation Protection", 2nd Edition, John Wiley & Sons, Inc. ISBN: 0-471-59581-0, 1995

[22] E.E. Lewis, "Fundamentals of Nuclear Reactor Physics", 1st Edition, Academic Press, ISBN: 978-0-12-370631-7, 2008

[23] W.M. Stacey, "Nuclear Reactor Physics", John Wiley & Sons Inc., USA, ISBN: 0-471-39127-1, 2001

[24] J.W. Keyes, "Clinical Applications of SPECT", International Journal of Cardiac Imaging, Vol. 5, 1989, pp. 25 - 32

[25] B.L. Holman, S.S. Tumeh, "Single-Photon Emission Computed Tomography (SPECT) Applications and Potential", Topics in Radiology/Nuclear Radiology, Journal of the American Medical Association, Vol. 263, No. 4, 1990, pp. 561-564

[26] P. Blake, B. Johnson, J.W. VanMeter, "Positron Emission Tomography (PET) and Single Photon Emission Computed Tomography (SPECT): Clinical Applications", Journal of Neuro-Ophthalmology, Vol. 23, No. 1, 2003, pp. 34-41

[27] A. Bell, G.A. McRae, R. Wassenaar, R.G. Wells, D. Faber, "nSPECT: A Radioisotope-Free Approach to Nuclear Medicine Imaging", IEEE Transactions on Nuclear Science, Vol. 62, No. 3, June 2015

[28] L. Jodal, C. Le Loirec, C. Champion, "Positron Range in PET Imaging: an Alternative Approach for Assessing and Correcting the Blurring", Physics in Medicine and Biology, Vol. 57, 2012, pp. 3931 - 3943

[29] R.J. Jaszczak, "The Early Years of Single Photon Emission Computed Tomography (SPECT): an Anthology of Selected Reminiscences", Physics in Medicine and Biology, Vol. 51, 2006, pp. R99-R115

[30] S. Tavernier, A. Gektin, B. Grinyov, W.W. Moses, "Radiation Detectors for Medical Applications", Springer Netherlands, 2006, Available online from <http://www.myilibrary.com?ID=65692> , Accessed July 6, 2014

[31] E.B. Sokole, A. Plachcinska, A. Britten, "Routine quality control recommendations for nuclear medicine instrumentation", European Journal of Nuclear Medicine and Molecular Imaging, Vol. 37, 2010, pp. 662 - 671

[32] P.H. Murphy, "Acceptance Testing and Quality Control of Gamma Cameras, Including SPECT", Journal of Nuclear Medicing, Vol. 28, 1987, pp. 1221 - 1227

[33] RadQual Global Sources, "Quality Control Devices for Molecular Imaging", http://www.raditec.ch/wp-content/uploads/2015/01/Radqual-Catalog.pdf, Accessed October 10, 2015

[34] Direct Scientific, "Flood Sources, Co-57", http://www.drct.com/dss/sources/floodsrc.htm, Accessed October 10, 2015

[35] E.B. Sokole, A. Heckenberg, H. Bergmann, "Influence of high-energy photons from cobalt-57 flood sources on scintillation camera uniformity images", European Journal of Nuclear Medicine, Vol. 23, No. 4, April 1996

[36] A. Sinclair, "X-Ray versus Gamma Irradiation of Blood Components for Prevention of Transfusion-Associated Graft Versus Host Disease", Technology Assessment Unit of the McGill University Health Centre, Report Number 51, 2011 April 12, Available online at http://www.mcgill.ca/tau, Accessed November 25, 2015

[37] H.L. Kronholz, C. Moustakis, T. Schange, "The desired dose distribution in blood irradiators - requirements and experience - ", Z. Medical Physics, Vol. 8, 1998, pp. 97-102

[38] S. Shastry, B. Ramya, J. Ninan, G.C. Srinidhi, S.S. Bhat, D.J. Fernandes, "Linear accelerator: A reproducible, efficacious and cost effective alternative for blood irradiation", Transfusion and Apheresis Science, Vol. 49, 2013, pp. 528 - 532

[39] International Atomic Energy Agency - Radioisotope Products and Radiation Technology Section, "Gamma Irradiators for radiation processing", July 2005, IAEA Brochure, Accessed online at http://www-naweb.iaea.org/napc/iachem/Brochure%20on%20gamma%20irradiators.pdf, Accessed October 18, 2014

[40] International Atomic Energy Agency, "Effects of ionizing radiation on blood and blood components: a Survey", IAEA-TECDOC-934, Vienna, 1997

[41] J.S. Hendricks, "A Monte Carlo Code for Transport - an Algorithm for All Seasons", Los Alamos Science, Number 22, pp. 30 - 43, 1994

[42] R.L. Harrison, "Introduction to Monte Carlo Simulation", American Institute of Physics Conference Proceedings, Vol. 1204, pp. 17-21, 2010, DOI: http://dx.doi.org/10.1063/1.3295638

[43] Los Alamos National Laboratory, "A General Monte Carlo N-Particle (MCNP) Transport Code", Online Reference Collection, Validation & Verification Reports, https://laws.lanl.gov/vhosts/mcnp.lanl.gov/references.shtml#mcnp5_refs, Accessed September 16, 2015

[44] W.B. Wilson, R.T. Perry, W.S. Charlton, T.A. Parish, "Sources: A code for calculating (alpha, n), spontaneous fission, and delayed neutron sources and spectra", Progress in Nuclear Energy, Vol. 51, Issues 4–5, May–July 2009, pp. 608-613, ISSN 0149-1970

[45] W.B. Wilson, R.T. Perry, E.F. Shores, W.S. Charlton, T.A. Parish, G.P. Estes, J.E., Stewart, "SOURCES 4C : a code for calculating ([alpha],n), spontaneous fission, and delayed neutron sources and spectra", LA-UR-02-1839, 2002, Retrieved from http://www.osti.gov/scitech/servlets/purl/976142 on October 3, 2015

[46] Los Alamos National Laboratory, L.P. Tucker, "Student Progress Report: Summer 2012", SOURCES-4C Benchmarking Exercises, LA-UR-12-23850, August 2012

[47] D.L. Bowers, E.A. Rhodes, C.E. Dickerman, "A switchable radioactive neutron source: Proof-of-principle", Journal of Radioanalytical and Nuclear Chemistry, Vol. 233, Issue 1-2, 1998, pp. 161-165

[48] R.E. Boyar, A. DeVolpi, G.S. Stanford, E.A. Rhodes, "Switchable radioactive neutron source device", US Patent Application US 4829191 A, 1989 May

[49] K.L. Hertz, N.R. Hilton, J.C. Lund, J.M. Van Scyoc, "Alpha-emitting radioisotopes for switchable neutron generators", Nuclear Instruments and Methods in Physics Research A, Vol. 505, 2004, pp. 41-45

[50] K.W. Geiger, L. van der Zwan, "Radioactive neutron source spectra from ^{9}Be(α,n) Cross Section Data", Nuclear Instruments and Methods, Vol. 131, 1975, pp. 315-321

[51] Electric Power Research Institute (EPRI), "Proceedings: 2006 EPRI Radiation Protection Conference/ISOE North American ALARA Symposium", Session 6: Alpha Monitoring and Radiation Protection, Document ID 1014354, October 2006, Available online at http://www.epri.com/abstracts/Pages/ProductAbstract.aspx?ProductId=000000000001014354, Accessed November 10, 2015

[52] H. Kluge, K. Weise, "The Neutron Energy Spectrum of a Am-241/Be (α, n) Source and Resulting Mean Fluence to Dose Equivalent Conversion Factors", Radiation Protection Dosimetry, Vol. 2, No. 2, 1982, pp. 85-93

[53] Oak Ridge National Laboratory, "Scale: A Comprehensive Modelling and Simulation Suite for Nuclear Safety Analysis and Design", Module M8 - Standard Composition Library, ORNL/TM-2005/39, Version 6.1 (June 2011), Scale Manual available with software licence from RSICC

[54] B.A. Cheadle, "The Physical Matallurgy of Zirconium Alloys", Atomic Energy of Canada Limited, CRNL-1208, 1975, Available online at

http://www.iaea.org/inis/collection/NCLCollectionStore/_Public/43/103/43103507.pdf, Accessed November 23, 2015

[55] International Atomic Energy Agency, "Heavy Water Reactors: Status and Project Development", Chapter 7 - Environmental Considerations, Technical Reports Series No. 407, Vienna, 2002, Available online at http://www-pub.iaea.org/MTCD/publications/PDF/TRS407_scr/D407_scr3.pdf, Accessed on September 10, 2013

[56] The Consortium for Advanced Simulation of LWRs (CASL), "Initial Boiling Water Reactor (BWR) Input Specifications", CASL-U-2015-0040-000, Available online at http://www.casl.gov/docs/CASL-U-2015-0040-000.pdf, Accessed July 12, 2015

[57] Dr. Glenn Wells, Medical Physicist, Department of Nuclear Cardiology, University of Ottawa Heart Institute, *Private Communication*, September 2012

[58] S. Glasstone, A. Sesonske, "Nuclear Reactor Engineering", 3rd Edition, Van Nostrand Reinhold Company, ISBN: 0-442-20057-9, 1981

[59] International Atomic Energy Agency, "Emerging applications of radiation in nanotechnology", Proceedings of a consultants meeting held in Bologna, Italy, 22-25 March 2004, IAEA-TECDOC-1438, Published online March 2005, http://www-pub.iaea.org/MTCD/publications/PDF/te_1438_web.pdf, Accessed November 28, 2015